Synchronization in Emerging Wireless Communication Systems

by

Yuzhe Yao
B.Sc., Xi'an Jiaotong University, 2005
M.Sc., Xi'an Jiaotong University, 2007

A Dissertation Submitted in Partial Fulfillment of the
Requirements for the Degree of

DOCTOR OF PHILOSOPHY

in the Department of Electrical and Computer Engineering

Synchronization in Emerging Wireless Communication Systems

by

Yuzhe Yao
B.Sc., Xi'an Jiaotong University, 2005
M.Sc., Xi'an Jiaotong University, 2007

Supervisory Committee

Dr. Xiaodai Dong, Supervisor
(Department of Electrical and Computer Engineering)

Dr. Hong-Chuan Yang, Departmental Member
(Department of Electrical and Computer Engineering)

Dr. Kui Wu, Outside Member
(Department of Computer Science)

Supervisory Committee

Dr. Xiaodai Dong, Supervisor
(Department of Electrical and Computer Engineering)

Dr. Hong-Chuan Yang, Departmental Member
(Department of Electrical and Computer Engineering)

Dr. Kui Wu, Outside Member
(Department of Computer Science)

ABSTRACT

Synchronization is one of the most important issues in wireless communication systems design and implementation. The requirement for synchronization is going high as the signal bandwidth and the system complexity increases. For instance, the ultra-short pulse width in ultra-wideband (UWB) communication systems poses problems to the conventional timing synchronization methods and the multi-node transmission poses problems to the existing carrier frequency offset (CFO) synchronization methods. Moreover, the impact of imperfect synchronization in these systems on the system performance is more negative than that of the conventional communication systems. Therefore, efficient synchronization algorithms are really in need.

This dissertation presents several synchronization methods aiming to either improve the synchronization performance or reduce the synchronization complexity. The focus of this dissertation is on UWB systems and cooperative systems. Both timing synchronization and carrier frequency synchronization problems have been investigated. Several different systems are considered, including the point to point block transmission based UWB communications, orthogonal frequency division multiplexing (OFDM) based one way and two way relaying communication systems and narrow band cooperative communication systems. For block transmission UWB systems, i.e.,

both OFDM and single carrier frequency domain equalization (SC-FDE) UWB systems, a new generic timing estimation method based on channel impulse response (CIR) estimation is proposed. The newly proposed method is superior to the existing methods not only in synchronization performance, but also in the algorithm complexity.

For the multi-node cooperative communications, the CFO mitigation issue is studied with OFDM signaling. Due to the distributed nature of the cooperative system, the multiple CFO problem is inevitable and hard to solve. A two-step compensation scheme is designed to suppress the interference introduced by multiple CFO with low complexity. Moreover, timing synchronization in cooperative communications is studied, including the broadband OFDM based cooperative communication and the narrow band cooperative communication. A means of determining the optimal timing of the OFDM signal in asynchronous two way relay networks (TWRN) has been designed. A correlation based multi-delay estimation method is proposed for narrow band asynchronous cooperative communication systems.

The synchronization issues covering both timing and carrier synchronization have been extensively studied in this dissertation. New synchronization methods have been proposed for the emerging transmission schemes such as high rate UWB transmission and the distributed cooperative transmission with challenges different from conventional wireless transmission schemes.

Contents

List of Tables

List of Figures

List of Abbreviations

AF	Amplify-and-Forward
ARQ	Automatic Repeat-reQuest
AWGN	Additive White Gaussian Noise
BER	Bit Error Rate
BC	Broadcast
BPSK	Binary Phase Shift Keying
CFO	Carrier Frequency Offset
CDMA	Code Division Multiple Access
CE	Channel Estimation
CF	Compress-and-Forward
CIR	Channel Impulse Response
CO-OFDM	Cooperative OFDM
CP	Cyclic Prefix
CDF	cumulative distribution function
CRC	Cyclic Redundancy Check
C-DF	Correctly-Decode-and-Forward
CSI	Channel State Information
CTE	Coarse Timing Estimator
DSTBC	Distributed Space Time Coding
DSFC	Distributed Space Frequency Coding
DSTC	Distributed Space Time Coding
DF	Decode-and-Forward
DFT	Discrete Fourier Transform
FEC	Forward Error Correction
FFT	Fast Fourier Transform
FD	Frequency Domain
FDE	Frequency Domain Equalization
IBI	Inter-block Interference
IBI-R	IBI-Removal
ICI	Inter-carrier Interference
ICI-R	ICI-Removal
IR	Impulse Radio

ISI	Inter-symbol Interference
IMLD	Iterative Maximum Likelihood Decoding
IFFT	Inverse Fast Fourier Transform
LFSR	Linear Feedback Shift Registers
MA	Multiple Access
ML	Maximum Likelihood
MAE	Mean Absolute Error
MAC	Multiplication-and-Accumulation
MSE	Mean Square Error
MB-OFDM	Multi-band Orthogonal Frequency Division Multiplexing
MMSE	Minimum Mean Square Error
OFDM	Orthogonal Frequency Division Multiplexing
OTEQ	One Tap Equalization
OWRN	One Way Relay Network
PN	Pseudorandom noise
QPSK	Quadrature Phase-Shift Keying
RF	Radio Frequency
RMSE	Root Mean Square Error
RRC	Root Raised Cosine
SC-FDE	Single Carrier Frequency Domain Equalization
SER	Symbol Error Rate
SNR	Signal-to-noise Ratio
SINR	Signal to Interference plus Noise Ratio
STBC	Space Time Block Coding
TD	Time Domain
TWRN	Two Way Relay Network
UWB	Ultra-Wideband

ACKNOWLEDGEMENTS

In the first place, I would like to offer my sincerest gratitude to my Graduate Supervisor, Dr. Xiaodai Dong, for her advice and support throughout my PhD study at University of Victoria. This dissertation would not have been possible without her guidance and help. The discussion and experiment with her have been inspiring me during the entire PhD study.

I gratefully acknowledge my supervisory committee, Dr. Hong-Chuan Yang, Department of Electrical and Computer Engineering and Dr. Kui Wu, Department of Computer Science for their valuable advise on my research work. Many thanks to my external examiner, Dr. Witold A. Krzymien, Department of Electrical and Computer Engineering, University of Alberta for making my dissertation complete.

I would like to thank my wife Youjun for her care and support during the long journey of PhD study, especially all the holidays that she arranged to give me time to write, to think and to talk to her about this subject. Her support and encouragement was in the end what made this dissertation possible.

I also wish to thank our department staff Ms. Moneca Bracken and Ms. Janice Closson for their enormous support and continuous cooperation.

Finally, my special thanks go to my parents for their love and understanding during the pursuit of the degree.

DEDICATION

Just hoping this is useful!

Chapter 1

Introduction

1.1 Background

During the past few decades, wireless communication has been one of the most exciting technologies that have changed people's life significantly. Especially in the last decade, a surge of research activities on wireless communications has been witnessed, covering wireless transmission technologies such as multiple antenna transmission, orthogonal frequency division multiplexing (OFDM), ultra-wideband (UWB) and cooperative communications. These emerging transmission technologies are developed to provide faster and more reliable communication over the wireless channel.

UWB is an appealing technology for short range and low power transmission and it was traditionally accepted as impulse radio by transmitting information with ultra-short pulses. Now the Federal Communications Commission (FCC) defines UWB in terms of a transmission from an antenna for which the emitted signal bandwidth exceeds the lesser of 500 MHz or 20% of the center frequency. The FCC power spectral density emission limit for UWB emitters operating in the UWB band is -41.3 dBm/MHz. Different types of UWB are proposed for different applications. In low rate applications, which has a data rate usually of several Mbps, impulse radio UWB (IR-UWB) has been proposed [2]. Whereas in high rate applications, MB-OFDM has been proposed [1, 3]. Both IR-UWB and OFDM UWB must conform to the FCC spectrum mask regulation.

OFDM is another promising transmission technology that divides the whole spectrum into a large number of sub-carriers, and modulates different data symbols onto different sub-carriers and all the sub-carriers are orthogonal to each other. OFDM

has developed into a popular scheme for wideband digital communication, whether wireless or over copper wires, used in applications such as Asymmetric Digital Subscriber Line (ADSL), wireless local area networks (W-LAN), wireless metropolitan area networks (W-MAN), wireless personal area networks (W-PAN), terrestrial television broadcasting (DVB) and long term evolution (LTE) in cellular systems. The primary advantage of OFDM over single-carrier schemes is its ability to cope with severe channel conditions without complex equalization filters. Channel equalization is simplified because OFDM may be viewed as using many slowly modulated narrow band signals rather than one rapidly modulated wideband signal.

Cooperative communications has been attractive recently due to its ability to improve overall system capacity and communication range extension. Unlike the conventional one-hop transmission, signal experiences multi-hop from the source to the destination in cooperative systems. In some cases, the relay nodes not only relay the signal of other users, but also have their own information to send. This scenario forms a user cooperation system, where each user helps relay their partner's information while transmitting its own information as well. In other cases, relay nodes do not have their own information, they act as a real "relay station" to forward information to the next hop. According to the operation at the relay nodes, there are three relaying schemes including amplify-and-forward (AF), decode-and-forward (DF) and compress-and-forward (CF). The AF strategy allows the relay node to amplify the received signal from the source node and to forward it to the destination station. DF relay nodes decode the source information and forward to the destination when the message is decoded successfully. The compress-and-forward strategy allows the relay station to compress the received signal from the source node and forward it to the destination without decoding the signal where Wyner-Ziv coding can be used for optimal compression. According to the topology, there is serial relay transmission and parallel relay transmission. The serial relay transmission is mainly used for range extension while parallel relay transmission is often employed to improve the robustness against fading channels. In the parallel topology, signal propagates through multiple relay path in same hop and destination combines the signals received with the help of various combining schemes, which provides power gain and diversity gain simultaneously.

1.2 Problem Statement

Synchronization is the first crucial task in digital communication systems. Nothing can be done without synchronization. Imperfect synchronization also causes performance degradation. Synchronization issue in wireless communications covers a lot of areas, including signal appearance detection, symbol timing, frame boundary estimation, carrier frequency offset estimation and compensation and time synchronization in networks. In this dissertation, the physical layer signal level synchronization will be investigated. Several transmission schemes have been exploited, including UWB, OFDM, and cooperative communications. Specifically, the research work of this dissertation is focused on the following problems.

1. **Timing Synchronization in Block Transmission UWB Systems**

   Block transmission has been well received for high-rate UWB communications, including OFDM UWB and single carrier frequency domain equalization (SC-FDE) UWB. The OFDM UWB has been standardized by both the IEEE and European Computer Manufacturers Association (ECMA) in [1, 3] and the SC-FDE for UWB has been proposed in [68]. In cyclic prefixed block transmission UWB systems, the block is short due to the high bandwidth hence the cyclic prefix (CP) length is often not enough to cover the delay spread. The long delay spread and the dense multipath has raised great challenge to the timing synchronization. As shown in Fig. 1.1, the task of timing synchronization is to detect the presence of the signal and locate the block boundary. The UWB channel has much more multipath components than the conventional broadband wireless channels. Furthermore, the first significant path is sometimes weak and is not the strongest path, especially in non-line of sight channels. The delay spread of the multipath channel is sometimes even longer than the CP length. As a result, the synchronization task becomes complicated and difficult in such a system. For instance, Fig. 1.2 is a realization of UWB channel obtained with the IEEE 802.15.3a channel model. The CP length in Fig. 1.1 is 64ns if the symbol number is 32 and the symbol duration is 2ns. But the channel delay spread can be more than 100ns in Fig. 1.2. Therefore, synchronization methods for conventional wideband OFDM signal cannot work well in UWB channels. New methods need to be developed to adapt to the complicated channel environment.

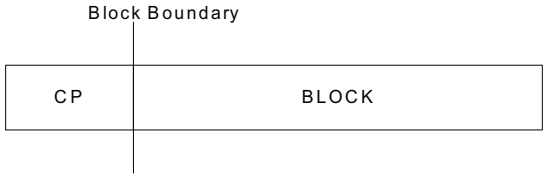

Figure 1.1: Cyclic prefixed block transmission.

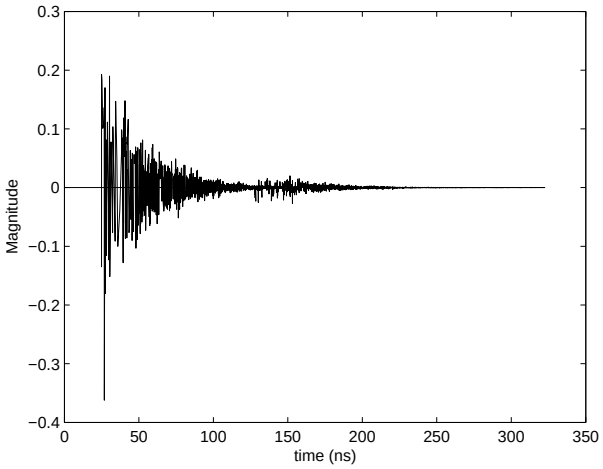

Figure 1.2: A UWB Channel Realization.

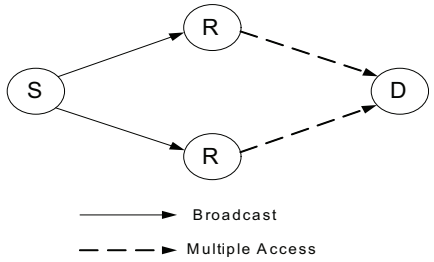

Figure 1.3: Illustration of a two relays network.

2. **Multiple CFO Mitigation in Cooperative OFDM Systems**

   Synchronization in cooperative networks is an interesting topic and has attracted a lot of research attention recently. Let's consider a simple one way relay cooperative network shown in Fig. 1.3. The network comprises of one source node, two relay nodes and one destination node. The source is trying to send OFDM modulated signal to the destination with the help of the two relays. This network forms a simple cooperative OFDM (CO-OFDM) network. Typically, the transmission is divided into two phases (time slots). During the first phase, the source node broadcasts the signal to the two relays and the relays temporarily sample and store the signal. Then in the second phase, the relays cooperatively forward the signal to the destination node with distributed space time coding (DSTC). In the second phase, the destination receives the superposition of the signal from two relays. Therefore, the destination receiver will suffer two distinct carrier frequency offsets (CFO). As we know, OFDM modulation is very sensitive to the CFO. Unlike the single hop OFDM transmission where the single CFO can be easily compensated, the multiple CFO distortion is hard to compensate even can be well estimated. In this situation, special care has to be taken to deal with the multiple CFO distortion.

3. **Optimal Timing Estimation in Two Way Relay Networks with OFDM Signaling**

   The communication in Fig. 1.3 is one way, which is called one way relay network (OWRN). However, communication is usually bidirectional. The two way communication network with the help of relays is called two way relay network (TWRN). TWRN is not simply two OWRNs. As shown in Fig. 1.4, which shows the smallest TWRN. In this case, the transmission is also divided into two phases. The first phase is called multiple access (MA) phase, in which the

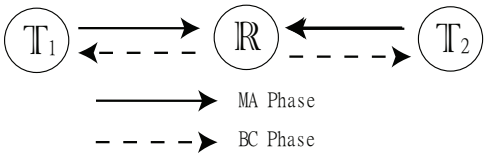

Figure 1.4: Illustration of a TWRN.

two source nodes transmit the signal to the relay at the same time. The second phase is called broadcast (BC) phase, in which the relay broadcasts the received signal to the source nodes. Since the signals from the two source nodes are sent simultaneously, the signal at the relay is the addition of the two. In the BC phase, the signal that each source node received contains the signal component from its own. Fortunately, each source node has knowledge of its own signal. Given the channel information, the self interference signal component can be easily subtracted from the composite received signal, remaining only the desired signal component.

Consider the TWRN with OFDM signaling. Due to the distributed nature of the network, the time slot at each node is not perfectly aligned to each other and the propagation delay of each channel is not the same. As a result, the signal blocks from the two source nodes are misaligned at the relay receiver and it is up to the relay node to determine a point to establish the discrete Fourier transform (DFT) window. Therefore, how to establish the DFT window as to achieve the best forwarded signal quality is an open problem that is crutial in such a system.

4. **Multiple Delay Estimation of DF Cooperative Transmission with Narrowband Signaling**

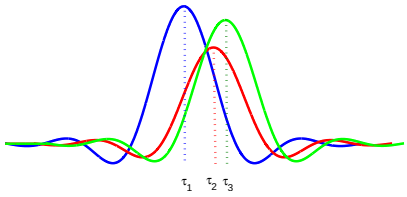

Figure 1.5: Received signal at the destination with 3 relays.

In cooperative OFDM systems, timing is flexible because of the use of CP. As will be discussed in later chapters, there is a region in the CP called inter-block

interference (IBI) free region. As long as the DFT window starts from the IBI-free region, there is no extra interference. However, in narrow band cooperative communications, the different delays from each relay node must be taken into consideration. As shown in Fig. 1.5, the signals from three relays arrive at the destination receiver with different delays. The multiple delays introduce inter-symbol interference (ISI) at the destination. To solve this problem, one way is to feedback the delay parameters to the relays and then each relay is able to adjust its transmit time in order for the signal to arrive at the destination at the same time. The other way is to eliminate the ISI at the destination using resynchronization filter which has been proposed in [62]. Therefore, accurate estimation of the delays from distributed relay nodes is essential in this type of cooperative transmission system. To save overhead, the relays transmit the training symbols at the same time. Then it is a multi-parameter estimation problem at the destination receiver.

1.3 Contributions

The synchronization problems introduced above have been investigated in this dissertation. The contributions made in this research work include impact analysis of imperfect synchronization, and proposing new methods for timing and frequency synchronization in several emerging transmission schemes. Those contributions are summarized as follows.

- A new joint timing and channel estimation scheme has been proposed for block transmission UWB systems, including the OFDM UWB and SC-FDE UWB. The scheme is based on a newly designed preamble for both coarse timing and the subsequent channel estimation. Despite of the presence of coarse timing error, the estimated channel impulse response (CIR) is simply the cyclic shifted version of the real CIR, thanks to the unique structure of the preamble. The proposed scheme saves preamble overhead by performing joint synchronization and channel estimation, and outperforms existing timing acquisition methods in the literature in dense multipath UWB channels. In addition, the impact of timing error on channel estimation and the performance of SC-FDE UWB systems are analyzed, and the bit-error-rate (BER) degradation with respect to a certain timing error is derived.

- The multiple CFO compensation problem in cooperative communications has been investigated. Specially, the system under study is AF cooperative OFDM with Alamouti distributed space time block coding (DSTBC). A joint time domain (TD) and frequency domain (FD) compensation method has been proposed. The proposed method saves complexity and is able to achieve better performance compared to the existing methods.

- For the TWRN with OFDM signaling, the optimal timing at the relay has been investigated. One OFDM block is dedicated to the timing estimation. A timing estimation method is proposed for the relay to establish the timing position in the MA time slot with the lowest interference power based on the superimposed training block from the two source nodes. The proposed estimator is a sliding window estimator evaluating the interference power at each timing position, and the timing position which minimizes the evaluation metric is the optimal position to establish the DFT window. The metric function is derived to measure the total interference power based on the training blocks. Finally, the performance of the proposed estimator is evaluated by computer simulation in the presence of different amounts of signal misalignment.

- In cooperative transmission with narrow band signaling, a low complexity correlation based multiple delay estimator has been proposed. The proposed method requires that each relay transmit a PN sequence with different phase. At the destination receiver, the discrete superimposed signal is first interpolated to the required resolution and then correlated with each relay's PN sequence modulated waveform template sampled at the same resolution. The peak of each correlation yields the estimation of the delay of the corresponding relay. The proposed correlation based method saves substantial complexity compared to the existing ML estimator and is able to achieve satisfactory performance.

1.4 Outline

The remaining chapters of the dissertation are organized as follows.

- Chapter 2 will introduce the newly proposed joint timing and channel estimation algorithm for block transmission UWB systems. Firstly, the existing work has been reviewed and the signal model is presented. Before introducing the

new algorithm, the impact of timing error on SC-FDE UWB system has been analyzed which has not appeared in the literature yet. Then the proposed joint timing and channel estimation method has been described and analyzed, including the coarse timing, channel estimation, fine timing and channel adjustment. To evaluate the proposed algorithm, simulation results have been presented including the mean absolute error (MAE) and channel estimation mean square error (MSE).

- Chapter 3 will present a multiple CFO mitigation algorithm for Alamouti DSTBC coded AF CO-OFDM system. The proposed method is a joint TD-FD scheme compared to the existing schemes which are all purely FD processing. In Chapter 3, the TD processing is described first then the corresponding FD processing is introduced. Complexity analysis is also conducted. Then simulation results and discussion on the algorithm will be presented.

- The timing issue in TWRN will be discussed in Chapter 4. The signal model of the TWRN is first presented in detail and the signal misalignment at the relay node is demonstrated. Then the maximum likelihood (ML) timing estimator is derived. The ML timing estimator is further derived and transformed into a sliding window correlator. The output of the correlator will be used as the metric for determining the optimal timing position to establish the DFT window. The proposed method has then been examined with computer simulation.

- The multiple delay estimation problem in a typical cooperative narrow band transmission system will be studied in Chapter 5. In this chapter, DF relays are employed in the network. Based on the existing ML multi-delay estimation in [62], we design a low complexity correlation based estimator. The estimator first interpolates the sampled signal into desired estimation resolution. Then correlation is performed for each relay to find out the corresponding delay parameter. The performance of the proposed estimator is slightly worse than the ML estimator but it saves substantial complexity.

- Finally, Chapter 6 concludes the whole dissertation and proposes the potential future work.

Chapter 2

Timing Synchronization in Block Transmission UWB Systems

As introduced in Chapter 1, UWB is expected to serve in short range communications. So far, there are two main categories of UWB, i.e., impulse-radio UWB (IR-UWB) [2] and multi-band OFDM (MB-OFDM) UWB [1] for low rate applications and high rate applications respectively. In this chapter, only high rate UWB systems will be discussed, including both OFDM UWB and SC-FDE UWB. The block transmission UWB schemes compare favorably to the impulse based UWB systems for high rate applications in terms of equalization complexity and energy collection in dense multipath UWB channels. Comparing SC-FDE UWB and OFDM UWB, SC-FDE has lower peak to average power ratio (PAPR) and lower sensitivity to carrier frequency offset (CFO) than OFDM, but is less robust to timing error [70]. The timing synchronization issue for both OFDM and SC-FDE block transmission UWB systems will be discussed in this chapter and a novel generic joint timing and channel estimation method will be introduced.

The rest of this chapter is organized as follows. Section 2.1 gives the background knowledge and the literature review on this subject. Section 2.2 presents the signal model. Before introducing the proposed algorithm, the impact of timing error on SC-FDE UWB systems is analyzed, which has not been well studied in the literature yet. Then the proposed algorithm will be introduced and analyzed in detail in Section 2.4. Section 2.5 presents the simulation results and Section 2.6 summaries the chapter.

2.1 Overview and Related Works

The high-rate UWB has pulse duration less than 2ns and the signal is sent without interval between adjacent pulses at high rate. The inter-symbol interference (ISI) is severe given the high bandwidth and the dense multipath, thus the requirement on the synchronization accuracy is much more stringent than conventional wideband systems. Moreover, the highly dispersive nature of UWB channels presents additional challenges to timing acquisition.

The literature is abundant with research on preamble assisted synchronization methods for OFDM in conventional wideband channels [56, 41, 27, 12]. Since only timing synchronization is the focus of our discussion, publications that only studied the OFDM carrier frequency offset synchronization are not discussed. Generally, synchronization methods can be classified into two categories: auto-correlation based [56, 41, 27] and cross-correlation with a clean preamble template, e.g., [12]. Schmidl and Cox are the first to propose a low complexity joint timing and CFO synchronization method using a two-symbol preamble pattern in additive white Gaussian noise (AWGN) channels [56]. The drawback of the scheme in [56] is the large timing variance due to the plateau of the timing metric function. In [27], Minn *et. al.* have designed a robust time and frequency synchronization method with improved training patterns and a timing metric function that has a sharp trajectory. The training symbol has L identical parts with possible sign inversions and the channel impulse response (CIR) estimated from one identical part is used for fine timing. A joint timing and channel estimation (CE) method has been proposed in [12], where the computational complexity of correlating with a preamble template is higher than the auto-correlation based methods. In [17], a joint timing and CE scheme has been proposed for WLAN systems, which performs a ML channel estimation at every trial of the timing instant estimation. For UWB systems, however, these timing schemes do not perform well due to the fact that dense multipath UWB channels are much longer than wideband channels. A UWB system from the implementation perspective cannot employ a large size fast Fourier transform (FFT) because of the cost and complexity constraints. In order to maintain a reasonable overhead, cyclic prefix (CP) must be short corresponding to the small FFT size. Sometimes a highly dispersive channel is even longer than CP, causing inter-block interference (IBI). Since perfect timing is achieved in the IBI-free region of CP, little or no room is left for synchronization deviation from the exact timing position, depending on the relative

UWB channel length to the CP length. Both the channel estimator and the search algorithm for the first tap proposed in [27] would not be sufficient in UWB channels due to the large coarse timing error caused by severe channel dispersion. For the CE method in [12], the large number of UWB channel taps requires a prohibitively large number of cross-correlation computations.

There are only a few publications in the literature on synchronization for multi-band (MB) OFDM UWB systems [15, 13, 32, 52, 76], all using the preamble defined in the WiMedia standard [1] except [13]. Cross-correlation with the preamble template is used in [15, 13, 32] for synchronization, leading to high complexity. The methods in [52, 76] employ auto-correlation of the received signal as the timing metric and take the maximum of the metric to be the timing point, which tend to synchronize to the strongest path but not necessarily the first significant path.

As discussed above, the timing issue in high rate UWB transmission has not been well addressed. A generic synchronization method for block transmission UWB transmission is needed. In the following, a generic joint timing and CE scheme for block transmission UWB systems will be presented, which begins with an auto-correlation based coarse timing estimator using a newly designed preamble, followed by CE and CE assisted timing adjustment. In the coarse timing stage, the coarse FFT window position is established and the initial CE is performed. The particular preamble structure makes the CE robust to the coarse timing error, and the proposed technique to accurately estimate the coarse timing error allows both fine timing adjustment and CIR adjustment for later data demodulation. Both synchronization and CE are acquired from the procedure. This design saves the preamble overhead and improves the synchronization performance in UWB channels. The fine timing estimation task is related to the time of arrival (ToA) estimation. For ToA estimation in MB-OFDM UWB systems, energy detectors can be found in [31, 14], and an energy jump detector has been proposed in [30]. The proposed timing estimator is equipped with a new energy jump detector for fine timing estimation.

2.2 System Model

Although the system model adopts cyclic prefixed single carrier block transmission with frequency domain equalization over UWB channels, the synchronization technique developed directly applies to an OFDM system. The pth transmitted block is composed of digitally modulated symbols $x_{p,k}$ $(0 \leq k \leq N-1)$, where N is the

block length. A cyclic prefix of length N_g is used to avoid IBI as in an OFDM system. Denote the symbol-spaced equivalent CIR by $\mathbf{h} = [h_0, h_1, ..., h_L]$, where L is the maximum channel delay. The UWB channel is assumed to be constant over the data blocks. As long as the maximum channel delay is shorter than the CP length ($L < N_g$), there is no IBI in data demodulation with perfect timing. The task of synchronization is to find the beginning of the data block, also referred to as finding the FFT window position. Perfect synchronization in cyclic prefixed block transmission systems can be achieved in the IBI-free region of the CP ($[-N_g + L, 0]$) [41]. As long as the FFT window starts within the IBI-free region, data demodulation can be carried out perfectly. Otherwise timing error will cause performance degradation to a system. In the following section, the effect of timing offset on the performance of SC-FDE UWB will be analyzed.

2.3 The Impact of Timing Error on the SC-FDE Performance

Before introducing the proposed timing estimator, the impact of timing error on SC-FDE systems will be analyzed in this section first. The timing error impact on a general OFDM system and on a MB-OFDM system has been analyzed in [67] and [28] respectively. However, the timing error impact on SC-FDE UWB systems has not been well studied. The sub-symbol level timing offset analysis and timing jitter analysis on SC-FDE UWB systems were studied in [70], where it was shown that the sub-symbol level timing offset determines the sampling position of the equivalent channel and even the worst sub-symbol level timing offset only results in small performance degradation. Timing jitter was found to be more detrimental to system performance. Here, we study the symbol level timing offset which will be shown to have more adverse effect than sub-symbol level timing offset.

2.3.1 Small Delay Spread Channels

Small delay spread channels refer to channels with the maximum delay shorter than CP, i.e. $N_g > L$. Let m denote the timing error, and assume $|m| < N_g - L$. When $m < 0$, the starting point of the established FFT window falls in the IBI-free part of CP, leading to the same performance as that of the exact timing point. However, when $m > 0$, the established FFT window is on the right of the correct window, meaning

that the current block window contains m samples of the next block. Assuming carrier frequency is perfectly synchronized, the pth received block as shown in Appendix I can be written as

$$\mathbf{y}(p) = \tilde{\mathbf{h}}\mathbf{x}^m(p) + \tilde{\mathbf{h}}_1^m\tilde{\mathbf{x}}_1^m(p) + \mathbf{n} \tag{2.1}$$

where $\tilde{\mathbf{h}}$ is the Toeplitz channel matrix with $[h_0\ 0\ \ldots\ 0\ h_L\ h_{L-1}\ \ldots\ h_1]_{1\times N}$ as its first row. $\mathbf{x}^m(p)$ is the $N\times 1$ desired pth data block left cyclic shifted by m (>0), $\mathbf{n}$ is the Gaussian noise,

$$\begin{aligned}\tilde{\mathbf{x}}_1^m(p) =&[\underbrace{0,...,0}_{N-m}, x_{p+1,-N_g} - x_{p,0},\ x_{p+1,-N_g+1} - x_{p,1},\ ...,\\ &x_{p+1,-N_g+m-1} - x_{p,m-1}]_{N\times 1}^T\end{aligned} \tag{2.2}$$

where $x_{p,n}$ denotes the nth ($-N_g \le n \le N-1$) symbol in the pth block, and

$$\tilde{\mathbf{h}}_1^m = \begin{bmatrix} \mathbf{0}_{(N-m)\times(N-m)} & \mathbf{0}_{(N-m)\times m} \\ & \begin{matrix} h_0 & 0 & \ldots & 0 \\ h_1 & h_0 & \ldots & 0 \\ \vdots & & \ddots & \vdots \\ h_{m-1} & & \ldots & h_0 \end{matrix} \\ \mathbf{0}_{m\times(N-m)} & \end{bmatrix}. \tag{2.3}$$

The received block in (2.1) can be seen as the combination of two convolutions plus the AWGN: one is the circulant convolution between $\mathbf{x}^m(p)$ and the channel $\mathbf{h}$, and the other one is the linear convolution between $\mathbf{h}$ and $\tilde{\mathbf{x}}_1^m(p)$. After FFT, FDE, and IFFT, the demodulated block can be written as

$$\hat{\mathbf{x}}(p) = \mathbf{F^H C\Lambda F}\mathbf{x}^m(p) + \mathbf{F^H CF}\tilde{\mathbf{h}}_1^m\tilde{\mathbf{x}}_1^m(p) + \mathbf{F^H CFn} \tag{2.4}$$

where $\mathbf{F}$ and $\mathbf{F^H}$ are the $N\times N$ FFT and IFFT operation matrices respectively, and $\mathbf{\Lambda}$ is diagonal representing the frequency domain channel response $H_k = \sum_{i=0}^{L} h_i e^{-j2\pi ik/N}$. The $\mathbf{C}$ is the diagonal FDE matrix with MMSE coefficients $C_k = \frac{\hat{H}_k^*}{|\hat{H}_k|^2 + N_0/(2E_b)}$ as its elements [69], where $\hat{H}_k$ is the estimated frequency domain channel response. In the presence of timing offset, the quality of CE is degraded as will be shown in Section 2.3.3. However, employing our proposed preamble and the joint timing and CE algorithm in Section 2.4, the effect of timing offset on CE is only a phase shift in

the frequency domain. Therefore, $\hat{H}_k = H_k e^{j2\pi km/N}$ ignoring the noise effect, where the phase shift is directly included in the CE. Let $\mathbf{\Psi}^{1,m} = \mathbf{F^H C F \tilde{h}}_1^m$, and the (k,n)th (the matrix index starts from 0) element of $\mathbf{\Psi}^{1,m}$ is given by

$$\Psi_{k,n}^{1,m} = \begin{cases} 0 & n<N-m \\ \frac{1}{N}\sum_{i=0}^{N-1}\sum_{t=n}^{N-1} C_i h_{t-n} e^{j\frac{2\pi i(m-t+k)}{N}} & N-m\le n\le N-1 \end{cases}. \tag{2.5}$$

Then the demodulated block can be rewritten as

$$\hat{\mathbf{x}}(p) = \frac{1}{N}\sum_{k=0}^{N-1}\mu_k \mathbf{x}(p) + \mathbf{I}_{isi} + \mathbf{\Psi}^{1,m}\tilde{\mathbf{x}}_1^m(p) + \tilde{\mathbf{n}} \tag{2.6}$$

where $\mu_k = \frac{|H_k|^2}{|H_k|^2 + N_0/(2E_b)}$, $\mathbf{I}_{isi}$ is the inter-symbol interference from the current block due to the fact that an MMSE receiver is not inter-symbol interference (ISI) free [68], and $\tilde{\mathbf{n}}$ is the Gaussian noise term with variance $\sigma_{\tilde{n}}^2 = \frac{N_0}{2N^2}\sum_{l=0}^{N-1}|\sum_{k=0}^{N-1} C_k e^{-\frac{j2\pi lk}{N}}|^2$. The ith element of $\mathbf{I}_{isi}$ is $\sum_{\substack{n=0\\ n\neq i}}^{N-1} S_n(i)x_{p,n}$ where $S_n(i) = \frac{1}{N}\sum_{k=0}^{N-1}\mu_k e^{-j2\pi(n-i)k/N}$. The third term in (2.6) is the timing error induced interference. Define the index set $[0, N-1]$ as U and the subset $[0, m-1]$ as U_1. Then for $i \in U_1$, the demodulated symbol can be written as

$$\begin{aligned} \hat{x}_{p,i} =& (\frac{1}{N}\sum_{k=0}^{N-1}\mu_k - \Psi_{i,N-m+i}^{1,m})x_{p,i} \\ &+ \overbrace{\sum_{n=m}^{N-1} S_n(i)x_{p,n} + \sum_{\substack{n=0\\ n\neq i}}^{m-1}(S_n(i) - \Psi_{i,N-m+n}^{1,m})x_{p,n}}^{\text{in-block ISI}} \\ &+ \underbrace{\sum_{n=0}^{m-1}\Psi_{i,N-m+n}^{1,m}\, x_{p+1,-N_g+n}}_{\text{IBI}} + \tilde{n}_i, \end{aligned} \tag{2.7}$$

and for $i \in U/U_1$, the demodulated symbol can be written as

$$\hat{x}_{p,i} = \frac{1}{N}\sum_{k=0}^{N-1}\mu_k x_{p,i} + \underbrace{\sum_{n=0}^{m-1}\Psi_{i,N-m+n}^{1,m}\, x_{p+1,-N_g+n}}_{\text{IBI}} + \overbrace{\sum_{n=m}^{N-1} S_n(i)x_{p,n} + \sum_{n=0}^{m-1}(S_n(i) - \Psi_{i,N-m+n}^{1,m})x_{p,n}}^{\text{in-block ISI}} + \tilde{n}_i. \tag{2.8}$$

The interference includes the in-block ISI which comes from the current block and the IBI coming from the succeeding block. There are a large number of independent interference symbols in (2.7) and (2.8), therefore Gaussian approximation can be applied to the sum of ISI according to the Lyapunov's central limit theorem as shown in the Appendix A.2. The variance of the interference for the ith desired symbol is denoted by $\sigma_s^2(i)$ which can be written as

$$\sigma_s^2(i) = \sum_{n=m}^{N-1}|S_n(i)|^2 + \sum_{\substack{n=0\\ n\neq i}}^{m-1}|S_n(i) - \Psi_{i,N-m+n}^{1,m}|^2 + \sum_{n=0}^{m-1}|\Psi_{i,N-m+n}^{1,m}|^2. \tag{2.9}$$

Without loss of generality, considering the BPSK symbols, the bit error rate (BER) is given by $P_e(x_{p,i}) = P(\Re(\hat{x}_{p,i}) > 0 | x_{p,i} = -1)$. Therefore, the error probability is given by

$$P_e(x_{p,i}) = Q\left(\frac{\sum_{k=0}^{N-1}\mu_k - \Re(\Psi_{i,N-m+i}^{1,m})}{N\sqrt{\sigma_s^2(i) + \frac{\sigma_{\tilde{n}}^2}{E_b}}}\right), \quad i \in U_1 \tag{2.10}$$

$$P_e(x_{p,i}) = Q\left(\frac{\sum_{k=0}^{N-1}\mu_k}{N\sqrt{\sigma_s^2(i) + \frac{\sigma_{\tilde{n}}^2}{E_b}}}\right), \quad i \in U/U_1 \tag{2.11}$$

where $\Re\{\cdot\}$ is taking the real part of a complex number. Then the overall average BER can be obtained by $\bar{P}_e = \frac{1}{N}\sum_{i=0}^{N-1} P_e(x_{p,i})$.

2.3.2 Large Delay Spread Channels

In the large delay spread channels, there is often no IBI-free region within the CP, and hence timing error on both sides of the exact timing point may cause performance degradation. When $m > 0$, the established FFT window contains multipath components from both the previous and the next block. Considering the case when timing error is small, i.e., $m < L - N_g$, and letting $\nu = L - N_g - m$, the demodulated block can be written as [1]

$$\begin{aligned}\hat{\mathbf{x}}(p) =&\mathbf{F^H C \Lambda F x}^m(p) + \mathbf{F^H C F}(\tilde{\mathbf{h}}_1^m \tilde{\mathbf{x}}_1^m(p) + \tilde{\mathbf{h}}_2^\nu \tilde{\mathbf{x}}_2^\nu(p)) \\ &+ \mathbf{F^H C F n},\end{aligned} \tag{2.12}$$

where $\tilde{\mathbf{x}}_2^\nu(p)$ and $\tilde{\mathbf{h}}_2^\nu$ are given by

$$\begin{aligned}\tilde{\mathbf{x}}_2^\nu(p) =&[x_{p-1,N-\nu} - x_{p,N-L},\ x_{p-1,N-\nu+1} - x_{p,N-L+1}, \\ &...,\ x_{p-1,N-1} - x_{p,N-N_g-1},\ \underbrace{0,...,0}_{N-\nu}]^T_{N\times 1}\end{aligned} \tag{2.13}$$

$$\tilde{\mathbf{h}}_2^\nu = \begin{bmatrix} h_{L-1} & h_{L-2} & \dots & h_{L-\nu} & \\ 0 & h_{L-1} & \dots & h_{L-\nu+1} & \mathbf{0}_{\nu\times(N-\nu)} \\ 0 & 0 & \ddots & \vdots & \\ 0 & 0 & \dots & h_{L-1} & \\ & \mathbf{0}_{(N-\nu)\times\nu} & & & \mathbf{0}_{(N-\nu)\times(N-\nu)} \end{bmatrix}. \tag{2.14}$$

The IBI has contribution from the preceding block and the succeeding block. Note that $\tilde{\mathbf{h}}_1^m \tilde{\mathbf{x}}_2^\nu(p) = \tilde{\mathbf{h}}_2^\nu \tilde{\mathbf{x}}_1^m(p) = \mathbf{0}$, and then (2.12) can be rewritten as

$$\begin{aligned}\hat{\mathbf{x}}(p) =&\mathbf{F^H C \Lambda F x}^m(p) + \mathbf{F^H C F}(\tilde{\mathbf{h}}_1^m + \tilde{\mathbf{h}}_2^\nu)(\tilde{\mathbf{x}}_1^m(p) + \tilde{\mathbf{x}}_2^\nu(p)) \\ &+ \mathbf{F^H C F n}.\end{aligned} \tag{2.15}$$

Let $\mathbf{\Psi}^{2,m,\nu} = \mathbf{F^H C F}(\tilde{\mathbf{h}}_1^m + \tilde{\mathbf{h}}_2^\nu)$ and define the index subsets $U_2 = [0, m-1]$ and $U_3 = [N - L + \nu, N - N_g]$. Following the same procedure in the previous subsection,

[1] For large timing error $m > L - N_g > 0$, the problem becomes the same as Subsection 2.3.1.

the variance of the interference can be obtained as

$$\sigma_s^2(i) = \sum_{\substack{n\in U_2\\ n\neq i}} |S_n(i) - \Psi_{i,N-m+i}^{2,m,\nu}|^2 + \sum_{\substack{n\in U_3\\ n\neq i}} |S_n(i) - \Psi_{i,n-N+L-m}^{2,m,\nu}|^2 + \sum_{\substack{n\notin U_2\cup U_3\\ n\neq i}}^{n\in U} |S_n(i)|^2 + \sum_{n\in U_2\cup U_3} |\Psi_{i,n}^{2,m,\nu}|^2. \tag{2.16}$$

Then the error probability of the ith symbol of the pth block is given by

$$P_e(x_{p,i}) = Q\left(\frac{\sum_{k=0}^{N-1}\mu_k - \Re(\Psi_{i,N-m+i}^{2,m,\nu})}{N\sqrt{\sigma_s^2(i) + \frac{\sigma_n^2}{E_b}}}\right), \quad i \in U_2 \tag{2.17}$$

$$P_e(x_{p,i}) = Q\left(\frac{\sum_{k=0}^{N-1}\mu_k - \Re(\Psi_{i,i+L-N}^{2,m,\nu})}{N\sqrt{\sigma_s^2(i) + \frac{\sigma_n^2}{E_b}}}\right), \quad i \in U_3 \tag{2.18}$$

$$P_e(x_{p,i}) = Q\left(\frac{\sum_{k=0}^{N-1}\mu_k}{N\sqrt{\sigma_s^2(i) + \frac{\sigma_n^2}{E_b}}}\right), \quad i \in (U - U_2 \cup U_3). \tag{2.19}$$

When the timing point is to the left of the exact timing point, i.e., $m < 0$, the interference comes only from the previous block, and the demodulated block is given by

$$\hat{\mathbf{x}}(p) = \mathbf{F^H C \Lambda F x}^m(p) + \mathbf{F^H C F}\tilde{\mathbf{h}}_2^\nu \tilde{\mathbf{x}}_2^\nu(p) + \mathbf{F^H C F n} \tag{2.20}$$

where $\nu > L - N_g$, resulting in more multipath components from the previous block. The variance of the interference can be written as

$$\sigma_s^2(i) = \sum_{\substack{n\in U_4\\ n\neq i}} |S_n(i) - \Psi_{i,n-N+L-m}^{3,\nu}|^2 + \sum_{\substack{n\notin U_4\\ n\neq i}}^{n\in U} |S_n(i)|^2 + \sum_{n=0}^{\nu-1} |\Psi_{i,n}^{3,\nu}|^2 \tag{2.21}$$

where $\mathbf{\Psi}^{3,\nu} = \mathbf{F^H C F}\tilde{\mathbf{h}}_2^\nu$ and U_4 is defined as $[N - N_g - \nu, N - N_g]$. Thus, the ith

symbol error probability can be derived as

$$P_e(x_{p,i}) = Q\left(\frac{\sum_{k=0}^{N-1}\mu_k - \Re(\Psi_{i,i-N+L-m}^{3,\nu}}{N\sqrt{\sigma_s^2(i)+\frac{\sigma_n^2}{E_b}}}\right), \quad i \in U_4 \tag{2.22}$$

$$P_e(x_{p,i}) = Q\left(\frac{\sum_{k=0}^{N-1}\mu_k}{N\sqrt{\sigma_s^2(i)+\frac{\sigma_n^2}{E_b}}}\right), \quad i \in U \text{ and } i \notin U_4. \tag{2.23}$$

2.3.3 The Impact of Timing Error on Channel Estimation

In the literature, CE and synchronization often employ separate preamble blocks instead of the single preamble proposed in Section 2.4, for example in the Multi-band OFDM standard proposal [1]. Conventional preambles usually begin with synchronization blocks, followed by CE pilot blocks and then data symbols. This subsection considers timing error induced degradation in CE with conventional preamble blocks. Note that channel estimation in SC-FDE is identical to OFDM. Consider the least square CE with one pilot block $\mathbf{p}_t$. Under a timing error of m (> 0) samples, the frequency domain received pilot block can be written as

$$\mathbf{P}_r(m) = \Lambda\mathbf{\Omega}(m)\mathbf{P}_t + \mathbf{F}\tilde{\mathbf{h}}_1^m\tilde{\mathbf{p}}_t^m + \tilde{\mathbf{n}}, \tag{2.24}$$

where $\mathbf{\Omega}$ and $\mathbf{P}_t$ are diagonal matrix with elements $e^{j2\pi im/N}$ and the frequency domain pilot block respectively, $\tilde{\mathbf{p}}_t^m$ is defined as $[0, ..., 0, x_{0,-N_g} - p_{t,0},\ x_{0,-N_g+1} - p_{t,1},\ ...,\ x_{0,-N_g+m} - p_{t,m-1}]_{N\times 1}^T$ where $\mathbf{x}_0$ is the data block following the pilot block. Define $\mathbf{\Phi}_{(N\times m)}^+$ as the last m columns of the matrix $\mathbf{F}\tilde{\mathbf{h}}_1^m$, and its (k,n)th element is given by

$$\Phi_{k,n}^+(m) = \sum_{l=0}^{m-n} h_l e^{-j2\pi k(l+n-m)/N}, \quad m > 0. \tag{2.25}$$

Then the kth sub-carrier of $\mathbf{P}_r$ can be written as

$$P_r(k|m) = H_k e^{j2\pi km/N}P_t(k) + \sum_{n=0}^{m-1}\Phi_{k,n}^+(x_{0,n} - p_{t,n}) + \tilde{n}_k. \tag{2.26}$$

The estimated channel at the kth sub-carrier is $\hat{H}_k = \frac{P_r(k|m)}{P_t(k)}$. The signal-to-interference-ratio (SIR) on the kth sub-carrier can be written as

$$\begin{aligned} SIR_k &= \frac{\mathbb{E}[|H_k P_t(k)|^2]}{\mathbb{E}[|\sum_{n=0}^{m-1} \Phi_{k,n}^{+}(x_{0,n} - p_{t,n})|^2]} \\ &= \frac{|H_k|^2 |P_t(k)|^2}{\sum_{n=0}^{m-1} |\Phi_{k,n}^{+}|^2 E_s + |\sum_{n=0}^{m-1} \Phi_{k,n}^{+} p_{t,n}|^2} \end{aligned} \tag{2.27}$$

where E_s is the average energy of the data symbols. For $m < 0$, since the length of the channel delay spread spans L sampling periods, only $q = \max(L-(N_g+m), 0)$ block symbols are corrupted by the multipath components from the previous block. Assuming that there is a synchronization block preceding the CE block in a non-joint scheme and with the same transmitting power, it can be derived that the SIR is given by

$$SIR_k = \begin{cases} \infty, & q = 0 \\ \frac{|H_k|^2 |P_t(k)|^2}{\sum_{n=0}^{q-1} |\Phi_{k,n}^{-}|^2 E_s + |\sum_{n=0}^{q-1} \Phi_{k,n}^{-} p_{t,\rho+n}|^2}, & q > 0 \end{cases} \tag{2.28}$$

for $m < 0$ where $\Phi_{k,n}^{-} = \sum_{i=0}^{n} h_{L-n+i} e^{-j2\pi ik/N}$ and $\rho = N - N_g - q$. It can be seen that timing error also affects the CE accuracy and will further degrade the system performance derived in Subsections 2.3.1 and 2.3.2 when the conventional preamble pattern is used.

2.4 The Proposed Joint Timing and Channel Estimation Scheme

Timing within the IBI-free region does not cause extra interference to the detection. However, in UWB systems, the IBI-free interval given a short CP is often very small or even zero, depending on channel realizations. Thus, it is necessary to locate the first significant arrival path of the transmitted signal block, which is defined as the exact timing point in the following. With the definition of the exact timing point, we define the timing error as the offset between the established timing point and the

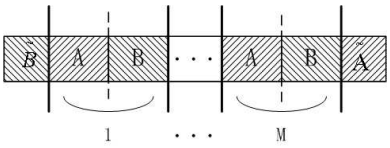

Figure 2.1: The proposed preamble structure, $\tilde{B}$: cyclic prefix; $\tilde{A}$: cyclic suffix

exact timing point.

2.4.1 Preamble Structure and Coarse Timing

In dense multipath channels, coarse timing obtained by evaluating a metric function cannot provide sufficient accuracy, since coarse timing often falls far away from the exact timing due to the large channel dispersion. We propose to use the estimated channel information to fine tune the timing position. A new preamble structure is designed to have the periodical property for acquisition and cyclic structure for accurate CE whose result will be used in the subsequent timing adjustment and frequency domain equalization. As shown in Fig. 2.1, in addition to the CP, a cyclic suffix is padded after the preamble body. Note that the suffix is used only for the preamble, and data blocks have CP only as in conventional OFDM. In the proposed preamble shown in Fig. 2.1, A and B represent the first half and the second half of one block generated by

$$p_t(n) = \frac{1}{\sqrt{N}} \sum_{k=0}^{N-1} P_t(k) e^{j2\pi nk/N} \quad 0 \le k \le N-1 \tag{2.29}$$

where $P_t(k)$ is a random ± 1 sequence in frequency domain (FD), referred to as FD pilot block, which results in flat amplitude in FD for good CE performance. The [A B] structure can be repeated M times and finally a prefix and a suffix are added to have [$\tilde{\text{B}}$ A B ... B $\tilde{\text{A}}$], where $\tilde{\text{A}}$ and $\tilde{\text{B}}$ are the first N_x samples of A and last N_x samples of B respectively. The length of the prefix and suffix denoted by N_x needs to be larger than the maximum coarse timing error, and $2N_x$ should be larger than the channel length L to avoid IBI. By repeating [A B] we can achieve noise averaging for more accurate CE, and the adjacent [A B] blocks serve as cyclic extension. For the case of $M = 1$, the whole preamble becomes [$\tilde{\text{B}}$ A B $\tilde{\text{A}}$], thus the synchronization and CE overhead is $2N_x + N$, smaller than the preamble pattern proposed in [1] where the overhead is $2(N + N_g)$. Following the conventional auto-correlation based metric

function, we define our timing metric function as

$$M(d) = \frac{2|C(d)|}{R(d)} = \frac{2\left|\sum_{i=0}^{2N_x+(M-1)N-1} r_{d+i}^* r_{d+N+i}\right|}{\sum_{i=0}^{2N_x+(M-1)N-1} (|r_{d+i}|^2 + |r_{d+N+i}|^2)} \tag{2.30}$$

and coarse timing is established by finding the maximum of (2.30) as given by $\theta_c = \max_d M(d)$. Note the range of d to look for the maximal can be defined as $[\theta_s, \theta_s + Q]$, where θ_s is the point where the metric function first exceeds the preset threshold and Q can be set as N. Simply speaking, the metric calculator activates the maximization procedure once the arrival of the signal is sensed. To reduce the computation complexity at the implementation stage, the metric can be implemented in an iterative manner similar to [56] as

$$C(d+1) = C(d) - r_d^* r_{d+N} + r_{d+2N_x+(M-1)N}^* \; r_{d+2N_x+MN} \tag{2.31}$$

and

$$R(d+1) = R(d) - |r_d|^2 - |r_{d+N}|^2 + |r_{d+2N_x+(M-1)N}|^2 + |r_{d+2N_x+MN}|^2, \tag{2.32}$$

which implies a sliding window implementation. For every received sample, only 3 new multiplication and 6 add operations are needed to compute the iterative timing metric. This sliding window correlator saves substantial complexity compared to the metrics proposed in [12] and [15] which need to perform the whole correlation for every sample.

2.4.2 Channel Estimation and Timing Adjustment

In this step, CE is carried out using the same preamble after the initial acquisition and the estimation accuracy is not affected by the timing error. Denote the coarse timing error (CTE) by ε_c which is in the number of symbols. Consider the low complexity least square (LS) CE. If $M = 1$, the frequency domain CE is given by $\hat{H}(k) = \frac{P_r(k)}{P_t(k)}$, where $P_r(k)$ and $P_t(k)$ denote the received and transmitted frequency domain training symbol at the kth subchannel respectively. The estimation can be

improved by employing the repetitive [A B] structure to reduce the noise effect. In addition, the cyclic structure given by $\tilde{\mathrm{B}}$ and $\tilde{\mathrm{A}}$ provides IBI-free CE as long as the coarse timing error $|\varepsilon_c| < N_x$. In this case, the estimated channel is given by

$$\hat{H}_k = H_k e^{j2\pi\varepsilon_c k/N} + W_k \tag{2.33}$$

where W_k is the Gaussian noise in frequency domain.

Since the proposed preamble has a cyclic structure, the estimated frequency domain channel using this preamble does not suffer from the coarse timing error induced IBI that is usually present in conventional schemes. The impact of coarse timing error on the CE with conventional preambles will be shown in Section 2.3.3. Performing inverse FFT (IFFT) on $\hat{H}_k$, the estimated CIR $\hat{\mathbf{g}}$ is the CIR $\mathbf{h}$ cyclicly shifted by the timing error of ε_c samples, plus the Gaussian noise. The CTE ε_c can be estimated from $\hat{\mathbf{g}}$ and then used to adjust timing for the subsequent data blocks, which has no cyclic property to use as the preamble does. The coarse timing error estimation is obtained by an energy jump detector written as

$$\hat{\varepsilon}_c = \begin{cases} -\hat{\tau}_0 & \text{if } 0 \le \hat{\tau}_0 < \frac{N}{2} \\ N_p - \hat{\tau}_0 & \text{if } \frac{N}{2} \le \hat{\tau}_0 < N \end{cases} \tag{2.34}$$

where

$$\hat{\tau}_0 = \max_i E(i) \quad 0 \le i \le N-1, \tag{2.35}$$

$$E(i) = \begin{cases} 0 & \text{if } |\hat{g}_i| < \eta|\hat{g}_{\max}| \\ e_r(i) - e_l(i) & \text{if } |\hat{g}_i| \ge \eta|\hat{g}_{\max}| \end{cases} \tag{2.36}$$

and

$$\begin{aligned} e_r(i) &= \sum_{k=0}^{\xi-1} |\hat{g}_{(i+k) \ mod \ N}|^2 \\ e_l(i) &= \sum_{k=0}^{\xi-1} |\hat{g}_{(i-k-1) \ mod \ N}|^2 \end{aligned} \tag{2.37}$$

where $|\hat{g}_{\max}|$ is the maximum absolute value of the elements in $\hat{\mathbf{g}}$ and η is a preset threshold whose determination will be given in Section 2.5.

Fig. 2.2 is an example of $\hat{\mathbf{g}}$ obtained by simulation using the CM2 channel model. In this example, the block length is $N = 128$. Due to the coarse timing error, the

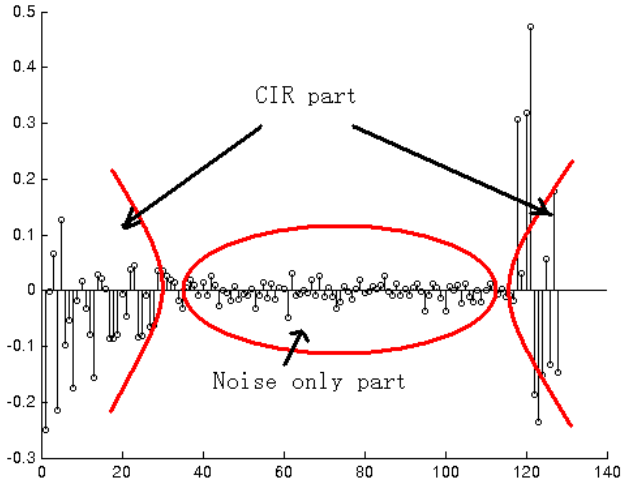

Figure 2.2: An example of CE $\hat{\mathbf{g}}$, obtained from IFFT of $\hat{\mathbf{H}}$, $N = 128$, and $E_b/N_0 = 10$ dB.

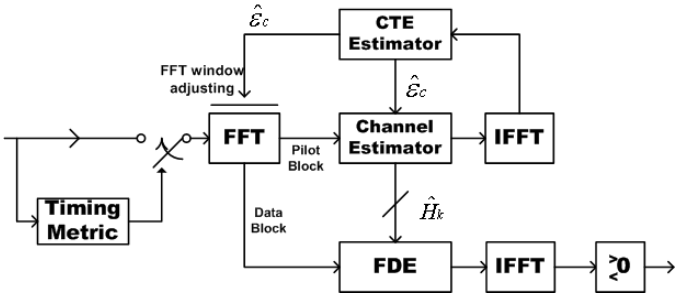

Figure 2.3: Block diagram of the proposed timing synchronizer for SC-FDE UWB systems.

actual CIR is cyclic shifted, and thus some strong taps at the end of the vector $\hat{\mathbf{g}}$ are observed which correspond to the channel taps shifted. The first significant tap is near the end of the vector $\hat{\mathbf{g}}$, meaning that the current timing is several samples to the right of the exact timing point. The first tap of $\hat{\mathbf{g}}$ can be determined by (2.34)-(2.37) and explained as follows. Once an estimated channel tap $\hat{g}(i)$ is above a normalized threshold $\eta\hat{g}_{\max}$, the energy of ξ channel taps on the right side of i represented by $e_r(i)$ is compared to the energy of ξ channel taps on the left side of i represented by $e_l(i)$, to evaluate the energy jump on the point i. The first channel tap τ_0 is detected at the position where the energy jump is the largest. Having a window of ξ channel taps is to reduce the occurrence of mistakenly choosing a noise tap as the first tap. Since before the first tap there are only noise, whereas $e_r(i)$ contains energy from the channel taps and noise, $e_r(i) - e_l(i)$ cancels the noise and can well detect the jump point from the noise only region to the starting of the CIR $\hat{\mathbf{g}}$. The determination of parameters η and ξ will be discussed in Section 2.5. Upon obtaining the coarse timing error, the synchronizer can adjust timing position by $\hat{\varepsilon}_c$ samples, and at the same time, the CE result should also be modified corresponding to the timing adjustment by $\hat{H}'_k = \hat{H}_k e^{-j2\pi\hat{\varepsilon}_c k/N}$. Note that in (2.34), we determine the timing error to the left or right of the exact timing by the search result being in the first half or the second half of the CIR. Therefore, the fine timing can handle at most $\frac{N}{2}$ coarse timing error, which is usually more than sufficient.

The block diagram of the entire timing synchronizer for SC-FDE UWB systems is shown in Fig. 2.3. When the timing metric module detects the coarse timing point, it passes the received signal to the subsequent modules. The LS estimator estimates FD channel response $\hat{H}_k$ based on the coarse FFT window, and then the coarse timing error is estimated by the CTE estimator based on the coarse CE result. Finally the

CTE estimation is used to adjust the FFT window position and the FDE channel coefficients.

2.4.3 Performance of Fine Timing Adjustment

The performance of the fine timing adjustment is solely dependent on the accuracy of the first tap search, given a set of estimated channel taps. The conventional energy detector [14, 27, 31] usually measures the energy in a window of channel taps and takes the starting point of the maximal measurement window as the first tap position. However, this method requires the knowledge of the exact channel length, which is usually difficult to estimate accurately in UWB channels. Setting the window too long may lead to an early timing while having the window too short may lead to a late timing. The proposed energy jump detector overcomes this drawback of the conventional energy detector. Its window length does not need to equal the exact channel length and usually a window length less than the channel length is sufficient. With a moderate window length, the energy jump detector can achieve accurate timing. Note that another energy jump detector has been proposed in [30], where the metric is in an energy ratio form while that of the proposed detector is in a subtraction form. The detector in [30] is able to deal with the more realistic channel with continuously varying delays at the cost of higher complexity. That is, CIR is estimated more frequently in [30]. In the following, we study the timing error probability of the proposed energy jump detector in comparison with that of the conventional energy detector. The energy jump factor at the exact timing point d can be written as

$$\begin{aligned} E(d) &= \sum_{k=0}^{\xi-1} |\hat{g}_{(d+k) \ mod \ N}|^2 - \sum_{k=0}^{\xi-1} |\hat{g}_{(d-k-1) \ mod \ N}|^2 \\ &= \sum_{k=0}^{\xi-1} (|h_k + w_{(d+k) \ mod \ N}|^2 - |w_{(d-k-1) \ mod \ N}|^2) \end{aligned} \tag{2.38}$$

where w_k is the noise component of the kth element of the estimated CIR vector. We study the case where the window length is less than the channel length ($\xi < L$), usually resulting in late timing with the conventional energy detector. For the case of $\xi > L$, the analysis is similar.

Consider a late timing event of t samples where $t > 0$. For the conventional energy

detector, the error probability that a late timing of t samples occurs is given by

$$P_{ED}(t) = \Pr(\sum_{k=0}^{t-1} |h_k + w_{(d+k) \ mod \ N}|^2 < \sum_{k=0}^{t-1} |h_{\xi+k} + w_{(d+\xi+k) \ mod \ N}|^2). \tag{2.39}$$

Following [14], we consider the complex Gaussian channel taps with variances decaying along the index. Assume the small number of t adjacent channel taps on the right side of (2.39) have the same variance σ_1^2. Similarly, the t adjacent taps on the left side of (2.39) have approximately equal variance denoted by σ_2^2. Then both sides of (2.39) are scaled Chi-square distributed random variables (r.v.s) with $2t$ degrees of freedom and the component Gaussian's variance $\sigma_1^2 + \sigma_w^2$ and $\sigma_2^2 + \sigma_w^2$ respectively, where σ_w^2 is the variance of the noise component in the coarse CE result. Then the probability in (2.39) can be written as

$$P_{ED}(t) = \int_0^\infty f_l(x) \int_x^\infty f_r(y) dy dx \tag{2.40}$$

where $f_l(x)$ and $f_r(x)$ represent the probability density function (PDF) of the left side and right side of (2.39) respectively. The PDF of a scaled Chi-square r.v. of $2t$ degrees of freedom is $f(x) = \frac{1}{\sigma^{2t} 2^t \Gamma(t)} x^{t-1} e^{-x/2\sigma^2}$, where σ^2 is the component Gaussian's variance. Substituting the PDF of the Chi-square r.v. into (2.40), the error probability can be written as

$$\begin{aligned} P_{ED}(t) &= \frac{1}{\Gamma(t)} \sum_{k=0}^{t-1} \frac{1}{k!} \frac{(\frac{\sigma_1^2+\sigma_w^2}{\sigma_2^2+\sigma_w^2})^k}{(1+\frac{\sigma_1^2+\sigma_w^2}{\sigma_2^2+\sigma_w^2})^{t+k}} \Gamma(t+k) \\ &= \frac{1}{\Gamma(t)} \sum_{k=0}^{t-1} \frac{1}{k!} \frac{\gamma_0^k}{(1+\gamma_0)^{t+k}} \Gamma(t+k) \end{aligned} \tag{2.41}$$

where $\Gamma(\cdot)$ is the Gamma function with $\Gamma(k) = (k-1)!$ and $\gamma_0 = \frac{\sigma_1^2+\sigma_w^2}{\sigma_2^2+\sigma_w^2}$. Indeed γ_0 represents the energy ratio of the estimated channel tap (including noise) at the actual first channel tap position over that at the $\xi + 1$ actual tap position. This definition takes into account the power decaying over time.

For the proposed energy jump detector, the event of timing error of t samples

happens when $E(d) < E(d+t)$. Similar to (2.38),

$$\begin{aligned} E(d+t) &= \sum_{k=0}^{\xi-1} |\hat{g}_{(d+t+k) \ mod \ N}|^2 - \sum_{k=0}^{\xi-1} |\hat{g}_{(d+t-k-1) \ mod \ N}|^2 \\ &= \sum_{k=0}^{\xi-1} |h_{k+t} + w_{(d+k+t) \ mod \ N}|^2 \\ &\quad - \sum_{k=0}^{\xi-1-t} |w_{(d-k-1) \ mod \ N}|^2 - \sum_{k=0}^{t-1} |h_k + w_{(d+k) \ mod \ N}|^2. \end{aligned} \tag{2.42}$$

Then the probability of the event for the proposed energy jump detector can be written as [1]

$$\begin{aligned} P_{EJ}(t) &= \Pr(E(d) < E(d+t)) \\ &= \Pr(2 \sum_{k=0}^{t-1} |h_k + w_{(d+k) \ mod \ N}|^2 \\ &< \sum_{k=0}^{t-1} (|h_{\xi+k} + w_{(d+\xi+k)}|^2 + |w_{(d-\xi+k) \ mod \ N}|^2)). \end{aligned} \tag{2.43}$$

The left side of (2.43) is a scaled Chi-Square r.v. with $2t$ degrees of freedom and the component Gaussian's variance $2(\sigma_1^2 + \sigma_w^2)$, while the right side of (2.43) is a sum of two scaled Chi-Square random variables with $2t$ degrees of freedom and the component Gaussian's variances $\sigma_2^2 + \sigma_w^2$ and σ_w^2. Then the timing error probability can be written as

$$P_{EJ}(t) = \int_0^\infty f_l(x) \int_x^\infty f_r(y) dy dx = \int_0^\infty f_l(x) \Upsilon(x) dx \tag{2.44}$$

where $\Upsilon(x) = \int_x^\infty f_r(y) dy$. According to [51], $\Upsilon(x)$ can be written as

$$\Upsilon(x) = \beta_1^t \beta_2^t \sum_{k=1}^{2} \sum_{l=1}^{t} \frac{\Theta_{k,l}(-\beta_k)}{(l-1)! \beta_k^{t-l+1}} \sum_{i=0}^{t-l} \frac{(\beta_k x)^i e^{-\beta_k x}}{i!} \tag{2.45}$$

[1] For the case of early timing, the corresponding probability can be written as $\Pr(2 \sum_{k=0}^{|t|-1} |w_{(d-k-1) \ mod \ N}|^2 > \sum_{k=0}^{|t|-1} (|h_{\xi-|t|+k} + w_{(d+\xi-|t|+k)}|^2 + |w_{(d-\xi-k) \ mod \ N}|^2))$ with $t < 0$. The subsequent derivation is similar to the case of late timing.

where

$$\beta_1 \equiv \frac{1}{2(\sigma_2^2+\sigma_w^2)} \tag{2.46}$$

$$\beta_2 \equiv \frac{1}{2\sigma_w^2} \tag{2.47}$$

$$\Theta_{1,l}(x) \equiv (-1)^{l-1}\frac{(t+l-2)!}{(t-1)!(\beta_2-\beta_1)^{t+l-1}} \tag{2.48}$$

$$\Theta_{2,l}(x) \equiv (-1)^{l-1}\frac{(t+l-2)!}{(t-1)!(\beta_1-\beta_2)^{t+l-1}}. \tag{2.49}$$

Defining $\beta_0 = \frac{1}{4(\sigma_1^2+\sigma_w^2)}$, and substituting (2.45) and the PDF of the Chi-square r.v. into (2.44), we have

$$\begin{aligned}
P_{EJ}(t) =& \frac{\beta_0^t\beta_1^t\beta_2^t}{\Gamma(t)}\sum_{k=1}^{2}\sum_{l=1}^{t}\sum_{i=0}^{t-l} \\
& \frac{\Theta_{k,l}(-\beta_k)\beta_k^{i+l-t-1}}{i!(l-1)!}\int_0^\infty x^{i+t-1}e^{-(\beta_0+\beta_k)x}dx \\
=& \frac{\beta_0^t\beta_1^t\beta_2^t}{\Gamma(t)}\sum_{k=1}^{2}\sum_{l=1}^{t}\sum_{i=0}^{t-l}\frac{\Theta_{k,l}(-\beta_k)\beta_k^{i+l-t-1}\Gamma(i+t)}{i!(l-1)!(\beta_0+\beta_k)^{i+t}} \\
=& \frac{1}{\Gamma(t)}\sum_{l=1}^{t}\sum_{i=0}^{t-l}\frac{(-1)^{l-1}(t+l-2)!\Gamma(i+t)}{(t-1)!i!(l-1)!} \\
& \left(\frac{\gamma_1^{i+l-1}\gamma_2^t}{(\gamma_2-\gamma_1)^{t+l-1}(1+\gamma_1)^{i+t}}\right. \\
& \left. + \frac{\gamma_2^{i+l-1}\gamma_1^t}{(\gamma_1-\gamma_2)^{t+l-1}(1+\gamma_2)^{i+t}}\right)
\end{aligned} \tag{2.50}$$

where $\gamma_1 = 2\frac{\sigma_1^2+\sigma_w^2}{\sigma_2^2+\sigma_w^2}$ and $\gamma_2 = 2\frac{\sigma_1^2+\sigma_w^2}{\sigma_w^2}$. The energy ratio defined by γ_0, γ_1 and γ_2 are related to the signal-to-noise-ratio (SNR) and the UWB channel statistics, and they determine the performance of the estimator. Fig. 2.4 shows the timing error probability comparison of the proposed energy jump detector and the conventional energy detector with specific energy ratios. In the proposed energy jump detector, the first channel tap searching algorithm has a slightly higher computation complexity than the conventional energy detector. It requires to calculate the energy of two windows and perform a subtraction while the conventional detector only computes one. However, the window in the energy jump detector is usually shorter than the channel-long window of the conventional energy detector.

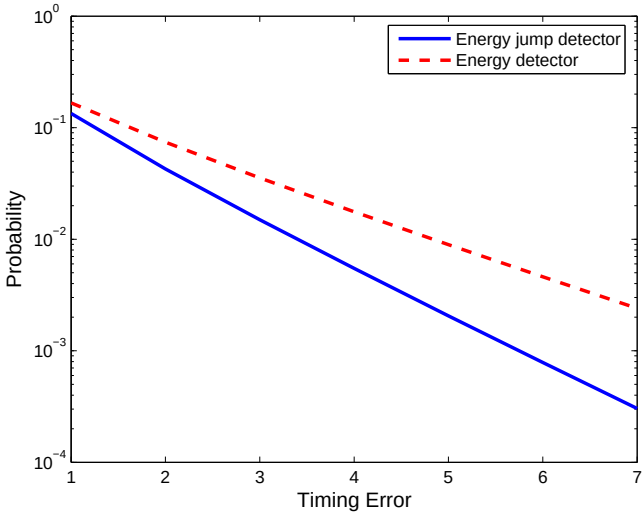

Figure 2.4: The timing error probability of the first channel tap search with $\gamma_0 = 5$, $\gamma_1 = 10$ and $\gamma_2 = 20$.

2.5 Simulation Results and Discussion

MB-OFDM and SC-FDE block transmission schemes are for high-rate UWB systems. Thus, in the simulation, we set the block length $N = 128$, CP length $N_g = 32$, following [1]. This block length is determined based on practical implementation complexity. However, the resulting CP does not guarantee to be always longer than a UWB channel. The UWB channels simulated follow CM1-CM4 models proposed by the IEEE 802.15.3a Working Group [1]. A root raised cosine (RRC) pulse with a roll-off factor of 0.5 and span of $[-3T_s, 3T_s]$ is used. Since the focus of this chapter is timing synchronization, perfect carrier frequency synchronization is assumed in the simulation. The design parameters N_x and ξ are determined according to the channel statistics. Fig. 2.5(a) gives the coarse timing error statistics, which shows the empirical cumulative distribution function (CDF) of the coarse timing error at $\frac{E_b}{N_0} = 10$ dB in CM1-CM4 UWB channels. It can be seen that the coarse timing error is most severe in CM4 which is the most dispersive channel model, indicating that the performance of the auto-correlation based coarse timing estimator is highly dependent on the channel condition. The more dispersive the channel is, the larger the coarse timing error. According to Fig. 2.5(a) we set $N_x = 30$. The choice of design parameter ξ in the CTE estimator depends on the channel length statistics. If ξ is too small, the estimation error probability is higher; Otherwise, the computation complexity is higher. We choose ξ to be the average number of channel taps carrying 50% of the channel energy for different channel models. Fig. 2.5(b) shows the CDF of number of taps carrying 50% of the channel energy, using the channel sampling rate of 2 ns, and 1000 channel realizations for each channel model. It indicates that in CM4 ξ can be chosen as 30, in CM3 $\xi = 25$, while in CM1 and CM2 $\xi = 15$ and $\xi = 20$ respectively. The parameter η determines whether a tap should be considered as a valid channel tap for further examination and can be set conservatively at 0.1, since the proposed algorithm does not simply rely on the threshold η to determine the first tap. A slightly larger η can reduce more computation complexity.

First, the impact of timing error on SC-FDE system with MMSE equalization is simulated and compared with the theoretical result. Fig. 2.6 shows the BER performance in CM1 and CM2 channels with different positive timing errors, from which we can observe the match between the theory and the simulation.

Fig. 2.7 shows the occurrence of the BER floor even with perfect timing in severely dispersive channels where the dense multipath channel is sometimes longer than the

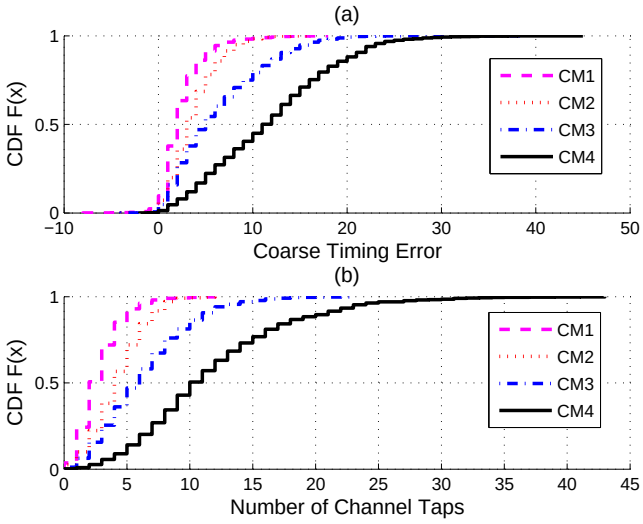

Figure 2.5: (a) The empirical CDF of coarse timing error, $M = 1$ and $E_b/N_0 = 10$ dB; (b) CDF of the number of channel taps carrying 50% of the channel energy, from 1000 channel realizations.

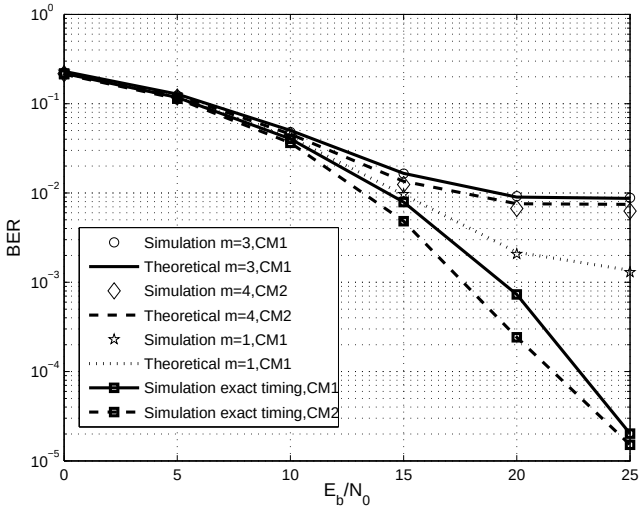

Figure 2.6: BER of SC-FDE with different timing error under short channel conditions.

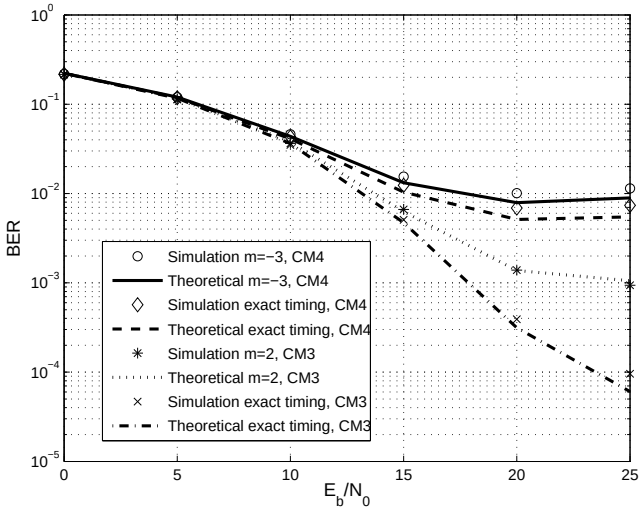

Figure 2.7: BER of SC-FDE with and without timing error in long UWB channels.

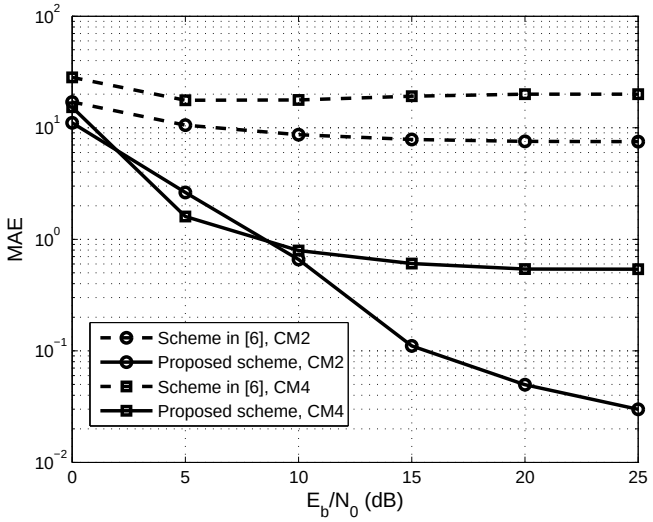

Figure 2.8: MAE performance of the proposed timing scheme and Minn's timing method in UWB systems.

designated CP length, especially in CM4 (severe error floor). At low SNRs, the noise and residual in-block ISI from MMSE equalization dominate the performance. Therefore, the performance for different timing offsets are almost the same. However, at high SNRs, the timing error induced extra in-block ISI and IBI dominate the performance. Therefore, error floor occurs when there is timing error. From Fig. 2.7, we can also see that in heavily dispersive channels, timing error at the left of the exact timing point degrades the performance, meaning no IBI-free region within the CP. Therefore, very precise timing scheme will be required in such channel conditions.

Timing synchronization is often evaluated in terms of mean absolute error (MAE). For each channel model, 1000 channel realizations are generated and in each channel realization, the timing algorithm is repeatedly tested for 100 times. The performance of the proposed timing scheme is compared with Minn's algorithm [27] with $N = 128$, 4 identical parts, and sign pattern of [- + - -] in Figs. 2.8 and 2.9 for the reason that both timing methods are CE aided. The MAE performance shows that the proposed CE aided timing method outperforms conventional OFDM timing method significantly in UWB channels. The timing performance improvement of the proposed method over the conventional method comes from the more accurate coarse CE and the first tap searching algorithm. The proposed cyclic extended preamble structure can provide an IBI-free coarse stage CE regardless where the coarse timing position is. For the conventional method in [27], the preamble block is divided into 4 parts with

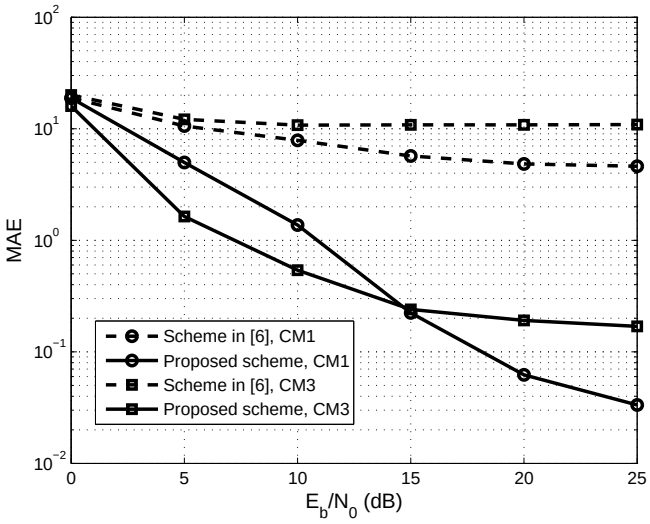

Figure 2.9: MAE performance of the proposed timing scheme and Minn's timing method in UWB systems.

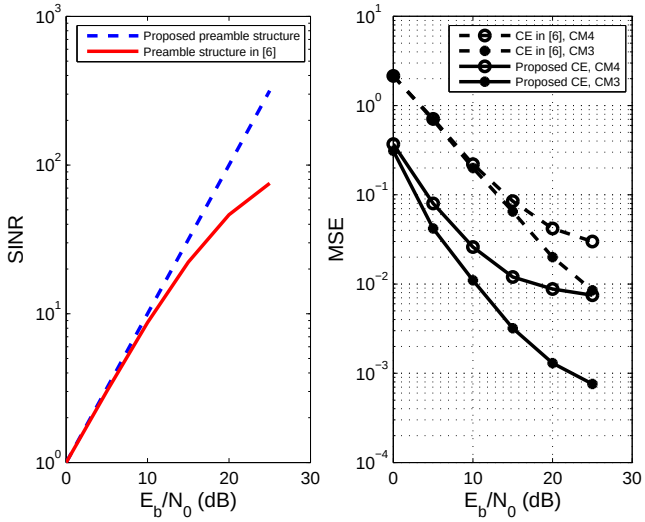

Figure 2.10: (a) Average SINR of the coarse CE in CM1; (b) MSE performance of the channel estimator, with proposed preamble pattern and with the conventional preamble pattern.

each one having a small length of $\kappa = N/4$. However, in the extremely dispersive UWB channel environment, the coarse stage CE may suffer severe IBI due to the coarse timing offset and the excessive channel length. For example, when the coarse timing position is on the right side of the true position, the coarse CE in [27] will include $\zeta = \varepsilon_c + L - \kappa$ samples of IBI. According to (2.27) in Section 2.3, the SIR of the coarse CE is given by $SIR_k = \frac{|H_k|^2 |P_t(k)|^2}{\sum_{n=0}^{\zeta-1} |\Phi_{k,n}^{+}(\zeta)|^2 E_s + |\sum_{n=0}^{\zeta-1} \Phi_{k,n}^{+}(\zeta) p_{t,n}|^2}$, where $\Phi_{k,n}^{+}(\zeta)$ is defined as in (2.25). The SINR results of the coarse CE obtained from simulation are plotted in Fig. 2.10(a) for the proposed scheme and that of [27] in CM1. In addition, the MSE performance of the channel estimator in CM3 and CM4 are compared in Fig. 2.10(b). Furthermore, the first tap searching algorithm in [27] is a conventional energy detector, whose performance is inferior to the proposed energy jump detector as described in Section 2.4.3.

Fig. 2.11 shows the timing performance with different design parameters, such as the number of repeated [A B] (M) and ξ in the first tap search algorithm. It can be seen from Fig. 2.11 that in short channel conditions such as CM1 or CM2, increasing ξ does not improve performance significantly, whereas increasing M from 1 to 2 can provide 3 dB gain in CE due to noise averaging (though not shown here), thus leading to better timing performance. However, increasing M in long channel conditions such as CM3 and CM4 can not improve the performance at high SNRs, whereas increasing ξ is more effective.

2.6 Summary

In this chapter, a joint timing and CE scheme that employs a unique preamble design and CIR assisted fine timing have been presented for UWB block transmission systems. The proposed preamble saves the overhead and has the cyclic property which results in CE and fine timing estimation robust to coarse timing error. Based on the CE result, a novel algorithm for estimating the coarse timing error has been developed for UWB channels. Furthermore, the impact of symbol level timing error on an SC-FDE system has been analyzed. Simulation results have shown that the proposed scheme yields accurate timing and superior channel estimation performance in UWB channels.

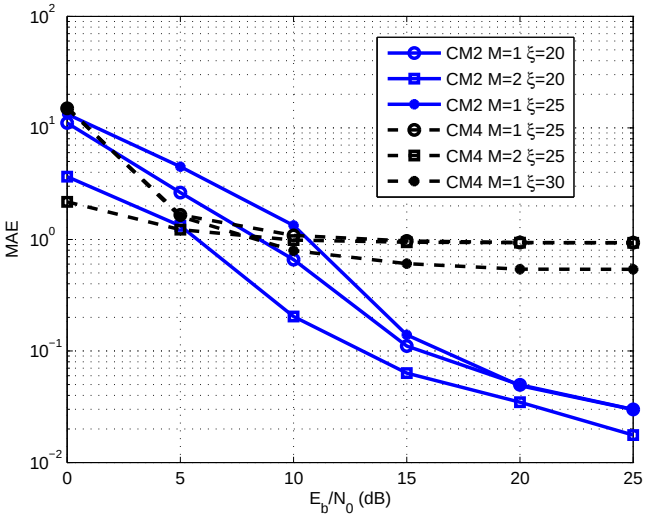

Figure 2.11: MAE performance of the proposed scheme with different parameters.

Chapter 3

Two Step Multiple CFO Mitigation Scheme in OFDM Based AF Cooperative Communications

From this chapter on, the research work will be focused on the synchronization issues in cooperative communication systems. Therefore, an overview on cooperative communication systems will be presented at the beginning of this chapter. Synchronization issues including both timing and frequency synchronization will be studied in Chapters 3, 4 and 5.

3.1 Overview on Cooperative Communications

In wireless networks, relays have been traditionally used to extend the range of communication systems. However, in recent years, other applications of relay communications have emerged. One such emerging application is to assist in the communication between the source and destination via some cooperation protocol to exploit cooperative diversity. By controlling medium access between source and relays coupled with the appropriate modulation or coding in such cooperative schemes, it has been found that the capacity of the system can be improved. In multi-user systems, different users can also act as cooperative partners or relays to share resources and assist each other in information transmission, thereby creating a cooperative network. Besides the one way traffic, there is two way relay network (TWRN) enabling the exchange of information between multiple users through relay(s). In such cases, by exploiting

the knowledge of one's own transmitted signal, the throughput of these systems can be drastically increased.

The basic ideas behind cooperative communication can be traced back to the groundbreaking work of Cover and El Gamal [55] on the information theoretic properties of the relay channel. The new frontier in research is now in cooperative communication which is the main terminology for cooperation among transceivers in a multiple users scenario in order to improve the systems overall capacity and coverage. This includes a family of configurations in which the information can be shared among transmitters and relayed to reach final destination which is one or more users. Different from conventional point-to-point communications, cooperative communications and networking allows different users or nodes in a wireless network to share resources to create collaboration through distributed transmission/processing, in which each user's information is sent out not only by the user, but also by collaborating users. Cooperative communications and networking is a new communication paradigm promising significant capacity and multiplexing gain increase in wireless networks. It realizes a new form of space diversity to combat the effects of severe fading that has been termed cooperative diversity, and it is also helpful in reducing the complexity of routing problems and realizing seamless networking. With the large benefits to be reaped from employing cooperative and relay techniques, several standardization groups, such as IEEE 802.16 and IEEE 802.11, have started standardization processes to include such technologies into their prevailing standards. These efforts will no doubt attract even more interest from the academia and industry, advancing cooperative and relay technologies even further in the coming years.

In this chapter, the multiple CFO compensation problem in an OFDM based cooperative system will be studied. The rest of the chapter is organized as follows. Section 3.2 introduces the motivation and related work. Section 3.3 presents the signal model for an ideal transmission without CFO. Section 3.4 formulates the signal model with CFO and proposes methods to mitigate the interference. The performance of the proposed schemes is evaluated through simulation in Section 3.5 and finally Section 3.6 summaries the chapter.

3.2 Introduction

Cooperation among wireless nodes can provide throughput enhancement, reliability improvement, and coverage extension for communication systems [34, 4]. Meanwhile,

orthogonal frequency division multiplexing (OFDM) is widely adopted for broadband communications because of its superb capability to combat frequency selective fading in wideband channels. OFDM also has relaxed timing requirement because perfect timing for OFDM systems is achieved within the inter-block interference (IBI) free region of cyclic prefix (CP), instead of only at an exact timing point. This can be a big advantage in a cooperative system where minor timing misalignments caused by the different propagation delays of the distributed nodes are unavoidable. Therefore, cooperative OFDM has gained significant attention recently when combined with distributed space time block coding (STBC) [22, 45, 73, 5, 26] or distributed space frequency coding (DSFC) [65, 37]. In particular, correctly-decode-and-forward (C-DF) is studied in [45, 73], where the relays only forward correctly decoded frames verified by the cyclic redundancy check (CRC) sequence. A series of algorithms covering various aspects of cooperative OFDM physical layer design are proposed in [45] with single relay C-DF, including frame structure, space-time design, synchronization, channel estimation and data detection. However, the C-DF scheme has a low forwarding probability when the source to relay link is poor. In [73], a two relay scenario without direct link is studied, and the space-time signaling considered is the same as that in [45], both adopting Alamouti space time code (STC) in a distributed manner. In [22], an amplify-and-forward (AF) with demodulation but no decoding at the relay combined with distributed Alamouti STC is proposed, and the optimal power allocation between the relay and source is investigated. Equalization methods for various distributed STBC schemes are analyzed in [26] for AF relaying, including distributed time-reversal (TR) STBC, single carrier with frequency domain equalization (SC-FDE) type distributed STBC and OFDM type distributed STBC.

Multiple carrier frequency offset (CFO) problem is an intrinsic problem in cooperative networks, especially in cooperative OFDM systems which are highly sensitive to CFO. The presence of multiple CFOs in the cooperative system causes significant performance degradation and hence erases the performance gain obtained through cooperative diversity. The estimation of multiple CFOs in cooperative systems can be found in [23, 25]. A coding approach is proposed to combat the multiple CFO problem of cooperative OFDM in [29], where a flat fading channel is assumed. The multiple CFO problem with delay diversity transmission in flat fading channels has been considered in [57], where a minimum mean square error decision feedback equalizer (MMSE-DFE) has been proposed to deal with the problem. The same problem has been studied with OFDM signaling in [44], where a linear equalizer has been

proposed. However, the flat fading channel is also assumed, while frequency selective channel has to be considered in broadband communications. The CFO mitigation problem in cooperative OFDM under frequency selective channels has been studied in [61, 60, 74, 72, 47]. The redundancy of cyclic prefix (CP) has been exploited in [61, 60] to address the multiple CFO problem, but distributed coding is not considered. To exploit the full diversity, distributed coding has to be applied. Therefore, it is more realistic to consider the multiple CFO problem with the consideration of coding schemes. Interference mitigation methods for STBC DF cooperative OFDM signals with multiple CFOs can be found in [74, 72, 47], and those for distributed space frequency block coding (SFBC) DF cooperative OFDM signals with multiple CFOs can be found in [16, 21, 18]. More specifically, a sub-matrix zero forcing (ZF) method is used in [74] to remove the inter-carrier interference (ICI) and IBI in the frequency domain (FD). An iterative method is proposed to cope with the multiple CFO problem in [72], where iterative decoding is used to eliminate ICI. On the other hand, the authors in [47] propose to first multiply the FD signal with a matrix to eliminate ICI and then perform iterative decoding to mitigate IBI. In [16] and [21], a system with generalized number of relays is considered with distributed space frequency coding. The problem is the high decoding complexity in frequency selective channels. Whereas in [18], simple decoding is employed for Alamouti style space frequency coding but assuming that the channel responses for adjacent subcarriers are the same, which is not the case in highly frequency selective channels. A multiple CFO compensation algorithm has been proposed for the spatial modulated OFDM system with multiple antennas in [8]. However, space time or space frequency coding is not considered, which is necessary in distributed antenna or cooperative transmission. An iterative reception mechanism has been proposed at the packet level with forward error correction (FEC) coding and Automatic Repeat-reQuest (ARQ) in [36].

We consider the Alamouti STBC coded AF cooperative OFDM transmission over frequency selective channels. At the destination receiver, instead of purely FD equalization, we present a joint time domain (TD) and FD mitigation method to mitigate the multiple CFO interference. Upon receiving the superimposed signal in the cooperative time slot (TS), we propose to first perform a partial TD compensation to recover the phase drift and part of the CFO terms. Then the remaining interference is mitigated in the FD. In this chapter, the TD partial compensation is designed to either remove IBI or remove ICI, while the preliminary results in [71] only considered the partial compensation for IBI removal. For each type of TD compensation, differ-

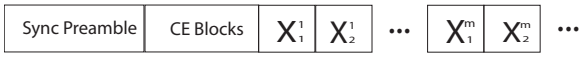

Figure 3.1: Source frame structure.

ent FD processing methods have been studied including sub-block equalization and iterative decoding. The contribution of this chapter is summarized as follows:

- While the existing methods for the multiple CFO mitigation deal with the FD received signal [74, 72, 47], we look at the problem from a different perspective, by performing joint TD and FD processing instead of pure FD interference mitigation. Relays will first perform TD partial compensation, followed by several different FD interference suppression methods, including FD equalization and iterative interference cancellation. We investigate and compare different combinations of TD partial compensation method and FD interference suppression method.

- In the stage of FD interference suppression, we propose reduced complexity methods for both FD equalization methods and FD iterative interference cancellation methods. Compared to the FD equalization methods in [74], the proposed joint TD and FD equalization method is able to reduce the FD equalization matrix to $N \times N$ instead of $2N \times 2N$. Compared to the FD iterative interference cancellation methods in [72, 47], the proposed joint TD and FD iterative interference cancellation achieves better performance with lower complexity.

3.3 Distributed STBC AF cooperative OFDM System without CFO

The considered relay system consists of one source, two relays and one destination, and the source is assumed to be unreachable to the destination. The cooperation protocol used is the two time slot relaying scheme. In particular, in the first time slot, the source broadcasts to the relays a frame of OFDM data blocks. The frame starts with a synchronization preamble, followed by the dedicated pilot blocks for channel estimation and then the data blocks as shown in Fig. 3.1. In the second TS, the two relays forward to the destination with distributed Alamouti STBC signaling.

Define the channel impulse response (CIR) of source-relays and relays-destination as $\mathbf{h}_j$ and $\mathbf{g}_j$ $(j = 1, 2)$. The corresponding frequency domain channel response

Table 3.1: Distributed STBC with AF cooperative OFDM in the second time slot

	OFDM Block 1	OFDM Block 2
Relay 1	$\lambda_1 \mathbf{Z}_{1,1}^m$	$\lambda_1 \mathbf{Z}_{1,2}^m$
Relay 2	$-\lambda_2 \mathbf{Z}_{2,2}^{m,*}$	$\lambda_2 \mathbf{Z}_{2,1}^{m,*}$

matrices are denoted by $\mathbf{H}_j$ and $\mathbf{G}_j$ $(j = 1, 2)$, where each one is a diagonal matrix of size $N \times N$ and has N subcarrier responses as its diagonal elements. The two relays perform Alamouti STBC every two OFDM blocks. We denote two consecutive OFDM blocks at the source by $\mathbf{X}_1^m$ and $\mathbf{X}_2^m$ $(1 \leq m \leq M)$, which will be STBC encoded by the two relays in the second TS. Therefore a frame consists of $2M$ OFDM blocks. Several assumptions are made for the simplicity of the analysis: 1) The receiver achieves perfect timing synchronization through the synchronization preamble; 2) The channel is static during each frame; 3) The perfect channel state information (CSI) is available at the receiver. In the first TS, the received ith OFDM block $(i = 1, 2)$ for the mth STBC codeword at the jth relay $(j = 1, 2)$ after FFT can be written as

$$\mathbf{Z}_{j,i}^m = \mathbf{H}_j \mathbf{X}_i^m + \boldsymbol{\nu}_{j,i}^m \tag{3.1}$$

where $\boldsymbol{\nu}_{j,i}^m$ is the noise vector of $\mathbf{X}_i^m$ at the jth relay. The distributed Alamouti STBC signaling with AF cooperative OFDM in the cooperative TS is illustrated in Table 3.1, where λ_1 and λ_2 are the power amplification factors at the two relays. Note that the conjugate operation in the STBC coding only takes place at relay 2, which not only conjugates the source symbols but also conjugates the FD channel responses of $\mathbf{H}_2$. In short, the operations at the relays include FFT, conjugation and block rearrangement.

At the destination, the received two consecutive blocks after FFT in the cooperative TS can be written as

$$\begin{aligned} \mathbf{Y}_1^m &= \lambda_1 \mathbf{G}_1 \mathbf{H}_1 \mathbf{X}_1^m - \lambda_2 \mathbf{G}_2 \mathbf{H}_2^* \mathbf{X}_2^{m,*} + \mathbf{W}_1^m \\ \mathbf{Y}_2^m &= \lambda_1 \mathbf{G}_1 \mathbf{H}_1 \mathbf{X}_2^m + \lambda_2 \mathbf{G}_2 \mathbf{H}_2^* \mathbf{X}_1^{m,*} + \mathbf{W}_2^m \end{aligned} \tag{3.2}$$

where $\mathbf{W}_1^m$ and $\mathbf{W}_2^m$ are the FD Gaussian noise, which includes the destination receiver noise and the forwarded noise from the relay. According to the STBC coding scheme, the equivalent channel of the source-relay-destination links can be written as $\boldsymbol{\Lambda}_1 = \lambda_1 \mathbf{G}_1 \mathbf{H}_1$ and $\boldsymbol{\Lambda}_2 = \lambda_2 \mathbf{G}_2 \mathbf{H}_2^*$. To simplify the analysis, we assume perfect

channel estimation at the destination receiver. In the cooperative TS, the destination receiver then decouples $\mathbf{X}_1^m$ and $\mathbf{X}_2^m$ as follows,

$$\begin{aligned}\bar{\mathbf{Y}}_1^m &= \mathbf{\Lambda}_1^* \mathbf{Y}_1^m + (\mathbf{\Lambda}_2^* \mathbf{Y}_2^m)^* \\ \bar{\mathbf{Y}}_2^m &= \mathbf{\Lambda}_1^* \mathbf{Y}_2^m - (\mathbf{\Lambda}_2^* \mathbf{Y}_1^m)^*\end{aligned} \tag{3.3}$$

where $\bar{\mathbf{Y}}_1^m$ and $\bar{\mathbf{Y}}_2^m$ are the decoupled signal components of $\mathbf{X}_1^m$ and $\mathbf{X}_2^m$ respectively. Substituting (3.2) into (3.3), we have

$$\bar{\mathbf{Y}}_i^m = \mathbf{\Xi} \mathbf{X}_i^m + \bar{\mathbf{W}}_i \quad i = 1, 2 \tag{3.4}$$

where $\mathbf{\Xi}$ is the overall channel gain and $\bar{\mathbf{W}}_i (i = 1, 2)$ is the the FD noise term as defined in (3.5) and (3.6).

$$\mathbf{\Xi} = \mathbf{\Lambda}_1^* \mathbf{\Lambda}_1 + \mathbf{\Lambda}_2^* \mathbf{\Lambda}_2 \tag{3.5}$$

$$\begin{aligned}\bar{\mathbf{W}}_1 &= \mathbf{\Lambda}_1^* \mathbf{W}_1^m + (\mathbf{\Lambda}_2^* \mathbf{W}_2^m)^* \\ \bar{\mathbf{W}}_2 &= \mathbf{\Lambda}_1^* \mathbf{W}_2^m + (\mathbf{\Lambda}_2^* \mathbf{W}_1^m)^*\end{aligned} \tag{3.6}$$

In (3.4), the signal to noise ratio (SNR) of the kth subcarrier in the cooperative TS can be written as $\gamma_2(k) = \frac{|\Lambda_1(k)|^2 + |\Lambda_2(k)|^2}{(1+\lambda_1^2 |G_1(k)|^2 + \lambda_2^2 |G_2(k)|^2) N_0}$.

It is worth pointing out that there are two types of AF relaying scheme for cooperative OFDM system, as shown in Fig. 3.2. The type I relaying scheme down-converts, samples and stores the received signal in the first TS. Then in the second TS, it mixes the baseband signal with the local carrier (f_r) which is used in the downconversion. Therefore, the equivalent carrier frequency for the forwarded signal remains the same as the source carrier (f_s). The type I relaying is simple, but it cannot perform distributed space time coding which is necessary to exploit the cooperative diversity. Another problem with type I relaying is that it linearly cascades the S-R and R-D channels, which may result in the equivalent channel impulse response (CIR) exceeding the CP length. On the other hand, the type II relaying shown in Fig. 3.2 does a bit more processing than type I relaying scheme, including CP removal, CFO compensation, FFT, distributed STBC (DSTBC) encoding in the first TS and IFFT, CP insertion in the second TS. It down-converts and up-converts the signal with f_r as well, but the equivalent carrier frequency for the forwarded signal is f_r, which is

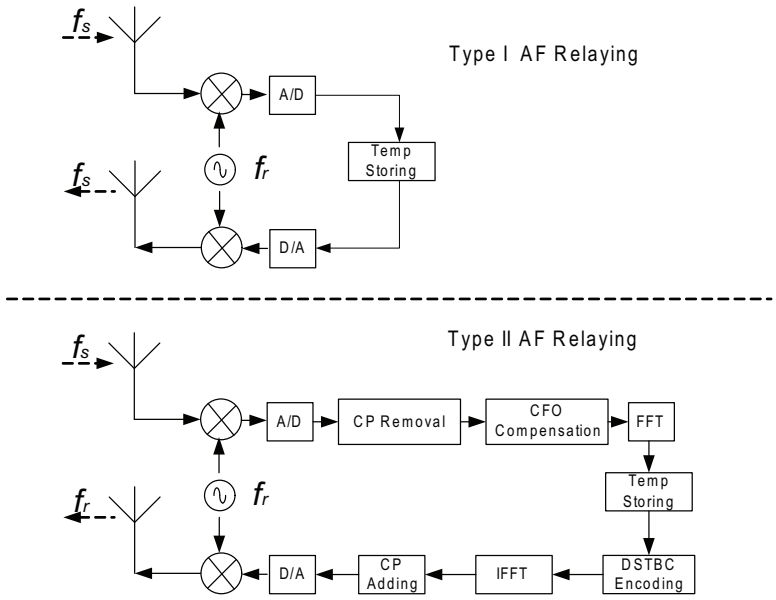

Figure 3.2: Two types of AF relaying scheme for cooperative OFDM system.

different from type I relaying scheme due to the CFO compensation operation. The CFO compensation in relay is a necessary step otherwise the DSTBC will introduce severe ICI. The type II relay also overcomes the channel cascading problem by reconstructing the CP. In our system, type II relay is employed since we consider the Alamouti STBC coding.

3.4 Distributed STBC AF cooperative OFDM System with CFO

3.4.1 Signal Model with CFO

When there are CFOs among the nodes, phase drift, ICI and IBI may occur at the destination when decoding the space time codewords. In the first phase, there is only one CFO at each relay node, which can be mitigated with the conventional CFO estimation and compensation method. For instance, the CFO estimation mean square error (MSE) can be lower than 10^{-4} at 20dB in [27], therefore the residual CFO in the first phase is negligible compared to the multiple CFOs in the second phase. We assume the CFOs between the source and the relays are compensated completely in the first phase. We only consider the CFO problem in the second phase, which

is more difficult to deal with. Denote the CFOs between the two relays and the destination by ε_1 and ε_2. We assume that the CFOs can be perfectly estimated at the destination receiver with the help of the synchronization preamble. Then the received time domain signal at the destination with multiple CFOs can be written as

$$\begin{aligned}\mathbf{y}_1^m &= \Phi(2m,\varepsilon_1)\mathbf{D}(\varepsilon_1)\mathbf{F}^H\mathbf{\Lambda}_1\mathbf{X}_1^m - \Phi(2m,\varepsilon_2)\mathbf{D}(\varepsilon_2)\mathbf{F}^H\mathbf{\Lambda}_2\mathbf{X}_2^{m,*} + \mathbf{w}_1^m \\ \mathbf{y}_2^m &= \Phi(2m+1,\varepsilon_1)\mathbf{D}(\varepsilon_1)\mathbf{F}^H\mathbf{\Lambda}_1\mathbf{X}_2^m + \Phi(2m+1,\varepsilon_2)\mathbf{D}(\varepsilon_2)\mathbf{F}^H\mathbf{\Lambda}_2\mathbf{X}_1^{m,*} + \mathbf{w}_2^m \end{aligned} \quad (3.7)$$

where $\Phi(n,\varepsilon) = e^{j2\pi(nN_s+N_g)\varepsilon/N}$ is the phase drift term, $N_s = N + N_g$ and N_g is the CP length, $\mathbf{D}(\varepsilon)$ is an $N \times N$ diagonal matrix with $e^{j2\pi(n-1)\varepsilon/N}$ as its nth element and $\mathbf{F}^H$ is the IFFT matrix. CFO induced terms include the common phase drift (CPD), e.g., $\Phi(2m,\varepsilon_1)$ which is the same for an entire block, and the intra-block phase distortion (IBPD) represented by $\mathbf{D}(\varepsilon_j)$, $j \in \{1,2\}$, that introduces ICI and IBI in frequency domain. In (3.7), the received block $\mathbf{y}_i^m$ $(i = 1,2)$ is written in 3 terms, where the first term is the signal from the first relay, the second term is the signal from the second relay and the third term is noise. The signal from each relay is written as the multiplication of the phase distortion term $\Phi(2m,\varepsilon_i)\mathbf{D}(\varepsilon_i)$ and the time domain signal after multipath channel distortion $\mathbf{F}^H\mathbf{\Lambda}\mathbf{X}_i^m$. The problem with multiple CFOs is that the CPD and the IBPD for each block cannot be completely compensated in time domain, since compensating one may result in misalignment of the other. Therefore, interference is inevitable in frequency domain. If we perform FFT to (3.7), the FD signal can be written as

$$\begin{bmatrix} \mathbf{Y}_1^m \\ \mathbf{Y}_2^{m,*} \end{bmatrix} = \begin{bmatrix} \mathbf{C}_{11} & \mathbf{C}_{12} \\ \mathbf{C}_{21} & \mathbf{C}_{22} \end{bmatrix} \begin{bmatrix} \mathbf{X}_1^m \\ \mathbf{X}_2^{m,*} \end{bmatrix} + \begin{bmatrix} \mathbf{W}_1^m \\ \mathbf{W}_2^m \end{bmatrix} \quad (3.8)$$

where $\mathbf{C}_{ij}$ is the $N \times N$ FD channel response matrix with $\mathbf{C}_{11} = \Phi(2m,\varepsilon_1)\mathbf{F}\mathbf{D}(\varepsilon_1)\mathbf{F}^H\mathbf{\Lambda}_1$, $\mathbf{C}_{12} = -\Phi(2m,\varepsilon_2)\mathbf{F}\mathbf{D}(\varepsilon_2)\mathbf{F}^H\mathbf{\Lambda}_2$, $\mathbf{C}_{21} = \Phi(2m+1,-\varepsilon_2)\mathbf{F}^H\mathbf{D}(-\varepsilon_2)\mathbf{F}\mathbf{\Lambda}_2^*$ and $\mathbf{C}_{22} = \Phi(2m+1,-\varepsilon_1)\mathbf{F}^H\mathbf{D}(-\varepsilon_1)\mathbf{F}\mathbf{\Lambda}_1^*$, $\mathbf{W}_1^m$ and $\mathbf{W}_2^m$ are the FD noise vectors. In the presence of CFO, the channel matrices $\mathbf{C}_{ij}$'s are not diagonal, and hence introduce ICI and IBI after performing the STBC decoding. However, the channel matrices are banded matrices which implies that the interference only spans over a small number of neighboring subcarriers as shown in Fig. 3.3. Based on this, existing works deal with the multiple CFO problem by purely FD equalization [74, 72, 47], which involves two channel matrices for each block. Instead of purely FD equalization, we

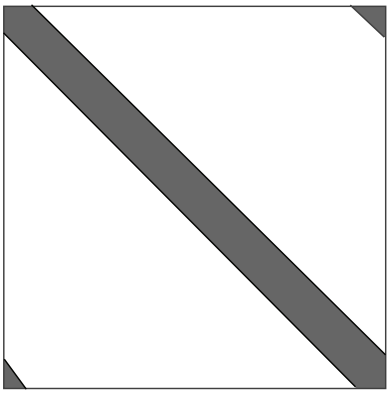

Figure 3.3: The banded feature of the channel matrices $\mathbf{C}_{ij}$.

consider performing TD partial compensation to remove either ICI or IBI before FD processing.

3.4.2 IBI-Removal Compensation

In (3.8), we can see the two transmit blocks $\mathbf{X}_1^m$ and $\mathbf{X}_2^m$ are superimposed both in $\mathbf{Y}_1^m$ and $\mathbf{Y}_2^m$, and they cannot be decoupled completely through conventional STBC decoupling due to the existence of multiple CFOs. Since the multiple CFOs cannot be compensated at the same time, we consider compensating part of them and deal with the remaining interference in the following FD decoding procedure. We will consider two kinds of TD partial compensation, i.e., ICI-removal scheme and IBI-removal scheme. As indicated by the names, ICI-removal scheme removes the ICI of $\mathbf{X}_1^m$ and $\mathbf{X}_2^m$ respectively, but the mutual interference of the two blocks remains there. On the other hand, IBI-removal scheme decouples $\mathbf{X}_1^m$ and $\mathbf{X}_2^m$ completely, but ICI remains in the decoupled blocks respectively. We will first look at the IBI-removal compensation, which is carried out as

$$\begin{aligned}\bar{\mathbf{Y}}_1^m &= \Phi(2m,-\varepsilon_1)\mathbf{\Lambda}_1^*\mathbf{F}\mathbf{D}(-\varepsilon_2)\mathbf{y}_1^m + \Phi(1,-\Delta\varepsilon)\Phi(2m+1,\varepsilon_2)\mathbf{\Lambda}_2(\mathbf{F}\mathbf{D}(-\varepsilon_1)\mathbf{y}_2^m)^* \\ \bar{\mathbf{Y}}_2^m &= \Phi(2m+1,-\varepsilon_1)\mathbf{\Lambda}_1^*\mathbf{F}\mathbf{D}(-\varepsilon_2)\mathbf{y}_2^m - \Phi(1,\Delta\varepsilon)\Phi(2m,\varepsilon_2)\mathbf{\Lambda}_2(\mathbf{F}\mathbf{D}(-\varepsilon_1)\mathbf{y}_1^m)^* \quad (3.9)\end{aligned}$$

where $\bar{\mathbf{Y}}_1^m$ and $\bar{\mathbf{Y}}_2^m$ contain the desired blocks for $\mathbf{X}_1^m$ and $\mathbf{X}_2^m$ and $\Delta\varepsilon = \varepsilon_1 - \varepsilon_2$. The operation in (3.9) cancels out the $\mathbf{X}_2^m$ component for $\bar{\mathbf{Y}}_1^m$ and the $\mathbf{X}_1^m$ component for $\bar{\mathbf{Y}}_2^m$, which can be derived by substituting (3.7) into (3.9). Then (3.9) can be written as

$$\bar{\mathbf{Y}}_i^m = \boldsymbol{\mathcal{T}}_i\mathbf{X}_i^m + \bar{\mathbf{W}}_i^m \quad i = 1,2 \qquad (3.10)$$

where

$$\boldsymbol{\mathcal{T}}_1 = \boldsymbol{\Lambda}_1^* \mathbf{F}\mathbf{D}(\Delta\varepsilon)\mathbf{F}^H\boldsymbol{\Lambda}_1 + \Phi(1,\Delta\varepsilon)\boldsymbol{\Lambda}_2\mathbf{F}^H\mathbf{D}(\Delta\varepsilon)\mathbf{F}\boldsymbol{\Lambda}_2^*$$
$$\boldsymbol{\mathcal{T}}_2 = \boldsymbol{\Lambda}_1^* \mathbf{F}\mathbf{D}(\Delta\varepsilon)\mathbf{F}^H\boldsymbol{\Lambda}_1 + \Phi(1,-\Delta\varepsilon)\boldsymbol{\Lambda}_2\mathbf{F}^H\mathbf{D}(\Delta\varepsilon)\mathbf{F}\boldsymbol{\Lambda}_2^* \tag{3.11}$$

and $\bar{\mathbf{W}}_1^m$ and $\bar{\mathbf{W}}_2^m$ are the FD noise vector after decoupling.

Remarks . *Observing (3.11), the ICI-inducing channel matrix $\boldsymbol{\mathcal{T}}_i$ depends only on $\Delta\varepsilon$ in addition to the channel response matrices. Hence, (3.9) if $\Delta\varepsilon$ is small can be reduced to*

$$\bar{\mathbf{Y}}_1^m = \Phi(2m,-\varepsilon_1)\boldsymbol{\Lambda}_1^*\mathbf{F}\mathbf{D}(-\varepsilon_2)\mathbf{y}_1^m + \Phi(2m+1,\varepsilon_2)\boldsymbol{\Lambda}_2(\mathbf{F}\mathbf{D}(-\varepsilon_1)\mathbf{y}_2^m)^*$$
$$\bar{\mathbf{Y}}_2^m = \Phi(2m+1,-\varepsilon_1)\boldsymbol{\Lambda}_1^*\mathbf{F}\mathbf{D}(-\varepsilon_2)\mathbf{y}_2^m - \Phi(2m,\varepsilon_2)\boldsymbol{\Lambda}_2(\mathbf{F}\mathbf{D}(-\varepsilon_1)\mathbf{y}_1^m)^*. \tag{3.12}$$

After substituting (3.7) into (3.12), and considering $\Phi(2m,\Delta\varepsilon) \approx \Phi(2m+1,\Delta\varepsilon)$, we have

$$\bar{\mathbf{Y}}_i^m \approx \boldsymbol{\mathcal{T}}\mathbf{X}_i^m + \bar{\mathbf{W}}_i^m \quad i = 1,2. \tag{3.13}$$

where $\boldsymbol{\mathcal{T}} = \boldsymbol{\Lambda}_1^*\mathbf{F}\mathbf{D}(\Delta\varepsilon)\mathbf{F}^H\Lambda_1 + \boldsymbol{\Lambda}_2\mathbf{F}^H\mathbf{D}(\Delta\varepsilon)\mathbf{F}\Lambda_2^*$ is the ICI-inducing channel matrix for both two blocks.

Since after TD compensation $\mathbf{X}_1^m$ and $\mathbf{X}_2^m$ are decoupled in $\bar{\mathbf{Y}}_i^m$, we decode them independently and drop the index i in (3.10). Then the detection problem is formulated as

$$\bar{\mathbf{Y}}^m = \boldsymbol{\mathcal{T}}\mathbf{X}^m + \bar{\mathbf{W}}^m. \tag{3.14}$$

To estimate $\mathbf{X}^m$ in (3.14), ZF equalization by multiplying $\boldsymbol{\mathcal{T}}^{-1}$ with $\bar{\mathbf{Y}}^m$ can be employed. Moreover, MMSE equalizer can also be used to equalize the ICI in (3.14). However, the equalization methods including ZF and MMSE require $N \times N$ matrix inversion operation, which is prohibitively complex in real time processing given that $\boldsymbol{\mathcal{T}}$ is not diagonal. Fortunately, it is observed that $\boldsymbol{\mathcal{T}}$ is a banded matrix which only has significant elements along the diagonal and on the left-bottom and right-top corner. Therefore, sub-block equalization methods can be developed to simplify the equalizer. Besides FD equalization, iterative decoding can also be employed to suppress the ICI in (3.14). The iterative method uses the decoded symbols to reconstruct the interference and then subtract the interference from $\bar{\mathbf{Y}}_m$. In the following, we will introduce the reduced complexity FD equalization methods and the iterative decoding method.

1. Sub-Block ZF (SB-ZF)

   To overcome the complex inversion operation of $\boldsymbol{\mathcal{T}}$ required by direct ZF equalization, SB-ZF takes advantage of the banded nature of $\boldsymbol{\mathcal{T}}$ by transforming the $N \times N$ matrix inversion problem into N matrix inversions with size $(2Q+1) \times (2Q+1)$, where $Q \ll N$ and the $(2Q+1) \times (2Q+1)$ matrices are taken along the main diagonal of $\boldsymbol{\mathcal{T}}$ [59]. However, the formulation of sub-blocks is slightly different from that in [59]. The SB-ZF is performed as $\mathcal{X}_k^m = \boldsymbol{\mathcal{T}}_k^{-1}\mathcal{Y}_k^m$ where

   $$\mathcal{Y}_k^m \triangleq [\bar{\mathbf{Y}}_{(k-Q)_N}^m \ \bar{\mathbf{Y}}_{(k-Q+1)_N}^m \ \ldots \ \bar{\mathbf{Y}}_{(k+Q)_N}^m]^T \tag{3.15}$$

   and $\boldsymbol{\mathcal{T}}_k$ is defined in (3.23), in which $(A)_N$ and $(A,B)_N$ are the mod operation of A mod N and (A mod N, B mod N) respectively. Then the estimation of the kth subcarrier is $\hat{X}_k^m = \mathcal{X}_k^m(Q+1)$. The choice of Q depends on the amount of CFO $\Delta\varepsilon$. When $\Delta\varepsilon$ is smaller, $\boldsymbol{\mathcal{T}}$ is more banded, meaning Q can be smaller. Typical values of Q will be discussed in the simulation.

2. Sub-Block MMSE (SB-MMSE)

   ZF detector has the drawback of noise enhancement, since it works only to eliminate the ICI component. MMSE estimator is designed to reduce both ICI and noise, and the optimized equalization taps minimize the mean square error. The MMSE design is equivalent to maximizing the signal to interference plus noise ratio (SINR) for the estimation problem of (3.14). Instead of N taps equalization, $2Q+1$ ($Q \ll N$) taps equalization is used. Denote the equalization coefficients with $\tilde{\xi}_k$, which is only a $(2Q+1) \times 1$ vector. First we have the following definition

   $$\mathcal{X}_k^m \triangleq [\mathbf{X}_{(k-2Q)_N}^m \ \mathbf{X}_{(k-2Q+1)_N}^m \ \ldots \ \mathbf{X}_{(k+2Q)_N}^m]^T \tag{3.16}$$

   $$\mathcal{W}_k^m \triangleq [\bar{\mathbf{W}}_{(k-Q)_N}^m \ \bar{\mathbf{W}}_{(k-Q+1)_N}^m \ \ldots \ \bar{\mathbf{W}}_{(k+Q)_N}^m]^T \tag{3.17}$$

   and $\mathcal{A}_k$ in (3.24). The auto-correlation matrix of $\mathcal{Y}_k^m$ is given by $\mathbf{R}_{yy}(k) = \mathbb{E}\{\mathcal{Y}_k^m \mathcal{Y}_k^{m,H}\} = \sigma_s^2 \mathcal{A}_k \mathcal{A}_k^H + \sigma_w^2 \boldsymbol{\Sigma}_k$ where $\boldsymbol{\Sigma}_k = diag\{\boldsymbol{\Xi}((k-Q)_N,(k-Q)_N)\ \boldsymbol{\Xi}((k-Q+1)_N,(k-Q+1)_N)\ \ldots\ \boldsymbol{\Xi}((k+Q)_N,(k+Q)_N)\}$, σ_s^2 and σ_w^2 are the signal power and noise power respectively. The cross correlation matrix $\mathbf{R}_{yx}(k) = \mathbb{E}\{\mathcal{Y}_k^m X_k^{m,*}\} = \sigma_s^2 \alpha_k$ where α_k is the kth column of $\mathcal{A}_k$. Then we have the

SB-MMSE equalization taps written as

$$\tilde{\xi}_k = \mathbf{R}_{yy}^{-1}(k)\mathbf{R}_{yx}(k) = \left(\mathcal{A}_k\mathcal{A}_k^H + \frac{\sigma_w^2}{\sigma_s^2}\mathbf{\Sigma}_k\right)^{-1}\alpha_k \tag{3.18}$$

and the SB-MMSE estimation of the kth subcarrier is given by $\hat{X}_k^m = \tilde{\xi}_k^H \mathcal{Y}_k^m$.

3. Recursive Matrix Inverse Computation

For SB-ZF and SB-MMSE, the detection of each data bearing subcarrier requires the inversion of $\boldsymbol{\mathcal{T}}_k$ and $\mathbf{R}_{yy}(k) = \mathcal{A}_k\mathcal{A}_k^H + \frac{\sigma_w^2}{\sigma_s^2}\mathbf{\Sigma}_k$ respectively, which leads to high complexity with a large Q. Note that there is a lot of common elements between $\mathbf{R}_{yy}(k)$ and $\mathbf{R}_{yy}(k+1)$, as well as $\boldsymbol{\mathcal{T}}_k$ and $\boldsymbol{\mathcal{T}}_{k+1}$. This gives chance to compute the series of matrix inversions recursively. Taking SB-ZF for example, we partition $\boldsymbol{\mathcal{T}}_k$ as

$$\boldsymbol{\mathcal{T}}_k = \begin{bmatrix} a_{11} & \mathbf{a}_{12}^H \\ \mathbf{a}_{21} & \mathbf{\Theta}_k \end{bmatrix} \tag{3.19}$$

where a_{11} is a scaler, $\mathbf{a}_{12}$ and $\mathbf{a}_{21}$ are $2Q\times 1$ vectors and $\mathbf{\Theta}_k$ is a $2Q\times 2Q$ matrix. $\boldsymbol{\mathcal{T}}_{k+1}$ and $\boldsymbol{\mathcal{T}}_k$ has $\mathbf{\Theta}_k$ in common. Therefore, we partition $\boldsymbol{\mathcal{T}}_{k+1}$ as

$$\boldsymbol{\mathcal{T}}_{k+1} = \begin{bmatrix} \mathbf{\Theta}_k & \mathbf{b}_{12} \\ \mathbf{b}_{21}^H & b_{22} \end{bmatrix} \tag{3.20}$$

where $\mathbf{b}_{12}$ and $\mathbf{b}_{21}$ are $2Q\times 1$ vectors and b_{22} is a scaler. Then the block-wise inversion of $\boldsymbol{\mathcal{T}}_{k+1}$ can be written as [9]

$$\boldsymbol{\mathcal{T}}_{k+1}^{-1} = \begin{bmatrix} \mathbf{\Theta}_k^{-1} + p\mathbf{\Theta}_k^{-1}\mathbf{b}_{12}\mathbf{b}_{21}^H\mathbf{\Theta}_k^{-1} & -p\mathbf{\Theta}_k^{-1}\mathbf{b}_{12} \\ -p\mathbf{b}_{21}^H\mathbf{\Theta}_k^{-1} & p \end{bmatrix} \tag{3.21}$$

where $p = \frac{1}{b_{22}-\mathbf{b}_{21}^H\mathbf{\Theta}_k^{-1}\mathbf{b}_{12}}$. This means $\boldsymbol{\mathcal{T}}_{k+1}^{-1}$ can be computed using $\mathbf{\Theta}_k^{-1}$ with a small number of multiplications between matrices and vectors. The inversion of the common portion $\mathbf{\Theta}_k$ can be obtained based on $\boldsymbol{\mathcal{T}}_k^{-1}$ as $\mathbf{\Theta}_k^{-1} = \mathbf{U}_k - \frac{\mathbf{c}_{21}\mathbf{c}_{12}^H}{c_{11}}$ if we write

$$\boldsymbol{\mathcal{T}}_k^{-1} = \begin{bmatrix} c_{11} & \mathbf{c}_{12}^H \\ \mathbf{c}_{21} & \mathbf{U}_k \end{bmatrix} \tag{3.22}$$

$$\boldsymbol{\mathcal{T}}_k \triangleq \begin{pmatrix} \boldsymbol{\mathcal{T}}_{(k-Q,k-Q)_N} & \cdots & \boldsymbol{\mathcal{T}}_{(k-Q,k)_N} & \cdots & \boldsymbol{\mathcal{T}}_{(k-Q,k+Q)_N} \\ & & \ddots & & \\ \boldsymbol{\mathcal{T}}_{(k,k-Q)_N} & \cdots & \boldsymbol{\mathcal{T}}_{k,k} & \cdots & \boldsymbol{\mathcal{T}}_{(k,k+Q)_N} \\ & & \ddots & & \\ \boldsymbol{\mathcal{T}}_{(k+Q,k-Q)_N} & \cdots & \boldsymbol{\mathcal{T}}_{(k+Q,k)_N} & \cdots & \boldsymbol{\mathcal{T}}_{(k+Q,k+Q)_N} \end{pmatrix} \tag{3.23}$$

$$\mathcal{A}_k \triangleq \begin{pmatrix} \boldsymbol{\mathcal{T}}_{(k-Q,k-2Q)_N} & \cdots & \cdots & \boldsymbol{\mathcal{T}}_{(k-Q,k)_N} & 0 & \cdots & 0 \\ & & & \ddots & & & \\ 0 & \cdots & \cdots & \boldsymbol{\mathcal{T}}_{k,k} & \cdots & \cdots & 0 \\ & & & \ddots & & & \\ 0 & \cdots & 0 & \boldsymbol{\mathcal{T}}_{(k+Q,k)_N} & \cdots & \cdots & \boldsymbol{\mathcal{T}}_{(k+Q,k+2Q)_N} \end{pmatrix} \tag{3.24}$$

---

where c_{11} is a scaler, $\mathbf{c}_{21}$ and $\mathbf{c}_{12}$ are $2Q \times 1$ vectors and $\mathbf{U}_k$ is a $2Q \times 2Q$ matrix. Thus, taking advantage of the common part between $\boldsymbol{\mathcal{T}}_k$ and $\boldsymbol{\mathcal{T}}_{k+1}$, the inversion can be computed recursively. The recursive method is able to reduce the complexity of sub-block equalization from $\mathcal{O}((2Q+1)^3)$ to $\mathcal{O}((2Q+1)^2)$.

4. Iterative ML Detection (IMLD)

   The iterative ML decoder performs interference cancellation (IC) at each subcarrier. In the pth iteration, the interference is reconstructed using the decoded symbols from the $(p-1)$th iteration. We propose a simple subcarrier ordering scheme, i.e., the detection starts from the subcarrier which has the largest signal power and goes along with the subcarrier index. The subcarrier with the largest power is determined by $\arg\max_k(|\Xi_{k,k}|)$, where $\Xi_{k,k}$ is the kth diagonal element of $\boldsymbol{\Xi}$ defined in (3.5). The process can be written in pseudocode shown in Table 3.2. In each step of the IMLD, individual symbol ML decoding is performed instead of joint ML decoding of two symbols since we have already decoupled the two blocks completely. The individual symbol ML decoding saves a lot of complexity compared to joint two symbol ML decoding, which will be discussed in Subsection 3.4.4.

Table 3.2: The pseudocode for iterative ML decoding with SIC:

$\hat{\boldsymbol{\mathcal{X}}}^m = \mathbf{0}$

$k_m = \arg\max_k(|\Xi_{k,k}|)$

for $it = 1$ **to** number of iterations

  for $k = k_m$ **to** $N-1$ **then from** 0 **to** $k_m - 1$

$$\tilde{\mathcal{Y}}^m(k) = \bar{\mathcal{Y}}^m(k) - \sum_{\substack{q=-Q \\ q\neq 0}}^{Q} \mathcal{T}_{k,(k+q)_N} \hat{\mathcal{X}}^m((k+q)_N)$$

$$\hat{\mathcal{X}}^m(k) = \arg\min_X \parallel \tilde{\mathcal{Y}}^m(k) - \mathcal{T}_{k,k} X \parallel^2$$

  endfor

endfor

3.4.3 ICI-Removal Compensation

The ICI-removal scheme and space time decoupling is carried out over the received time domain blocks $\mathbf{y}_1^m$ and $\mathbf{y}_2^m$ as

$$\begin{aligned}\bar{\mathbf{Y}}_1^m &= \Phi(2m,-\varepsilon_1)\mathbf{\Lambda}_1^*\mathbf{F}\mathbf{D}(-\varepsilon_1)\mathbf{y}_1^m + \Phi(2m+1,\varepsilon_2)\mathbf{\Lambda}_2(\mathbf{F}\mathbf{D}(-\varepsilon_2)\mathbf{y}_2^m)^* \\ \bar{\mathbf{Y}}_2^m &= \Phi(2m+1,\varepsilon_1)(\mathbf{\Lambda}_1^*\mathbf{F}\mathbf{D}(-\varepsilon_1)\mathbf{y}_2^m)^* - \Phi(2m,-\varepsilon_2)\mathbf{\Lambda}_2^*\mathbf{F}\mathbf{D}(-\varepsilon_2)\mathbf{y}_1^m \end{aligned} \tag{3.25}$$

where $\bar{\mathbf{Y}}_1^m$ and $\bar{\mathbf{Y}}_2^m$ contain the desired blocks for $\mathbf{X}_1^m$ and $\mathbf{X}_2^{m,*}$. The operation in (3.25) cancels out the ICI component of $\mathbf{X}_1^m$ for $\bar{\mathbf{Y}}_1^m$ and the ICI component of $\mathbf{X}_2^m$ for $\bar{\mathbf{Y}}_2^m$, which can be derived by substituting (3.7) into (3.25). To obtain $\bar{\mathbf{Y}}_1^m$, the CPD and IBPD terms for $\mathbf{X}_1^m$ are completely compensated, while for $\bar{\mathbf{Y}}_2^m$ those of $\mathbf{X}_2^m$ have been completely compensated. Therefore, unlike the IBI-removal scheme, the IBI component between $\mathbf{X}_1^m$ and $\mathbf{X}_2^m$ remains but the ICI has been removed. After the substitution, (3.25) can be written as

$$\begin{aligned}\bar{\mathbf{Y}}_1^m &= \mathbf{\Xi}\mathbf{X}_1^m + \mathbf{\Gamma}_1\mathbf{X}_2^{m,*} + \bar{\mathbf{W}}_1^m \\ \bar{\mathbf{Y}}_2^m &= \mathbf{\Xi}\mathbf{X}_2^{m,*} + \mathbf{\Gamma}_2\mathbf{X}_1^m + \bar{\mathbf{W}}_2^m \end{aligned} \tag{3.26}$$

where the IBI weighting matrices are

$$\begin{aligned}\mathbf{\Gamma}_1 &= \Phi(2m+1,-\Delta\varepsilon)\mathbf{\Lambda}_2\mathbf{F}^H\mathbf{D}(-\Delta\varepsilon)\mathbf{F}\mathbf{\Lambda}_1^* - \Phi(2m,-\Delta\varepsilon)\mathbf{\Lambda}_1^*\mathbf{F}\mathbf{D}(-\Delta\varepsilon)\mathbf{F}^H\mathbf{\Lambda}_2 \\ \mathbf{\Gamma}_2 &= \Phi(2m+1,\Delta\varepsilon)\mathbf{\Lambda}_1\mathbf{F}^H\mathbf{D}(\Delta\varepsilon)\mathbf{F}\mathbf{\Lambda}_2^* - \Phi(2m,\Delta\varepsilon)\mathbf{\Lambda}_2^*\mathbf{F}\mathbf{D}(\Delta\varepsilon)\mathbf{F}^H\mathbf{\Lambda}_1. \end{aligned} \tag{3.27}$$

The channel matrix $\mathbf{\Xi}$ in (3.26) is diagonal and that is why we call it ICI-removal, i.e., the ICI within each desired symbol is removed. Then the subsequent decoding is similar to the problem in [47], where an iterative joint maximum likelihood decoding (IJMLD) process is proposed to combat the interference introduced by the matrices $\mathbf{\Gamma}_1$ and $\mathbf{\Gamma}_2$. However, on subcarrier k, $X_1^m(k)$ and $X_2^m(k)$ are jointly ML decoded which requires a two dimensional search over the symbol set and the interference reconstruction on each subcarrier requires $2 \times 2N$ complex multiplications. To provide better performance and reduce complexity, we propose a modified IJMLD (MIJMLD) decoder as described by the pseudocode in Table 3.3. Note that in the proposed MIJMLD, only $2Q$ neighboring subcarriers are used for interference reconstruction. Furthermore, we have the subcarrier with the largest power decoded first, which leads to better initial decision. It has to be pointed out that the interference

Table 3.3: The pseudocode for the iterative joint ML decoding with SIC:

$\hat{\boldsymbol{\mathcal{X}}}_1^m = \mathbf{0}$, $\hat{\boldsymbol{\mathcal{X}}}_2^{m,*} = \mathbf{0}$
$k_m = \arg\max_k(|\Xi_{k,k}|)$
for $it = 1$ **to** number of iterations
  for $k = k_m$ **to** $N-1$ **then from** 0 **to** $k_m - 1$

$$\tilde{\mathcal{Y}}_1^m(k) = \bar{\mathcal{Y}}_1^m(k) - \sum_{\substack{q=-Q \\ q\neq 0}}^{Q} \Gamma_1(k,(k+q)_N)\hat{\mathcal{X}}_2^{m,*}((k+q)_N)$$

$$\tilde{\mathcal{Y}}_2^m(k) = \bar{\mathcal{Y}}_2^m(k) - \sum_{\substack{q=-Q \\ q\neq 0}}^{Q} \Gamma_2(k,(k+q)_N)\hat{\mathcal{X}}_1^{m}((k+q)_N)$$

$$\begin{bmatrix} \hat{\mathcal{X}}_1^m(k) \\ \hat{\mathcal{X}}_2^{m,*}(k) \end{bmatrix} = \arg \min_{X_1^m(k), X_2^{m,*}(k)} \| \begin{bmatrix} \tilde{\mathcal{Y}}_1^m(k) \\ \tilde{\mathcal{Y}}_2^m(k) \end{bmatrix} - \begin{bmatrix} \Xi_{k,k} & \Gamma_1(k,k) \\ \Gamma_2(k,k) & \Xi_{k,k} \end{bmatrix} \begin{bmatrix} X_1^m(k) \\ X_2^{m,*}(k) \end{bmatrix} \|^2$$

  endfor
endfor

matrices needed for IBI mitigation algorithms, i.e., $\mathbf{\Gamma}_1$ and $\mathbf{\Gamma}_2$, vary with the block index. Therefore, $\mathbf{\Gamma}_1$ and $\mathbf{\Gamma}_2$ have to be updated for every STBC codeword with the phase shift. For IBI-removal scheme, the subsequent decoder only needs to compute the two interference matrices once per frame according to (3.11), and for small $\Delta\varepsilon$ only one interference matrix is to be computed for both $\mathbf{X}_1^m$ and $\mathbf{X}_2^m$ according to (3.13). At this point, it is obvious that the IBI-removal scheme has lower complexity than the ICI-removal scheme. The detailed complexity analysis will be presented in Subsection 3.4.4. It is worth mentioning that for small $\Delta\varepsilon$ where the interference is not significant, simple one tap equalization (OTEQ) can be employed after IBI-removal or ICI-removal compensation to save complexity.

3.4.4 Complexity Analysis

So far, we have proposed three joint TD and FD schemes: IBI-removal with sub-block equalization, IBI-removal with IMLD and ICI-removal with MIJMLD. We will compare the proposed sub-block equalization method with the existing sub-block FDZF scheme in [74] and the proposed iterative methods with the existing iterative method in [47]. First take a look at the FDZF method and the IBI-R-SB-ZF method. For the FDZF scheme, one FFT operation is performed for each block first. Then the two blocks $\mathbf{X}_1^m$ and $\mathbf{X}_2^m$ are decoded jointly. With sub-block size Q, STBC decoding involves N matrix inversions of size $(4Q+2) \times (4Q+2)$. Assume that the FFT

operation requires $N \log_2 N$ multiplication-and-accumulation (MAC) operations, and the matrix inversions requires $N(4Q+2)^3$ MAC operations. Therefore, the total computation required by FDZF for a STBC codeword is approximately $2N \log_2 N + 8N(2Q+1)^3$ MAC operations. As for the proposed IBI-removal TD compensation and SB-ZF scheme, $4N$ multiplications and 4 FFT operations are required for each STBC codeword at the compensation stage. At the FD equalization stage, $2N$ inversions of $(2Q+1) \times (2Q+1)$ matrix are required. Thus the overall computation needed by the proposed scheme can be approximated as $4N + 4N \log_2 N + 2N(2Q+1)^3$ MAC operations. With $Q \geq 1$, most of the computation comes from the sub-block matrix inversions (the Q involved terms in the above computation approximations). Therefore, the proposed IBI-R with sub-block equalization scheme saves substantial complexity compared to the pure sub-block FD equalization method.

Then look at the iterative methods. Considering the complexity of the IBI-removal with IMLD, each subcarrier of $\mathbf{X}_1^m$ and $\mathbf{X}_2^m$ is decoded separately. For each subcarrier at one iteration, $2(Q+M)$ MAC operations are needed where M is the modulation size ($2Q$ MACs for the interference cancellation, $2M$ MACs for the ML estimation). As a result, the total number of MACs for each iteration becomes $4N(Q+M)$. As for the ICI-removal with modified iterative joint ML decoding and the iterative method in [47] (the decoding for the two schemes are similar), $8M^2+4Q$ MACs are required for each subcarrier and the total number of MACs for each iteration is $8M^2N$. Therefore, IBI-removal compensation with iterative decoding has much lower complexity than the joint two blocks decoding required by the ICI-removal and the method in [47] because the IBI-removal completely decouples the two blocks.

3.5 Simulation Results and Discussion

In the simulation, we set $N = 64$, CP length is 16. The multipath channel used in the simulation is modeled the same way as [40]. All the channels have the discrete impulse response with a maximum order of $L = 8$. Each channel has different number of taps chosen from $0 \sim 8$. We choose the channel delays for the four channels as $\tau_{sr1} = [0, 2, 4, 7]$, $\tau_{rd1} = [0, 1, 4]$, $\tau_{sr2} = [0, 1, 3, 6]$ and $\tau_{rd2} = [0, 1, 2]$. The taps are modeled as independent circularly symmetric Gaussian random variables with zero-mean (Rayleigh fading) and exponential power delay profile

$$E\{|h(\tau_l)|^2\} = \rho e^{-0.3\tau_l} \quad l = 0, 1, ..., L \tag{3.28}$$

where the constant ρ is chosen such that the channel power is normalized to unity. For each simulation, 100 channel realizations are generated to obtain the average performance. The data symbols are QPSK modulated. The power is allocated equally among the transmissions. However, better performance may be achieved with optimal power allocation according to the channel information, which is out of the scope of out discussion. In the following simulation, the proposed method is sometimes compared with the existing methods under AF relaying, while the existing methods have been proposed for DF relaying but we applied them in AF relaying for comparison purpose.

3.5.1 TD Compensation and One-tap Equalization

The symbol error rate (SER) of the proposed joint TD-FD CFO mitigation method is evaluated with different $\Delta\varepsilon$. We first test the performance of one tap equalization under small $\Delta\varepsilon$ values since OTEQ saves substantial complexity with acceptable performance when considering the tradeoff between the performance and the complexity. When $\Delta\varepsilon$ is small, the interference is not significant. Therefore, the IBI or ICI can be simply treated as noise and OTEQ can be considered in the decoding process. In IBI-removal scheme, the equalizer works as $\hat{X}_j^m(k) = \frac{\bar{Y}_i^m(k)}{\mathcal{T}_i(k,k)}$ $(i = 1, 2)$ at the kth subcarrier. In ICI-removal scheme, it works as $\hat{X}_j^m(k) = \frac{\bar{Y}_i^m(k)}{|\Lambda_1(k,k)|^2+|\Lambda_2(k,k)|^2}$ $(i = 1, 2)$ at the kth subcarrier. We evaluated the BER of OTEQ under different amounts of CFO in Fig. 3.4. The performance of OTEQ is determined by the SINR after TD partial compensation. Thus, we study the post TD compensation SIR. For IBI-removal, the desired signal in (3.10) only contains ICI and the SIR for the kth subcarrier of $\mathbf{X}_1^m$ can be written as

$$\gamma_1^{s1}(k) = \mathbb{E}\left[\frac{|\alpha(\Delta\varepsilon)|^2||\Lambda_1(k,k)|^2 + \Phi(1,\Delta\varepsilon)|\Lambda_2(k,k)|^2|^2}{\| \bar{\boldsymbol{\psi}}_1^{s2}(k) \|^2}\right] \tag{3.29}$$

where $\alpha(\Delta\varepsilon) = \frac{1-e^{j2\pi\Delta\varepsilon}}{N(1-e^{j2\pi\Delta\varepsilon/N})}$, $\bar{\boldsymbol{\psi}}_1^{s1}(k)$ is the kth row of the ICI-inducing channel matrix $\boldsymbol{\mathcal{T}}_1$ without diagonal elements and $\|\cdot\|$ represents the Euclidean norm of a vector. On the other hand, the compensated FD signal with ICI-removal in (3.26) is composed of the desired signal component, the interference term and the noise term. The SIR for the kth subcarrier of $\mathbf{X}_1^m$ can be written as

$$\gamma_1^{s2}(k) = \mathbb{E}\left[\frac{(|\Lambda_1(k,k)|^2 + |\Lambda_2(k,k)|^2)^2}{\| \boldsymbol{\psi}_1^{s2}(k) \|^2}\right] \tag{3.30}$$

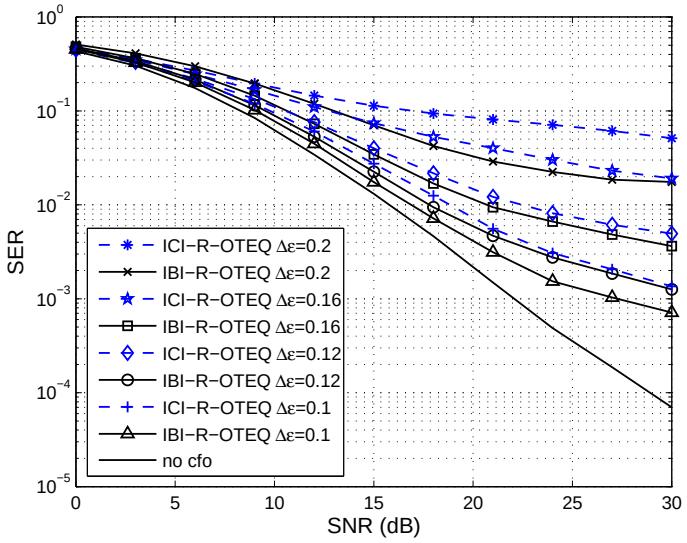

Figure 3.4: SER of one tap equalizer after IBI-removal and ICI-removal compensation with different $\Delta\varepsilon$ values.

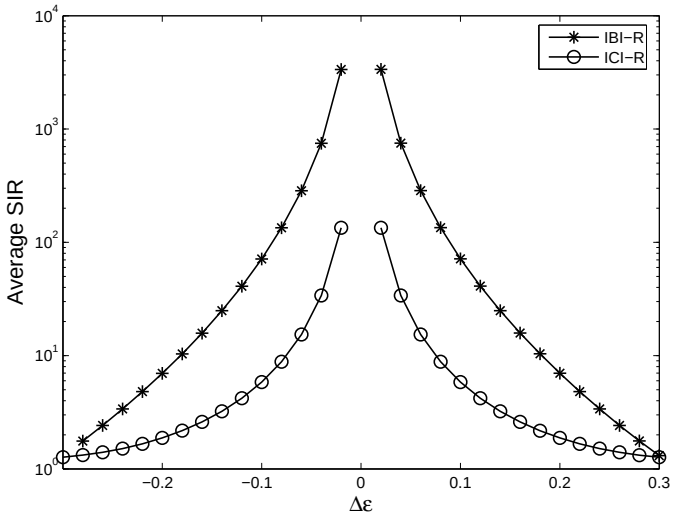

Figure 3.5: Numerical results of the SIR after partial compensation and STBC decoupling under different CFO settings.

where $\boldsymbol{\psi}_1^{s1}(k)$ is the kth row of the IBI matrix $\boldsymbol{\Gamma}_1$. Fig. 3.5 shows the numerical results of the SIR after the TD partial compensation and the FD STBC decoupling. According to the above analysis, SIR is found to be only dependent on the channel and $\Delta\varepsilon$. The numerical SIR result is averaged over 100 channel realizations. We can see from Fig. 3.5 that IBI-removal is better than ICI-removal in terms of post-compensation SIR, which leads to the result that OTEQ performs better with IBI-removal shown in Fig. 3.4.

3.5.2 TD Compensation and FD Interference Suppressing Decoding

As the CFO increases, the interference becomes more dominant and has to be suppressed. The proposed TD compensation and FD interference suppressing methods are examined in terms of SER, including IBI-R compensation followed by sub-block equalization or single symbol iterative ML decoding with interference cancellation, ICI-R and modified iterative joint symbol ML decoding with interference cancellation. For comparison, we also employ the FD sub-block ZF (FDZF) equalization method proposed in [74], and the FD iterative joint ML decoder (FD-IJMLD) in [47], although the signal models in [74] and [47] are not exactly identical to our system. Fig. 3.6 shows the BER performance of the above mentioned schemes with the CFO

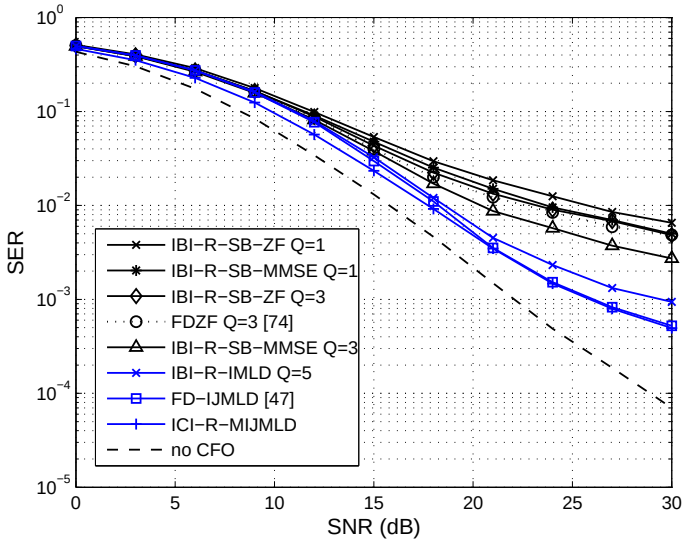

Figure 3.6: SER performance of different detection methods under $\varepsilon_1 = 0.1$, $\varepsilon_2 = -0.1$ and $\Delta\varepsilon = 0.2$.

setting being $\varepsilon_1 = 0.1$, $\varepsilon_2 = -0.1$ and $\Delta\varepsilon = 0.2$, and the number of iterations for the iterative methods are 2. The ICI-inducing channel matrices used for $\Delta\varepsilon = 0.2$ is from (3.11), which involves two different ICI-inducing channel matrices for the STBC codeword. From Fig. 3.6, it is shown that for the sub-block equalization methods SB-MMSE outperforms the SB-ZF equalization method with the same sub-block size. The performance of the FDZF method in [74] is close to the IBI-R-SB-ZF method with the same sub-block size but the complexity is much higher than the latter as discussed in Section 3.4.4. The ICI-R-MIJMLD performs the best and loses approximately 2 dB compared to the no CFO case. The proposed IBI-R-IMLD is close to FD-IJMLD in SER performance and it saves a lot of complexity compared to the FD-IJMLD as discussed in Subsection 3.4.4. Fig. 3.7 shows the SER performance under another CFO set of $\varepsilon_1 = 0.08$, $\varepsilon_2 = -0.08$ and $\Delta\varepsilon = 0.16$. From Fig. 3.7 smaller performance gap between the FD-IJMLD and the no CFO case is observed. The performance of IBI-R-IMLD is still close to that of the FD-IJMLD. Fig 3.8 shows the SER performance for IBI-R with SB-MMSE, ICI-R with MIJMLD and FD-IJMLD under CFO settings $\varepsilon_1 = 0.15$, $\varepsilon_2 = -0.15$ and $\Delta\varepsilon = 0.3$. The performances of IBI-R-SB-MMSE and IBI-R-IMLD degrade significantly and error floors occur. The ICI-R-MIJMLD and FD-IJMLD perform much better than the IBI-R schemes. From the above results, it can be observed that the performance of IBI-R with FD in-

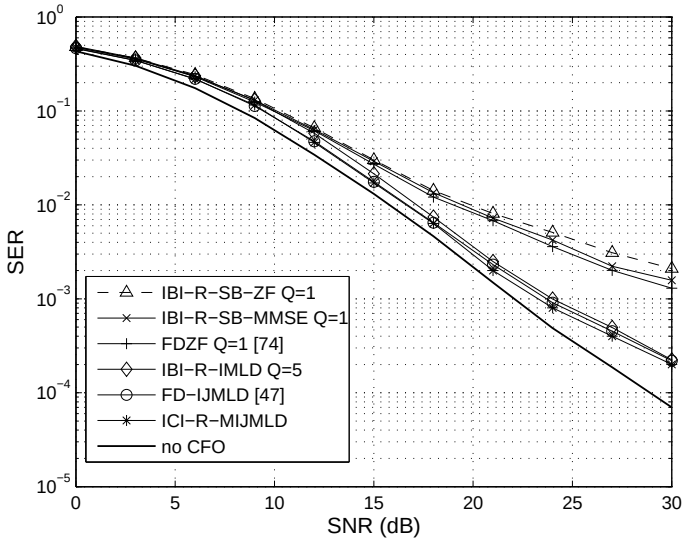

Figure 3.7: SER performance of different detection methods under $\varepsilon_1 = 0.08$, $\varepsilon_2 = -0.08$ and $\Delta\varepsilon = 0.16$.

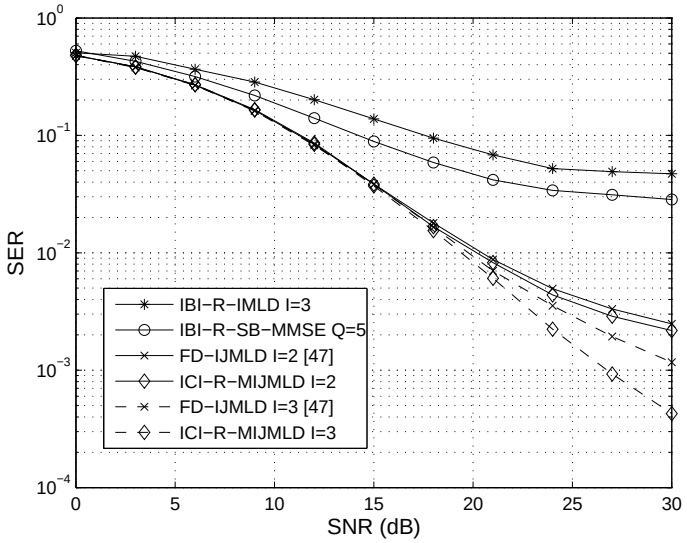

Figure 3.8: SER performance under $\varepsilon_1 = 0.15$, $\varepsilon_2 = -0.15$ and $\Delta\varepsilon = 0.3$.

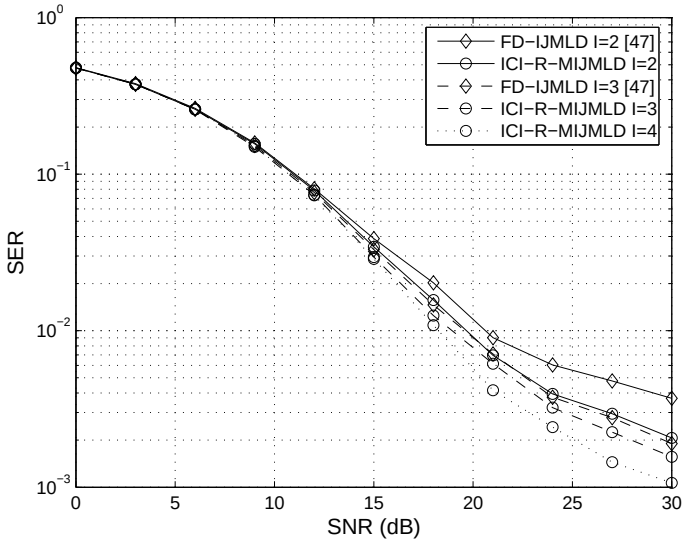

Figure 3.9: SER performance under $\varepsilon_1 = 0.2$, $\varepsilon_1 = -0.2$ and $\Delta\varepsilon = 0.4$.

terference suppression schemes deteriorates fast with the increase of $\Delta\varepsilon$. However, considering the complexity, the IBI-removal scheme is sufficient to achieve acceptable performance with much lower complexity under small $\Delta\varepsilon$.

When $\Delta\varepsilon$ is large, ICI-R-MIJMLD is examined and compared with FD-IJMLD in Fig. 3.9 with $\varepsilon_1 = 0.2$, $\varepsilon_2 = -0.2$ and $\Delta\varepsilon = 0.4$. It can be observed that the ICI-R-MIJMLD outperforms the FD-IJMLD slightly. The performance improvement comes from the simple detection ordering mechanism in addition to the joint ML decoding. It is observed that increasing the number of iterations has limited improvement on the performance after several iterations, and the choice of number of iterations depends on $\Delta\varepsilon$.

3.5.3 Impact of Imperfect CSI

In this subsection, we will characterize the impact of imperfect CSI on the performance of the proposed scheme. A two block based channel estimation method has been proposed for this cooperative transmission scheme in [71]. The proposed channel estimation method is able to estimate the channel in the presence of multiple CFOs with the same performance of that without CFO. In this case, the imperfect CSI only introduces additive Gaussian distributed interference. We first model the channel as the actual channel coefficients plus Gaussian distributed estimation error as done in many papers (e.g., [49, 24]). Denote the estimated channel matrix with $\hat{\mathbf{\Lambda}}_1$ and $\hat{\mathbf{\Lambda}}_2$,

which can be written as

$$\begin{aligned}\hat{\mathbf{\Lambda}}_1 &= \mathbf{\Lambda}_1 + \boldsymbol{\delta}_1 \\ \hat{\mathbf{\Lambda}}_2 &= \mathbf{\Lambda}_2 + \boldsymbol{\delta}_2\end{aligned} \tag{3.31}$$

where $\boldsymbol{\delta}_1$ and $\boldsymbol{\delta}_2$ are the Gaussian distributed estimation error matrices with variances $\mathbb{E}[\boldsymbol{\delta}_1^H \boldsymbol{\delta}_1] = \sigma_1^2 \mathbf{I}$ and $\mathbb{E}[\boldsymbol{\delta}_2^H \boldsymbol{\delta}_2] = \sigma_2^2 \mathbf{I}$. Consider the IBI-removal scheme for instance. Replacing $\mathbf{\Lambda}_1$ and $\mathbf{\Lambda}_2$ with $\hat{\mathbf{\Lambda}}_1$ and $\hat{\mathbf{\Lambda}}_2$ in (3.9), we can get

$$\begin{aligned}\bar{\mathbf{Y}}_1^m &= \boldsymbol{\mathcal{T}}_1 \mathbf{X}_1^m + \bar{\mathbf{W}}_1^m + \mathbf{\Upsilon}_1 \\ \bar{\mathbf{Y}}_2^m &= \boldsymbol{\mathcal{T}}_2 \mathbf{X}_2^m + \bar{\mathbf{W}}_2^m + \mathbf{\Upsilon}_2\end{aligned} \tag{3.32}$$

where $\mathbf{\Upsilon}_1$ and $\mathbf{\Upsilon}_2$ are the channel estimation error induced extra interference and $\bar{\mathbf{W}}_1^m$ and $\bar{\mathbf{W}}_1^m$ are the AWGN noise terms. Only take a look at $\mathbf{\Upsilon}_1$, which is written as

$$\begin{aligned}\mathbf{\Upsilon}_1 = \boldsymbol{\delta}_1^* (&\mathbf{F}\mathbf{D}(\Delta\varepsilon)\mathbf{F}^H \mathbf{\Lambda}_1 \mathbf{X}_1^m - \Phi(2m, -\Delta\varepsilon)\mathbf{\Lambda}_2 \mathbf{X}_2^{m,*}) \\ &+ \boldsymbol{\delta}_2 (\Phi(2m, -\Delta\varepsilon)\mathbf{\Lambda}_1^* \mathbf{X}_2^{m,*} + \Phi(1, \Delta\varepsilon)\mathbf{F}^H \mathbf{D}(\Delta\varepsilon)\mathbf{F}\mathbf{\Lambda}_2^* \mathbf{X}_1^m).\end{aligned} \tag{3.33}$$

Given $\mathbf{X}_1^m$ and $\mathbf{X}_2^m$ for each OFDM STBC codeword, each element of $\mathbf{\Upsilon}_1$ is the sum of several Gaussian distributed random variables, which also follows Gaussian distribution. Then we take an expectation over the data symbols. The variance of the extra interference can be written as

$$\mathbb{E}[\mathbf{\Upsilon}_1 \mathbf{\Upsilon}_1^H] = \sigma_s^2(\sigma_1^2 + \sigma_2^2)\mathbf{\Xi} \tag{3.34}$$

where σ_s^2 is the transmit power of the source symbol. The same characterization can be derived for $\mathbf{\Upsilon}_2$ and for ICI-removal scheme as well. Therefore, it can be seen that imperfect CSI only causes extra Gaussian interference that adds to the noise floor of the proposed scheme.

3.5.4 Impact of Residual CFO of the Source-Relay Link

So far it has been assumed that the CFOs between the source and relays during the first transmission stage have been perfectly estimated and compensated. However, in the presence of imperfect CFO estimation of the S-R links, the type II AF relay shown

in Fig. 3.2 would introduce extra interference to the overall transmission. Denote the residual CFO in the S-R links with ω_1 and ω_2 for relay 1 and 2 respectively. Note this is the normalized CFO (by subcarrier spacing), which means the phase of each sample will be drifting by $e^{j2\pi n\omega_1/N}$ and $e^{j2\pi n\omega_2/N}$ (n is the sample index). Eq. (3.2) can be rewritten as follows when considering the residual CFO ω_1 and ω_2,

$$\begin{aligned}
\mathbf{Y}_1^m &= \lambda_1\Phi(2m,\omega_1)\mathbf{G}_1\mathbf{F}\mathbf{D}(\omega_1)\mathbf{F}^H\mathbf{H}_1\mathbf{X}_1^m \\
&\quad -\lambda_2\Phi(2m+1,-\omega_2)\mathbf{G}_2\mathbf{F}^H\mathbf{D}(-\omega_2)\mathbf{F}\mathbf{H}_2^*\mathbf{X}_2^{m,*}+\mathbf{W}_1^m \\
\mathbf{Y}_2^m &= \lambda_1\Phi(2m+1\omega_1)\mathbf{G}_1\mathbf{F}\mathbf{D}(\omega_1)\mathbf{F}^H\mathbf{H}_1\mathbf{X}_2^m \\
&\quad +\lambda_2\Phi(2m,-\omega_2)\mathbf{G}_2\mathbf{F}^H\mathbf{D}(-\omega_2)\mathbf{F}\mathbf{H}_2^*\mathbf{X}_1^{m,*}+\mathbf{W}_2^m. \qquad (3.35)
\end{aligned}$$

Then the equivalent channel of the S-R-D links should be rewritten as

$$\begin{aligned}
\tilde{\mathbf{\Lambda}}_1 &= \lambda_1\Phi(2m,\omega_1)\mathbf{G}_1\mathbf{F}\mathbf{D}(\omega_1)\mathbf{F}^H\mathbf{H}_1 \\
\tilde{\mathbf{\Lambda}}_2 &= \lambda_2\Phi(2m,-\omega_2)\mathbf{G}_2\mathbf{F}^H\mathbf{D}(-\omega_2)\mathbf{F}\mathbf{H}_2^*. \qquad (3.36)
\end{aligned}$$

Comparing the equivalent channel with the case without CFO in Section 3.3, the terms $\mathbf{F}\mathbf{D}(\omega_1)\mathbf{F}^H$ and $\mathbf{F}^H\mathbf{D}(-\omega_2)\mathbf{F}$ will introduce extra interference to the forwarded signal and $\Phi(2m,\omega_1)$ and $\Phi(2m,-\omega_2)$ cause phase shift to each block. The average interference power can be approximated by [27]

$$\mathcal{I}_\omega \simeq \frac{\pi^2}{3}mse_\omega. \qquad (3.37)$$

where mse_ω is the MSE of ω estimation. According to the result in [27], the single CFO estimation algorithm is able to achieve estimation MSE as low as 10^{-5} at moderate SNR. Therefore, the interference introduced by the residual CFO is negligible at moderate SNR. Then we can approximate the equivalent channel with

$$\begin{aligned}
\tilde{\mathbf{\Lambda}}_1 &\simeq \lambda_1\Phi(2m,\omega_1)\mathbf{G}_1\mathbf{H}_1 \\
\tilde{\mathbf{\Lambda}}_2 &\simeq \lambda_2\Phi(2m,-\omega_2)\mathbf{G}_2\mathbf{H}_2^*. \qquad (3.38)
\end{aligned}$$

The phase shift terms $\Phi(2m,\omega_1)$ and $\Phi(2m,-\omega_2)$ are drifting along with the block index m, which could be large if the frame is long. The destination receiver only has the knowledge of the equivalent channel without the phase term, which will be used to apply the compensation and decoding algorithm. Therefore, we need to limit

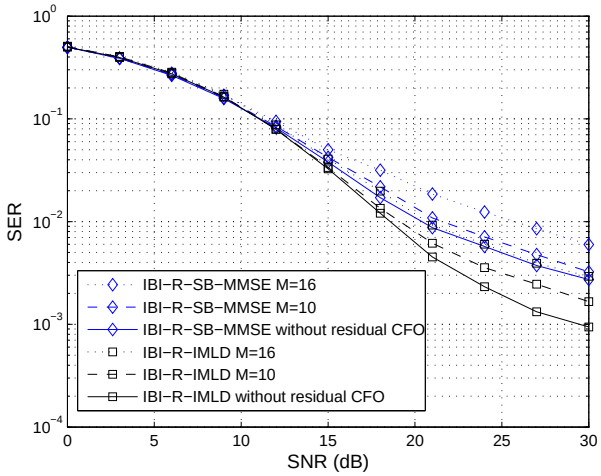

Figure 3.10: The performance of the proposed methods in the presence of the residual CFO from S-R links. The residual normalized CFO is modeled as normal distributed with variance 10^{-5}. The R-D CFO setting is $\varepsilon_1 = 0.1$, $\varepsilon_2 = -0.1$ and $\Delta\varepsilon = 0.2$. M is the number of blocks in a frame.

the number of blocks in a frame in order to keep the impact of the residual S-R CFO within an acceptable range. Fig. 3.10 depicts the performance of the IBI-R-SB-MMSE and IBI-R-IMLD methods in the presence of the residual S-R CFO. It can be seen that shorter frame yields better tolerance to the S-R residual CFO. However, we cannot have too short frames due to the synchronization overhead before the frame transmission. As a result, frame length has to be chosen carefully according to the implementation consideration and the average amount of S-R residual CFO.

3.6 Summary

A class of joint TD and FD interference mitigation methods has been proposed for the distributed Alamouti STBC coded AF cooperative OFDM system with multiple CFOs. Our study has analyzed two possible TD compensation schemes. The IBI-removal scheme decouples the STBC codeword completely which leads to subsequent low complexity decoding. However, the IBI-removal does not provide satisfactory performance when the CFO is large. With large CFO, the ICI-removal compensation with subsequent MIJMLD is proposed and shown to be effective. Therefore, with different amount of CFO, different approach can be employed depending on the performance requirement. In particular, with relatively small CFO, IBI-removal with

FD interference suppressing decoder can be considered to achieve satisfactory performance with much lower complexity. On the other hand, with relatively large CFO, the ICI-removal with MIJMLD can be employed to combat the severe interference.

Chapter 4

Optimal Timing Estimation at the Relay in OFDM based Two Way Relay Systems over Frequency Selective Channels

In this chapter, we are going to study the timing synchronization issue in the two way relay networks. Our study will focus on the scenario including two communicating terminals and multiple relay nodes in between of the two source nodes. The two source nodes do not have direct link to each other. The rest of the chapter is organized as follows. The motivation and related work are introduced in Section 4.1. Then signal model is presented in Section 4.2. The timing misalignment issue is illustrated in Section 4.3, and the interference power characterization is presented in Section 4.3 as well. Section 4.4 introduces the proposed timing estimator. The simulation results are presented in Section 4.5 and then Section 4.6 summaries the chapter.

4.1 Motivation and Related Work

A detailed implementation of cooperative communication has been first proposed by Laneman in [34, 35], followed by intensive research on the implementation of cooperative diversity. Efficient relaying strategies and distributed space time coding (DSTC) schemes are proposed to the OWRN transmission in [35, 48, 64, 22]. However, TWRN has not been well studied yet. The history of TWRN goes back to 1961

by Shannon [10], where the capacity analysis is provided. The capacity analysis of TWRN also appeared in [7, 58, 54]. The amplify-and-forward (AF) and decode-and-forward (DF) for OWRN are extended to half-duplex TWRN in [6]. Physical layer network coding for a two time slot transmission scheme is developed for TWRN in [50], where two communicating nodes are allowed to transmit simultaneously at the same frequency.

TWRN with orthogonal frequency division multiplexing (OFDM) signaling is studied in [19, 75, 11, 38, 23]. In [19], an ML channel estimation method is proposed for the TWRN with OFDM. An analog network coding scheme is proposed to achieve full diversity in [75] where multiple relay nodes are considered. Tone permutation and power allocation strategy at the relay node are studied in [11] assuming perfect channel state information (CSI) at the relay. Perfect timing and frequency synchronization are assumed in most of the existing work. However, synchronization in TWRN is not easy to acquire in practice. Carrier frequency offset (CFO) estimation is studied with one relay node between the terminal nodes in [38, 23]. The AF TWRN allows the two communicating source nodes to transmit at the same time in the first time slot. However, the time slot established at different nodes may not be accurately aligned in distributed relay networks. Together with the different propagation delays, signal misalignment may occur at the relay nodes. The work in [75] includes the signal misalignment into the design of the analog network coding, but only small amount of misalignment is considered which does not introduce timing-induced extra interference. When the signal misalignment is large, timing-induced extra interference is introduced and the amount of interference is dependent on the fast Fourier transform (FFT) window position. Therefore, it is necessary for the relay to take the signal misalignment into consideration in terms of the interference power when establishing the FFT window. To the best of our knowledge, this issue has not been well studied in the literature.

In this chapter, timing at the relay in OFDM based AF TWRN is investigated. We have derived the total interference power at the relay with different timing instants. Based on the total interference power, the optimal timing of the TWRN OFDM signal is defined as the timing point where the timing induced interference is minimized. An OFDM block is devoted for training purpose and the training blocks transmitted by the two terminals are superimposed at the relay. Based on the training block, a sliding window interference power estimator is developed and the timing position is determined according to the estimated interference power. The proposed sliding

window estimator approximates the interference power by a linear transformation of the observations at a given timing instant.

Notations: Vectors and matrices are boldface letters. The FFT size for OFDM block is denoted by N. $(\bullet^T)$ and $(\bullet^H)$ denote the transpose and the Hermitian transpose. $(*)$ is the linear convolution operation. $\mathbf{F}$ is the $N \times N$ discrete Fourier transform (DFT) matrix with $e^{-j2\pi(m-1)(n-1)/N}$ as its (m,n)th element, while $\mathbf{F}_L$ is taking the first L columns of $\mathbf{F}$. $diag(\mathbf{X})$ is a diagonal matrix with the vector $\mathbf{X}$ as its main diagonal. $\parallel \mathbf{A} \parallel$ is to take the Euclidean norm of the vector $\mathbf{A}$. $\mathbf{D}(m) = Diag\{e^{-j2\pi(k-1)m/N}\}$.

4.2 Signal Model

The two source nodes are denoted by $\mathbb{T}_1$ and $\mathbb{T}_2$. In AF TWRN, each transmission is divided equally into two phases, i.e., a multiple access (MA) phase and a broadcasting (BC) phase as shown in Fig. 4.1. In the MA phase, the two source nodes transmit data symbols according to their own time slot at the same time. Due to the half-duplex working pattern, each relay node has to store the signal samples received in the MA phase. Considering the fact that analog waveform cannot be stored, each relay node has to down-convert the radio frequency (RF) signal to the baseband and then store the baseband signal samples. In this case, the AF relay node has to establish an FFT window boundary to remove the cyclic prefix (CP) and store the superimposed OFDM signal block from $\mathbb{T}_1$ and $\mathbb{T}_2$. In the BC phase, each relay node re-inserts the cyclic prefix to the stored OFDM block in the MA phase and broadcasts to the two source nodes.

Denote the discrete channel impulse response (CIR) between $\mathbb{T}_1$ and the jth relay by $\mathbf{h}^{(j)} = [h_0^{(j)}, h_1^{(j)}, \dots, h_{C_j}^{(j)}]^T$ where C_j is the maximal delay spread of $\mathbf{h}^{(j)}$, and the channel between $\mathbb{T}_2$ and the jth relay by $\mathbf{g}^{(j)} = [g_0^{(j)}, g_1^{(j)}, \dots, g_{M_j}^{(j)}]^T$ where M_j is the maximal delay spread of $\mathbf{g}^{(j)}$. The channel defined above does not take the propagation delay into account, meaning that $h_0^{(j)}$ and $g_0^{(j)}$ are the first arriving paths. The corresponding frequency domain channel response for each channel is denoted by $\mathbf{H}_j$ and $\mathbf{G}_j$, which are diagonal matrices with $H_j(k,k) = \sum_{l=0}^{C_j} h_l^{(j)} e^{-j2\pi lk/N}$ and $G_j(k,k) = \sum_{l=0}^{M_j} g_l^{(j)} e^{-j2\pi lk/N}$. Due to the different propagation delay and the transmit time misalignment of the two source nodes, the signals of the two source nodes may have different time of arrival (ToA) at the relay. Combine the transmit time misalignment and the propagation delay into one delay term and denote it with $\tau_1^{(j)}$

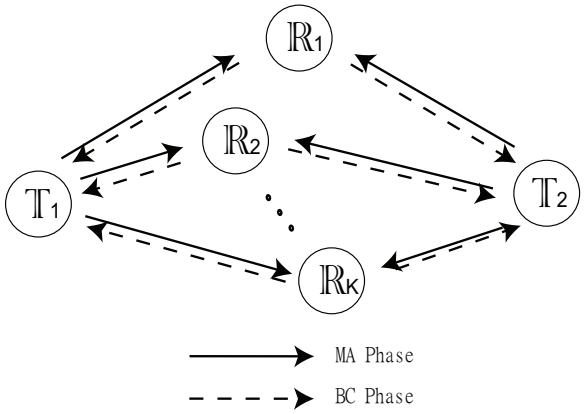

Figure 4.1: System Model.

and $\tau_2^{(j)}$ for $\mathbb{T}_1$ and $\mathbb{T}_2$ respectively, in sample intervals. Then the received signal at the jth relay can be written as

$$r_j(n) = \sum_{l=0}^{C_j} h_l^{(j)} x_1(n-l-\tau_1^{(j)}) + \sum_{l=0}^{M_j} g_l^{(j)} x_2(n-l-\tau_2^{(j)}) + \omega_j(n). \qquad (4.1)$$

It should be pointed out that the signal broadcast by each relay only experiences one channel to $\mathbb{T}_1$ or $\mathbb{T}_2$ in the BC phase. That means the OFDM block misalignment only comes from the MA transmission phase. For a TWRN with only one relay, the signal misalignment can be estimated and each source can adjust its time to align its signal arriving at the relay. However, when there are multiple relay nodes, this signal alignment cannot be guaranteed at all the relay nodes since the timing adjustment needed for different relay is different. Therefore, signal misalignment is inevitable in TWRN systems with multiple relays. In the presence of significant signal misalignment, how to establish the FFT window at each relay is crucial since the interference induced by signal misalignment is determined by the FFT window position.

4.3 Timing Misalignment of TWRN Signal

4.3.1 Signal Misalignment

Signal misalignment at the relay happens most of the time in multiple relay TWRN systems. The signals from different sources arrive at the relay node at different time instant. Therefore, the FFT window of the two signals are misaligned. For OFDM signal, it has been shown that the optimal time instant used to establish the FFT window is not a single timing point [41]. In particular, there is no timing-induced extra interference as long as the FFT window starts from a time instant in the inter-block interference (IBI) free region (IFR) of the CP. As a result, the interference power of the misaligned signal in TWRN systems depends on how the IFRs of the two source signals overlap and where to start the FFT window. We only look at one relay node because each relay performs timing, storing and broadcasting individually. Therefore, in the following we drop the relay index j since the processing for each relay is the same. Then the notations $\mathbf{h}^{(j)}$, $\mathbf{g}^{(j)}$, C_j, M_j, $\tau_1^{(j)}$, $\tau_2^{(j)}$, $\mathbf{H}_j$ and $\mathbf{G}_j$ are changed to $\mathbf{h}$, $\mathbf{g}$, C, M, τ_1, τ_2, $\mathbf{H}$ and $\mathbf{G}$.

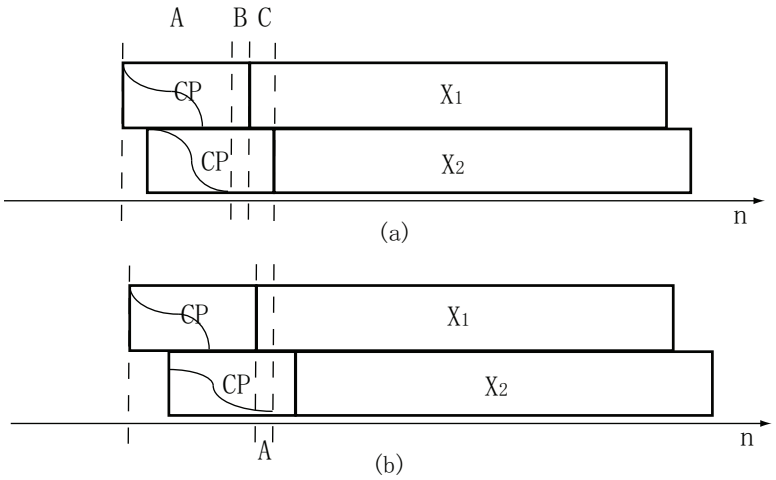

Figure 4.2: The received signal at $\mathbb{T}_1$.

Consider the case $\tau_2 > \tau_1$ which means in the MA phase the signal from $\mathbb{T}_2$ arrives later than that of $\mathbb{T}_1$. The received signal at the relay can be illustrated in Fig. 4.2 where $\mathbf{X}_1$ and $\mathbf{X}_2$ are the OFDM signal block from $\mathbb{T}_1$ and $\mathbb{T}_2$ respectively. In Fig. 4.2, part A and part B represent the IFR of the received block of $\mathbf{X}_1$ and $\mathbf{X}_2$ respectively. It can be seen that the IFRs of $\mathbf{X}_1$ and $\mathbf{X}_2$ overlap in Fig. 4.2(a). While in Fig. 4.2(b), there is no overlap between the two IFRs. Obviously the common part of the IFRs is good for establishing the FFT window. However, the overlap is not guaranteed. Generally, the existence of the overlap relies on (a) $C < N_g$, (b) $M < N_g$ and (c) $N_g > M + \tau_2 - \tau_1$. The conditions (a) and (b) can be easily satisfied since the guard interval is guaranteed larger than the channel dispersion. However, condition (c) cannot always be guaranteed.

Define $\Delta\tau = \tau_2 - \tau_1$. When $N_g < M + \Delta\tau$, there is no overlap between the IFRs of the two OFDM blocks as illustrated in Fig. 4.2(b). In this case, no matter where the FFT window is established, there is extra interference. In general, different FFT window establishment induces different amount of interference. However, the signal block misalignment induced interference for $\mathbf{X}_1$ and $\mathbf{X}_2$ can be characterized independently.

4.3.2 Interference Power Characterization

Given a relay node, consider the case $\tau_2 > \tau_1$ where the data block $\mathbf{X}_2$ from source $\mathbb{T}_2$ arrives later than the data block from source $\mathbb{T}_1$. Denote the start of the established FFT window in the relay node as θ, and let $\theta = 0$ represent the beginning of the

OFDM block of $\mathbf{X}_1$ excluding CP. Therefore, the signal block of $\mathbf{X}_2$ excluding CP starts from $\theta + \Delta\tau$. The frequency domain received signal at $\mathbb{R}$ in the MA phase can be written as

$$\mathbf{Y} = \tilde{\mathbf{H}}^{\theta}\mathbf{X}_1 + \tilde{\mathbf{G}}^{\theta+\Delta\tau}\mathbf{X}_2 + \mathbf{I}_1 + \mathbf{I}_2 + \mathbf{W} \tag{4.2}$$

where $\tilde{\mathbf{H}}^{\theta} = \mathbf{D}(\theta)\mathbf{H}$, $\tilde{\mathbf{G}}^{\theta+\Delta\tau} = \mathbf{D}(\theta+\Delta\tau)\mathbf{G}$, $\mathbf{I}_1$ and $\mathbf{I}_2$ are the interference component from $\mathbf{X}_1$ and $\mathbf{X}_2$ caused by inappropriate FFT window position, and $\mathbf{W}$ is the frequency domain noise term. Note that the diagonal channel response matrices $\tilde{\mathbf{H}}^{\theta}$ and $\tilde{\mathbf{G}}^{\theta+\Delta\tau}$ only have phase shift from $\mathbf{H}$ and $\mathbf{G}$. The timing error induced interference has been separated into $\mathbf{I}_1$ and $\mathbf{I}_2$ contributed by $\mathbf{X}_1$ and $\mathbf{X}_2$ respectively. $\mathbf{I}_i$ depends on θ, $\mathbf{h}$ and $\mathbf{X}_i$. For instance, if $C - N_g \leq \theta \leq 0$, $\mathbf{I}_1 = \mathbf{0}$. Then we can analyze the interference for $\mathbf{X}_1$ and $\mathbf{X}_2$ separately. Unlike the interference analysis of the timing offset in [67], we perform the interference analysis with instantaneous channel $\mathbf{h}$ and $\mathbf{g}$.

Consider the timing offset θ of $\mathbf{X}_1$. When $\theta > 0$, which means the FFT window starts to the right of the beginning of $\mathbf{X}_1$, the time domain received signal component of $\mathbf{X}_1$ can be written as

$$\tilde{\mathbf{y}}_1 = \mathbf{F}^H\tilde{\mathbf{H}}^{\theta}\mathbf{X}_1 + \tilde{\mathbf{\Theta}}^{\theta}\tilde{\mathbf{x}}_1^{\theta} \tag{4.3}$$

where

$$\begin{aligned}\tilde{\mathbf{x}}_1^{\theta} &= [\underbrace{0, ..., 0}_{N-\theta}, x_1^{\text{ne}}(-N_g) - x_1^{\text{cu}}(0),\ x_1^{\text{ne}}(-N_g+1) - x_1^{\text{cu}}(1),\ ..., \\ &\qquad x_1^{\text{ne}}(-N_g+\theta-1) - x_1^{\text{cu}}(\theta-1)]_{N\times 1}^T\end{aligned} \tag{4.4}$$

$$\tilde{\mathbf{\Theta}}^{\theta} = \begin{bmatrix} \mathbf{0}_{(N-\theta)\times(N-\theta)} & \mathbf{0}_{(N-\theta)\times\theta} \\ \mathbf{0}_{\theta\times(N-\theta)} & \begin{matrix} h_0 & 0 & \dots & 0 \\ h_1 & h_0 & \dots & 0 \\ \vdots & & \ddots & \vdots \\ h_{\theta-1} & & \dots & h_0 \end{matrix} \end{bmatrix}. \tag{4.5}$$

In (4.4), x_1^{ne} and x_1^{cu} are the time domain samples of the next OFDM symbol and the current OFDM symbol respectively. Thus, the first term in (4.4) is the desired signal component of $\mathbf{X}_1$ which is interference free and the second term in (4.4) represents the interference induced by imperfect timing. Then the interference in frequency domain can be obtained as $\mathbf{I}_1 = \mathbf{F}\tilde{\mathbf{\Theta}}^{\theta}\tilde{\mathbf{x}}_1^{\theta}$. Note that $\tilde{\mathbf{x}}_1^{\theta}$ has only last θ nonzero elements and

at the same time $\mathbf{F}\tilde{\mathbf{\Theta}}^{\theta}$ has only last θ nonzero columns. Let $\tilde{\mathbf{\Psi}}^{\theta} = \mathbf{F}\tilde{\mathbf{\Theta}}^{\theta}$, then the (k,n)th (the index starts from 0) element of $\tilde{\mathbf{\Psi}}^{\theta}$ can be given as

$$\tilde{\Psi}^{\theta}(k,n) = \begin{cases} 0, & n < N-\theta \\ \frac{1}{N}\sum_{m=n}^{N-1} h_1(m-n)e^{\frac{-j2\pi km}{N}}, & N-\theta \le n \le N-1 \end{cases}. \tag{4.6}$$

Then the average interference power on the kth subcarrier can be written as

$$\mathbb{E}\{I_1(k)\} = \sum_{n=N-\theta}^{N-1} |\tilde{\Psi}^{\theta}(k,n)|^2 \mathbb{E}\{|\tilde{x}_1^{\theta}(n)|^2\} = 2e_1 \sum_{n=N-\theta}^{N-1} |\tilde{\Psi}^{\theta}(k,n)|^2 \tag{4.7}$$

where e_1 is the average symbol energy of source $\mathbb{T}_1$.

In the case of $\theta < 0$, when $C - N_g < \theta < 0$, the FFT window falls into the IFR of $\mathbf{X}_1$. But the FFT falls out of the IFR of $\mathbf{X}_1$ if $\theta < C - N_g$. Then defining $\xi = C - N_g - \theta$, the received signal component of $\mathbf{X}_1$ can be written as

$$\bar{\mathbf{y}}_1 = \begin{cases} \mathbf{F}^H \bar{\mathbf{H}}^{\theta} \mathbf{X}_1 & \xi \le 0 \\ \mathbf{F}^H \bar{\mathbf{H}}^{\theta} \mathbf{X}_1 + \bar{\mathbf{\Theta}}^{\xi} \bar{\mathbf{x}}_1^{\xi} & \xi > 0 \end{cases} \tag{4.8}$$

where $\bar{\mathbf{\Theta}}^{\xi}\bar{\mathbf{x}}_1^{\xi}$ represents the interference term including the multipath component from the previous block and the missing multipath component of the current block and the definition of $\bar{\mathbf{\Theta}}^{\xi}$ and $\bar{\mathbf{x}}_1^{\xi}$ are given by

$$\begin{aligned} \bar{\mathbf{x}}_1^{\xi} =& [x_1^{\mathrm{pr}}(N-\xi) - x_1^{cu}(N-C),\ x_1^{\mathrm{pr}}(N-\xi+1) - x_1^{cu}(N-C+1),\ ..., \\ & x_1^{\mathrm{pr}}(N-1) - x_1^{cu}(N-N_g-1),\ \underbrace{0, ..., 0}_{N-\xi}]_{N\times 1}^{T} \end{aligned} \tag{4.9}$$

$$\bar{\mathbf{\Theta}}^{\xi} = \begin{bmatrix} h_{C-1} & h_{C-2} & \dots & h_{C-\xi} & \\ 0 & h_{C-1} & \dots & h_{C-\xi+1} & \mathbf{0}_{\xi\times(N-\xi)} \\ 0 & 0 & \ddots & \vdots & \\ 0 & 0 & \dots & h_{C-1} & \\ & \mathbf{0}_{(N-\xi)\times\xi} & & & \mathbf{0}_{(N-\xi)\times(N-\xi)} \end{bmatrix} \tag{4.10}$$

where x_1^{pr} is the time domain samples of the previous block. Then defining $\bar{\mathbf{\Psi}}^{\xi} = \mathbf{F}\bar{\mathbf{\Theta}}^{\xi}$, the average interference power in this case can be written as $\mathbb{E}\{|I_1(k)|^2\} =$

$2e_1\sum_{n=0}^{\xi-1}|\bar{\Psi}^{\xi}(k,n)|^2$.

In summary, the average interference power for $\mathbf{X}_1$ conditioned on θ can be written as

$$\mathbb{E}\{|I_1(k)|^2\} = \begin{cases} 2e_1\sum_{n=0}^{\xi-1}|\bar{\Psi}^{\xi}(k,n)|^2 & \theta < -N_g + C \\ 0 & -N_g + C \leq \theta \leq 0 \\ 2e_1\sum_{n=0}^{\theta-1}|\tilde{\Psi}^{\theta}(k,n)|^2 & \theta > 0 \end{cases} . \tag{4.11}$$

For $\mathbf{X}_2$, the timing error becomes $\theta - \Delta\tau$ since the OFDM block for $\mathbf{X}_2$ starts from $\Delta\tau$. As a result, the interference term $\mathbf{I}_2$ can be characterized following the same method. Specifically, replace e_1, θ, $\mathbf{h}$ and C in (4.11) with e_2, $\theta - \Delta\tau$, $\mathbf{g}$ and M.

The numerical result of the normalized total interference power with different FFT window positions is shown in Fig. 4.3, where the channel taps used are calculated using $h_l = \rho_1 e^{-0.1l}$ and $g_l = \rho_2 e^{-0.2l}$ where ρ_1 and ρ_2 are the normalizing factors. Since we only consider the integer part of the signal misalignment, the candidate timing positions are sample spaced. In Fig. 4.3, we assume $\mathbf{X}_2$ arrives later than $\mathbf{X}_1$. The curve with $\Delta\tau = 3$ is under the channel condition where $\mathbf{X}_1$ and $\mathbf{X}_2$ have overlapped IFR and the total interference power within the overlapped IFR is zero. On the other hand, the other curves in Fig. 4.3 are under the case where the IFRs of $\mathbf{X}_1$ and $\mathbf{X}_2$ do not overlap. Therefore, interference exists no matter where to establish the FFT window.

4.4 Timing at the Relay

In this section, the timing problem at each relay node is studied. Since different timing positions introduce different levels of interference power, it is important for the relay to establish the FFT window at the best position to forward better quality signal to the source nodes. The source nodes transmit preamble blocks before data blocks to assist synchronization and channel estimation. To save overhead, the two terminal nodes transmit the preamble simultaneously. Denote the training block of $\mathbb{T}_j$ with $\mathbf{P}_j$ $(N \times 1)$. Assume that the training symbols are known to each relay

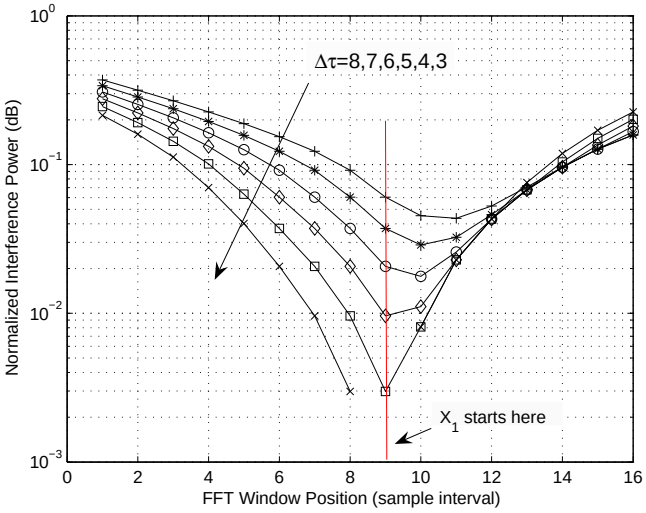

Figure 4.3: Normalized total interference power with different FFT window position. FFT size $N = 64$, $N_g = 8$, $C = 5$ and $M = 5$.

node and the relay node is able to achieve a coarse timing by auto-correlation based OFDM signal acquisition method using the periodic property of the training sequence [33, 27]. In this section, we assume $\mathbf{X}_2$ arrives later than $\mathbf{X}_1$, i.e., $\Delta\tau > 0$. The other case with $\Delta\tau < 0$ is symmetric and the proposed methods can be applied directly.

To determine where to establish the FFT window at the relay, a straightforward way is to estimate the timing offsets of the two signals. Then the FFT window can be easily established where the first arriving signal is. When the signal misalignment is significant, establishing the FFT window aligned to the first arriving signal may not be the optimal choice in terms of the total interference power. Therefore, in the case where the signal misalignment is significant, the timing induced interference power can be computed at each timing position according to the result in Section 4.3.2 and the relay should choose a position with the lowest timing induced interference to establish the FFT window for the subsequent OFDM data blocks.

4.4.1 Timing Offsets Estimation based Method

In this subsection, we introduce a method to estimate the timing offsets of $\mathbf{X}_1$ and $\mathbf{X}_2$ based on the received training block with a coarse timing. The timing offsets of $\mathbf{P}_1$ and $\mathbf{P}_2$ are denoted by θ_1 and $\theta_2 = \theta_1 + \Delta\tau$ respectively. Then the received time domain training block can be written as

$$\mathbf{y}_p = \tilde{\mathbf{H}}\mathbf{p}_1(\theta_1) + \tilde{\mathbf{G}}\mathbf{p}_2(\theta_2) + \boldsymbol{\nu} \tag{4.12}$$

where $\tilde{\mathbf{H}}$ and $\tilde{\mathbf{G}}$ are the $N \times N$ circulant Toeplitz channel matrices with $[\mathbf{h}^T\ \mathbf{0}_{1,N-C}]^T$ and $[\mathbf{g}^T\ \mathbf{0}_{1,N-M}]^T$ as the first columns, $\mathbf{p}_j(\theta_j)$ $(j = 1, 2)$ is the time domain training block cyclically shifted by the amount of θ_j and $\boldsymbol{\nu}$ is a $N \times 1$ vector containing the noise and interference. Performing FFT to $\mathbf{y}_p$, the frequency domain signal block can be written as

$$\mathbf{Y}_p = \mathbf{S}_1\mathbf{D}(\theta_1)\mathbf{F}_L\boldsymbol{\varpi}_L^{(1)} + \mathbf{S}_2\mathbf{D}(\theta_2)\mathbf{F}_L\boldsymbol{\varpi}_L^{(2)} + \mathbf{V} \tag{4.13}$$

where $\mathbf{S}_j = diag(\mathbf{P_j})$, $\boldsymbol{\varpi}_L^{(1)} = [\mathbf{h}^T \quad \mathbf{0}_{1\times(L-C)}]^T$, $\boldsymbol{\varpi}_L^{(2)} = [\mathbf{g}^T \quad \mathbf{0}_{1\times(L-M)}]^T$, L is an integer used for channel length when the actual channel length knowledge is not available. Therefore L should be sufficiently large such that $L > max(C, M)$, and $\mathbf{V}$ is the $N \times 1$ frequency domain noise and interference vector. Defining $\mathbf{Q}(\theta_1, \theta_2) =$

$[\mathbf{S}_1\mathbf{D}(\theta_1)\mathbf{F}_L \quad \mathbf{S}_2\mathbf{D}(\theta_2)\mathbf{F}_L]$ and $\boldsymbol{\varpi} = [\boldsymbol{\varpi}_L^{(1)T} \quad \boldsymbol{\varpi}_L^{(2)T}]^T$, eq. (4.13) can be rewritten as

$$\mathbf{Y}_p = \mathbf{Q}(\theta_1, \theta_2)\boldsymbol{\varpi} + \mathbf{V}. \tag{4.14}$$

The unknowns to be estimated in (4.14) include θ_j $(j = 1, 2)$ and $\boldsymbol{\varpi}$. We model the noise plus interference term $\mathbf{V}$ as Gaussian distributed. Then the joint ML estimator can be employed as

$$(\hat{\theta}_1,\ \hat{\theta}_2,\ \hat{\boldsymbol{\varpi}}) = \arg\min_{\tilde{\theta}_1, \tilde{\theta}_2 \tilde{\boldsymbol{\varpi}}} \parallel \mathbf{Y}_p - \tilde{\mathbf{Q}}\tilde{\boldsymbol{\varpi}} \parallel \tag{4.15}$$

where $\tilde{\mathbf{Q}} = \mathbf{Q}(\tilde{\theta}_1, \tilde{\theta}_2)$ and $\tilde{\boldsymbol{\varpi}}$ varies in the $2L$ dimension complex space C^{2L}. Fixing $\tilde{\theta}_j$ $(j = 1, 2)$, the ML estimation of $\boldsymbol{\varpi}$ is given by [39]

$$\hat{\boldsymbol{\varpi}} = (\tilde{\mathbf{Q}}^H\tilde{\mathbf{Q}})^{-1}\tilde{\mathbf{Q}}^H\mathbf{Y}_p. \tag{4.16}$$

Taking (4.16) into (4.15), the estimation of θ_j $(j = 1, 2)$ can be given by

$$(\hat{\theta}_1\ \hat{\theta}_2) = \arg\max_{\tilde{\theta}_1 \tilde{\theta}_2} \mathcal{M}(\tilde{\theta}_1, \tilde{\theta}_2) \tag{4.17}$$

where

$$\mathcal{M}(\tilde{\theta}_1, \tilde{\theta}_2) = \mathbf{Y}_p^H\tilde{\mathbf{Q}}(\tilde{\mathbf{Q}}^H\tilde{\mathbf{Q}})^{-1}\tilde{\mathbf{Q}}^H\mathbf{Y}_p. \tag{4.18}$$

The estimation in (4.17) involves a two dimensional search over $\tilde{\theta}_1$ and $\tilde{\theta}_2$. Considering θ_1 and θ_2 are integers, the searching complexity is not too high. The searching region of $\tilde{\theta}_j$ $(j = 1, 2)$ can be written as $[-\eta, \eta]$, where η should be able to cover the coarse timing error of both channels. After obtaining the estimation of θ_1 and θ_2, the channel estimation can be carried out through (4.16). Therefore, the proposed method is actually a joint timing and channel estimation scheme with superimposed training blocks from $\mathbb{T}_1$ and $\mathbb{T}_2$.

The timing offsets estimator in (4.17) is based on a block of observation which is usually established by a coarse timing. The variance of the noise plus interference term $\mathbf{V}$ in (4.13) is dependent on the timing offsets θ_j $(j = 1, 2)$. Therefore, if the timing offsets of the established FFT window are large, the variance of the noise plus interference term is significant which will result in a poor estimation performance. Next, we will present a sliding window method to determine the best sampling position.

4.4.2 Sliding Window Estimator

Instead of performing estimation on a fixed block of observation, we slide the block along the received samples in order to take more samples into consideration. At each position, we will have a block of observations based on which the interference power estimation can be performed.

Denote the start of $\mathbf{P}_1$ with d, and hence $\mathbf{P}_2$ starts from $d + \Delta\tau$. Then denote the start of the sliding window with $\tilde{d}$. Given a $\tilde{d}$, the frequency domain signal in the sliding window can be written as

$$\mathbf{Y}_p(\tilde{d}) = \mathbf{S}_1\mathbf{D}(\tilde{d} - d)\mathbf{F}_L\boldsymbol{\varpi}_L^{(1)} + \mathbf{S}_2\mathbf{D}(\tilde{d} - d - \Delta\tau)\mathbf{F}_L\boldsymbol{\varpi}_L^{(2)} + \mathbf{I}(\tilde{d}) + \mathbf{V}(\tilde{d}) \tag{4.19}$$

where $\mathbf{I}(\tilde{d})$ and $\mathbf{V}(\tilde{d})$ are the interference vector and noise vector respectively with both conditioned on $\tilde{d}$. The interference vector $\mathbf{I}(\tilde{d})$ includes the timing induced interference from both $\mathbf{P}_1$ and $\mathbf{P}_2$ and the power is determined by the position of $\tilde{d}$. The idea is to find a $\tilde{d}$ that minimizes the interference power, which will be the optimal timing point for the misaligned signal. Then we need a way to measure the interference power in terms of $\tilde{d}$. Looking at (4.19), we want to take $\tilde{d}$ into the channel vector.

If $\tilde{d} \leq d$, we define

$$\begin{aligned}
\boldsymbol{\varpi}_L^{(1)}(\tilde{d}) &= [\mathbf{0}_{1\times(d-\tilde{d})} \quad \boldsymbol{\varpi}^{(1)T} \quad \mathbf{0}_{1\times(L-d+\tilde{d}-C)}]^T \\
\boldsymbol{\varpi}_L^{(2)}(\tilde{d}) &= [\mathbf{0}_{1\times(d+\Delta\tau-\tilde{d})} \quad \boldsymbol{\varpi}^{(2)T} \quad \mathbf{0}_{1\times(L-d-\Delta\tau+\tilde{d}-M)}]^T
\end{aligned} \tag{4.20}$$

with a sufficiently large L. Then (4.19) can be rewritten as

$$\mathbf{Y}_p(\tilde{d}) = \mathbf{S}_1\mathbf{F}_L\boldsymbol{\varpi}_L^{(1)}(\tilde{d}) + \mathbf{S}_2\mathbf{F}_L\boldsymbol{\varpi}_L^{(2)}(\tilde{d}) + \mathbf{I}(\tilde{d}) + \mathbf{V}(\tilde{d}). \tag{4.21}$$

where $\boldsymbol{\varpi}_L^{(1)}(\tilde{d})$ and $\boldsymbol{\varpi}_L^{(2)}(\tilde{d})$ are the only unknown parameters to be estimated based on $\mathbf{Y}_p(\tilde{d})$.

On the other hand, when $\tilde{d} > d$, the channel vector for $\mathbf{P}_1$ should be circularly shifted as

$$\boldsymbol{\varpi}_N^{(1)}(\tilde{d}) = [\mathbf{h}_{\tilde{d}-d}, ..., \mathbf{h}_C, \ \mathbf{0}_{1\times(N-C)}, \mathbf{h}_0, ..., \mathbf{h}_{\tilde{d}-d-1}]^T \tag{4.22}$$

which is an $N \times 1$ vector. In order to bound the channel vector with L taps, we drop the zero elements in $\boldsymbol{\varpi}_N^{(1)}(\tilde{d})$ and use L_a and L_b to bound the head part of $\boldsymbol{\varpi}_N^{(1)}(\tilde{d})$ and the tail part of $\boldsymbol{\varpi}_N^{(1)}(\tilde{d})$ respectively ($L_a + L_b = L$). As a result, the channel

vector is rewritten as a $(L_a + L_b) \times 1$ vector $\boldsymbol{\varpi}_L^{(1)}$, and the frequency domain response can be written as $[\mathbf{F}_{L_a}\ \tilde{\mathbf{F}}_{L_b}]\boldsymbol{\varpi}_L^{(1)}$, where $\tilde{\mathbf{F}}_{L_b}$ is an $N \times L_b$ matrix taking the last L_b columns of $\mathbf{F}$. Similarly for $\mathbf{P}_2$, then (4.19) can be rewritten as

$$\mathbf{Y}_p(\tilde{d}) = \mathbf{S}_1[\mathbf{F}_{L_a}\ \tilde{\mathbf{F}}_{L_b}]\boldsymbol{\varpi}_L^{(1)}(\tilde{d}) + \mathbf{S}_2[\mathbf{F}_{L_a}\ \tilde{\mathbf{F}}_{L_b}]\boldsymbol{\varpi}_L^{(2)}(\tilde{d}) + \mathbf{I}(\tilde{d}) + \mathbf{V}(\tilde{d}). \tag{4.23}$$

Define $\boldsymbol{\varpi}(\tilde{d}) = [\boldsymbol{\varpi}_L^{(1)T}(\tilde{d}) \quad \boldsymbol{\varpi}_L^{(2)T}(\tilde{d})]^T$ and

$$\boldsymbol{\mathcal{S}} = \begin{cases} [\mathbf{S}_1\mathbf{F}_L\ \mathbf{S}_2\mathbf{F}_L] & \tilde{d} \le d \\ [\mathbf{S}_1[\mathbf{F}_{L_a}\ \tilde{\mathbf{F}}_{L_b}]\ \mathbf{S}_2[\mathbf{F}_{L_a}\ \tilde{\mathbf{F}}_{L_b}]] & \tilde{d} > d. \end{cases} \tag{4.24}$$

Then (4.21) and (4.23) can be written as

$$\mathbf{Y}_p(\tilde{d}) = \boldsymbol{\mathcal{S}}\boldsymbol{\varpi}(\tilde{d}) + \mathbf{I}(\tilde{d}) + \mathbf{V}(\tilde{d}). \tag{4.25}$$

Treating the interference term as noise as well, the ML estimation of the channel impulse response at location $\tilde{d}$ can be given as

$$\hat{\boldsymbol{\varpi}}(\tilde{d}) = (\boldsymbol{\mathcal{S}}^H\boldsymbol{\mathcal{S}})^{-1}\boldsymbol{\mathcal{S}}^H\mathbf{Y}_p(\tilde{d}). \tag{4.26}$$

Substituting (4.26) into (4.25), (4.25) can be written as

$$\mathbf{Y}_p(\tilde{d}) \approx \boldsymbol{\mathcal{S}}(\boldsymbol{\mathcal{S}}^H\boldsymbol{\mathcal{S}})^{-1}\boldsymbol{\mathcal{S}}^H\mathbf{Y}_p(\tilde{d}) + \tilde{\mathbf{V}}(\tilde{d}) \tag{4.27}$$

where $\tilde{\mathbf{V}}(\tilde{d})$ is the combined interference plus noise term as $\tilde{\mathbf{V}}(\tilde{d}) = \mathbf{I}(\tilde{d}) + \mathbf{V}(\tilde{d})$. Then the total interference plus noise power can be estimated as

$$\Upsilon_I(\tilde{d}) = \| \mathbf{Y}_p(\tilde{d}) - \boldsymbol{\mathcal{S}}(\boldsymbol{\mathcal{S}}^H\boldsymbol{\mathcal{S}})^{-1}\boldsymbol{\mathcal{S}}^H\mathbf{Y}_p(\tilde{d}) \|^2 . \tag{4.28}$$

The power of the interference plus noise term varies with $\tilde{d}$ and the optimal timing point can be found at $\tilde{d}$ which minimizes the total interference plus noise power in (4.28) as

$$\hat{d} = \underset{\tilde{d} \in [d_c - \varepsilon, d_c + \varepsilon]}{\arg\min}\ \Upsilon_I(\tilde{d}) \tag{4.29}$$

where $[d_c - \varepsilon, d_c + \varepsilon]$ is the region to search for the minimum (d_c is the coarse timing estimation).

The key element in the estimator is the matrix $\boldsymbol{\mathcal{S}}$ which is dependent on $\tilde{d} > d$

or $\tilde{d} \leq d$ as in (4.24). d is something that is not available. However, recognizing that our goal is to find the optimal timing point, we only have to consider how the channel vectors should be bounded at the optimal timing point. Generally, this will depend on whether the IFRs of the two source signals overlap. If the IFRs overlap, the optimal timing point is always within the overlapped IFR. That means we can use the form in (4.20) to bound the channel vectors in this case. Then $\boldsymbol{\mathcal{S}} = [\mathbf{S}_1\mathbf{F}_L$ $\mathbf{S}_2\mathbf{F}_L]$. Otherwise, we have to use $\boldsymbol{\mathcal{S}} = [\mathbf{S}_1[\mathbf{F}_{L_a}\ \tilde{\mathbf{F}}_{L_b}]\ \mathbf{S}_2[\mathbf{F}_{L_a}\ \tilde{\mathbf{F}}_{L_b}]]$. Moreover, it can be found that the case with $\tilde{d} \leq d$ is a subset of $\tilde{d} > d$. Since if we take $L_a = L$, then the lower case in (4.24) is adding $2L_b$ more columns to the upper case. That means we can always use the latter method to construct $\boldsymbol{\mathcal{S}}$ even without the overlap condition information. However, we will show in Section 4.5 that closer bounding of the channel vector provides better performance. In the following, we assume the overlap condition information of the the IFR is available for convenience of comparison.

4.5 Performance Evaluation

In this section, we evaluate the proposed sliding window timing estimator through simulation. We set the FFT size $N = 256$ and the CP length $N_g = 16$. The multipath channel is modeled the same way as in [40], i.e., the discrete channel taps are modeled as independent and circularly symmetric Gaussian random variables with zero-mean (Rayleigh fading) and with exponential power delay profile

$$\begin{aligned} E\{|h_l|^2\} &= \rho_1 e^{-\zeta_1 l} \quad l = 0, 1, ..., C \\ E\{|g_l|^2\} &= \rho_2 e^{-\zeta_2 l} \quad l = 0, 1, ..., M \end{aligned} \tag{4.30}$$

where ζ_j is the tap power decaying factor and ρ_j is chosen such that the channel power is normalized to unity. In the simulation, we set the power decaying factors to be $\zeta_1 = \zeta_2 = 0.1$. Similar to the above analysis, we assume that $\mathbf{X}_2$ arrives later than $\mathbf{X}_1$. $\mathbf{P}_1$ and $\mathbf{P}_2$ in the simulation are random BPSK symbol blocks.

4.5.1 Small Signal Misalignment

Consider the case where the IBI-free regions for $\mathbf{X}_1$ and $\mathbf{X}_2$ overlap, i.e., $\Delta\tau + M < N_g$. In this case, we evaluate the estimator in (4.29) in terms of the miss timing probability. The miss timing event is defined as the start of FFT window is out of the overlapped

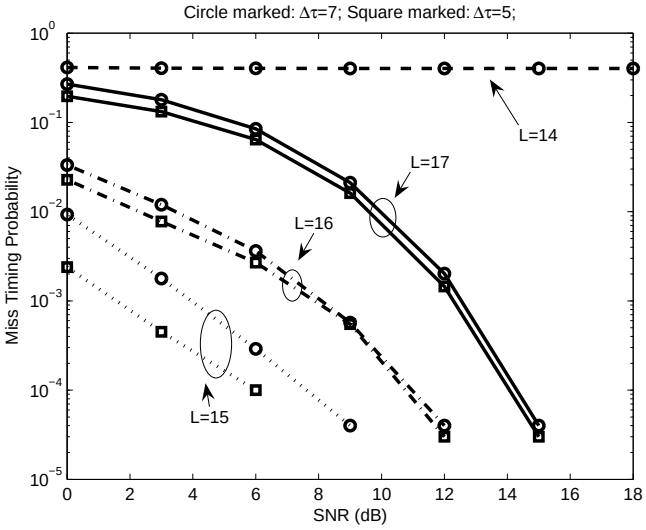

Figure 4.4: Miss timing probability of the proposed estimator in (4.29) in different channel environments. The searching region parameter in (4.29) is $\varepsilon = N_g$.

portion of the IBI-free regions. The simulation result is averaged over 1000 channel realizations with each channel realization repeating 100 times. Fig. 4.4 shows the miss timing probability with different channel parameters. In Fig. 4.4, the channel length for both channels are set to be $C = M = 8$, and the relay has no knowledge on the channel length. Therefore, the relay has to choose a sufficiently long vector to accommodate the channel length and $\Delta\tau$. Specifically, when the block exactly starts from the beginning of $\mathbf{X}_1$, $\mathbf{h}$ starts from $\boldsymbol{\varpi}_L^{(1)}(0)$ and $\mathbf{g}$ starts from $\boldsymbol{\varpi}_L^{(2)}(\Delta\tau)$. In this case, the CIR vector cannot be shorter than $M + \Delta\tau$. Considering the amount of misalignment $\Delta\tau$ is unknown to the relay, the relay has to choose a sufficiently large CIR vector length to be on the safe side.

If we vary L, it can been seen that the performance varies with L. The smaller L is, the better the performance as long as $L \geq M + \Delta\tau$. However, the estimator does not work when $L < M + \Delta\tau$. Therefore, to maintain a satisfactory performance for different channel conditions, L has to be chosen carefully. On the other hand, if the channel length and the misalignment knowledge are known to the relay, the relay could choose the smallest L to obtain the optimal performance.

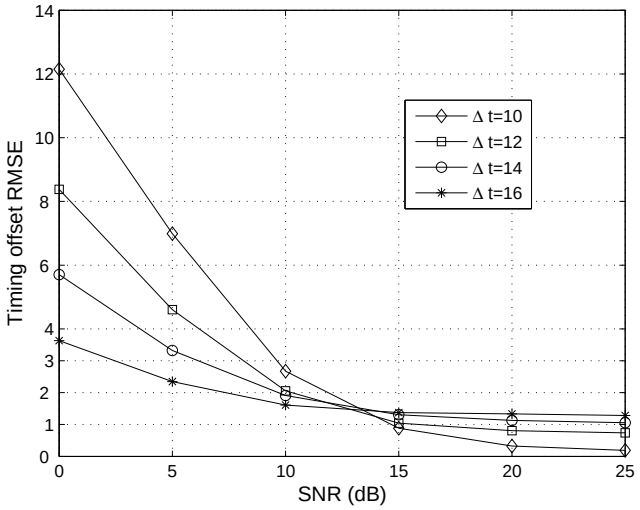

Figure 4.5: RMSE performance of the timing estimator under significant signal misalignments.

4.5.2 Significant Signal Misalignment

When significant misalignment happens between the two arriving signal blocks, the timing induced interference is inevitable according to the analysis in Section 4.3. In this case, there is an optimal FFT window position that minimizes the timing induced interference power. For each channel realization and $\Delta\tau$ value, we use the result in Section 4.3 to calculate the total timing induced interference power and find the optimal timing instant theoretically. Then the performance of the proposed estimator is evaluated in terms of timing offset of the estimated timing instant from the optimal instant. We examine the root mean square error (RMSE) of the timing estimator, which gives a statistical result on the average of timing estimation away from the calculated optimal instant. In this case, the interference plus noise power estimator in (4.28) has to use the lower case constructor in (4.24) for $\boldsymbol{\mathcal{S}}$, therefore L_a and L_b have to be decided. Without the knowledge of the channel length and the amount of misalignment, we choose sufficiently large L_a and L_b. In Fig. 4.5, the RMSE of timing offset with different amounts of misalignment is depicted. Assuming no channel length knowledge, we set $L_a = 24$ and $L_b = 5$ to deal with different conditions. It can be seen that as the SNR increases, the RMSE of timing offset drops to below 2 for even $\Delta\tau = 16$ and below 1 for smaller $\Delta\tau$.

The timing offset RMSE performance with different length of channel vector is

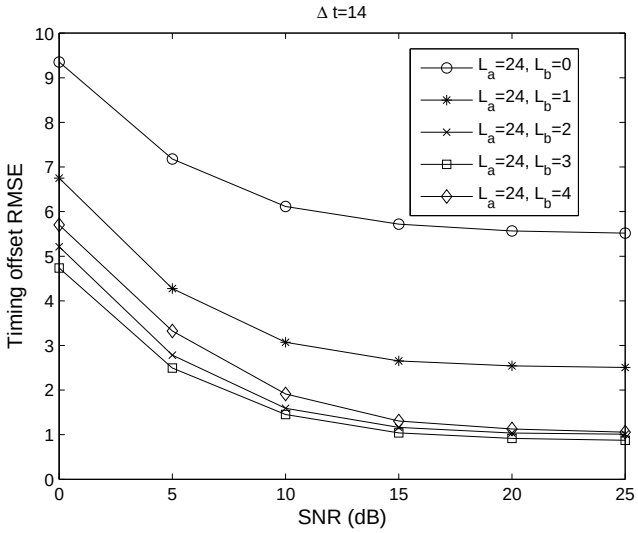

Figure 4.6: RMSE performance of the timing estimator with different channel length parameters, $\Delta t = 14$.

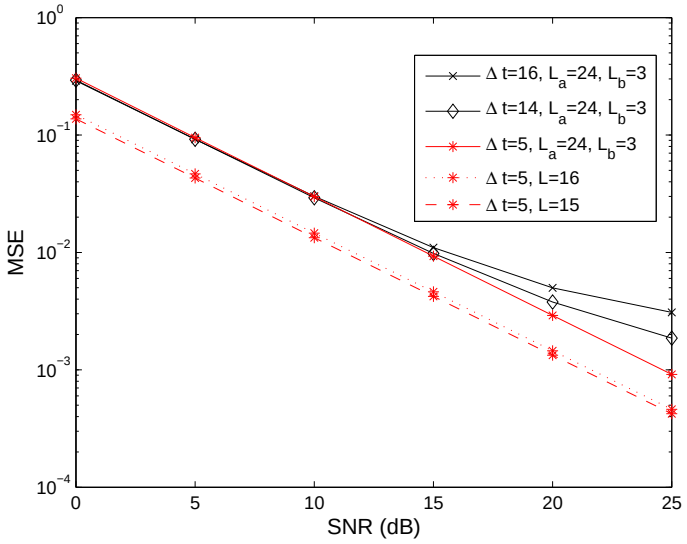

Figure 4.7: MSE performance of the channel estimation using (4.26) based on the timing estimation result.

depicted in Fig. 4.6. Setting $L_b = 0$ is equivalent to reduce the weighting matrix form of the lower case of (4.24) to the upper case form. We can see that $\boldsymbol{\mathcal{S}}$ is not able to deal with significant signal misalignment, since timing after the arrival of $\mathbf{X}_1$ is not allowed in this model. However, since most of the channel paths are located within the L_a part, L_b can be small. It can be seen that $L_b = 3$ achieves the best performance, and further increasing L_b degrades the performance.

4.5.3 Channel Estimation at the Relay

Although the AF relays do not decode the message, channel estimation at the relay is sometimes necessary in performance enhancing schemes such as subcarrier selection or distributed beamforming. In our case, the channel estimation can be performed based on the timing estimation result by (4.26). Therefore, the channel estimation performance depends on the timing performance significantly. We examine the performance of the channel estimator in (4.26) in terms of mean square error (MSE). A result of the evaluation is shown in Fig. 4.7. It is found that the channel estimation performance is affected by the length of the channel vector. The performance is better with closer bounding of the channel vector over the actual channel under the same channel condition.

4.6 Summary

In this chapter, the timing issue in OFDM based AF TWRN systems has been studied. The inherent signal misalignment problem in TWRN system introduces interference at the relay if the misalignment is significant. The total interference power at different timing positions has been derived and the optimal timing position is where the total interference power is minimized. Based on the superimposed training blocks, a linear method to measure the total interference power at different timing position is designed. In other words, the timing estimator performs total interference power estimation to locate the optimal timing position. Finally, the performance of the timing estimator is evaluated by simulation.

Chapter 5

Multi-Relay Delay Estimation for Cooperative DF Relaying over Fading Channels

So far, we have studied the synchronization issues for OFDM based cooperative transmission in Chapters 3 and 4. In this chapter, timing synchronization for narrow band signal over fading channels in cooperative communication scenarios will be discussed. As we know, the symbol duration of a narrow band signal is much longer than that of the a wideband OFDM based signal. Therefore, timing synchronization is no longer limited to the symbol level but down to the sub-symbol level. As introduced in Chapter 1, the signal misalignment within one symbol duration must be taken care of in order to reduce the ISI in a cooperative scenario.

5.1 Overview and Related Works

In typical two-hop cooperative communications, the AF relays amplify the received signal and forward to the destination while the DF relays decode the received signal, re-encode and then forward to the destination. Both AF and DF cooperative communications have been shown to be efficient. However, most of the current results on cooperative communications assume perfect synchronization at the relay and destination, which in real world is not a practical assumption due to the distributed nature of the network. Synchronization issues including performance analysis, timing estimation and compensation have not been well covered yet in the existing literature.

The impact of synchronization errors on the performance of cooperative multiple input multiple output (MIMO) systems has been studied in [53] under Rayleigh fading channels, where it is shown that the synchronization error at the destination introduces inter-symbol interference (ISI) as well as poor channel state information (CSI) estimation. Schemes for combating the synchronization errors have been proposed in [66, 63, 61, 20]. Most of the schemes for combating the synchronization error in cooperative systems are based on distributed space time coding (DSTC) [66, 61, 20], which try to overcome the synchronization error by special code structure. A time reversal space time code (TR-STC) and an orthogonal frequency division multiplexing (OFDM) space time coding (ST-OFDM) are proposed to combat synchronization errors in [66]. A space time block coding (STBC) based on a special frame-based multi-transmission scheme with packet-wise encoding has been proposed in [61], which is shown to be synchronization error tolerable. In [20], an STBC scheme has been proposed with OFDM modulation considering the imperfect synchronization in both timing and frequency. A parallel interference cancellation (PIC) method has been proposed in [63] to suppress the interference introduced by the synchronization error.

Synchronization algorithms for cooperative communications have been proposed in [43, 42, 62]. The method in [43] is designed for network time synchronization, which is the problem of synchronizing the local time of all the distributed nodes in a network. It has to be pointed out that network time synchronization is different from the timing synchronization in the signal detection stage, since the latter is to estimate the arrival of the desired signal. Synchronization methods for signal detection in cooperative communications can be found in [42, 62], where [42] is for carrier frequency offset (CFO) estimation and [62] is for the timing synchronization of DF cooperative transmission. A maximum likelihood (ML) multiple delay estimation method has been proposed in [62], where the signals from different relays experience different propagation delays. The ML estimator in [62] requires an exhaustive search over the possible range and the number of searches is determined by the step size and the number of relays. The complexity of the ML estimator is prohibitively high when the step size is small or the number of relays is large. In this chapter, a correlation based timing estimator for the multiple access (MA) phase of the DF cooperative transmission will be presented. The proposed estimator is a correlation based suboptimal estimator with some performance sacrifice, but it saves substantial complexity compared to the ML estimator.

The remainder of the chapter is organized as follows. Section 5.2 describes the signal model and the existing ML timing estimator. The proposed method is introduced and analyzed in Section 5.3. In Section 5.4, the performance of the proposed estimator is evaluated by simulation. Finally Section 5.5 summaries the chapter.

5.2 ML Timing Estimation

The system under consideration comprises of one source, K relays and one destination. The transmission is divided into 2 phases, i.e., the broadcast (BC) phase and the MA phase. In BC phase, the source broadcasts to the K relays and we assume the K relays successfully decode the message. In the MA phase, there are several cooperation schemes in order to achieve the diversity. Time slot divided relaying scheme needs the relays to forward the message within different time slots. Frequency divided relaying scheme requires that the relays transmit with different carrier frequencies. Distributed beamforming can also be employed where the relays transmit at the same time and frequency with the signal weighed so that they add constructively with the same phase at the destination. Special DSTC design also enables the simultaneous transmission of the relays. In this study, we only consider the synchronization stage before data transmission where the K relays transmit the training signal simultaneously to the destination without any processing since the channel state information (CSI) is not available. At the destination, the received signal from the kth relay is written as [62]

$$r_k(t) = h_k \sum_{i=-D}^{N_s+D-1} x_k(i) g(t - iT - \epsilon_k T) \tag{5.1}$$

where $x_k(i)$ is the ith training symbol of the kth relay, h_k is the channel response between the kth relay and the destination, T is the symbol interval, $g(t)$ is the pulse shaping filter with finite duration ($t \in [-DT,\ DT]$), N_s is the number of symbols for observation and ϵ_k is the normalized (by T) propagation delay of the kth relay. The received signal at the destination is oversampled at the rate of Q (≥ 2) samples per symbol, therefore the sampling interval is $T_s = T/Q$. Then the received discrete signal from each relay can be written as

$$\mathbf{d}_k = h_k \mathbf{A}_{\epsilon_k} \mathbf{x}_k + \mathbf{w} \tag{5.2}$$

where

$$\begin{aligned}
\mathbf{d}_k &\triangleq [r_k(0), r_k(T_s), ..., r_k((N_sQ-1)T_s)]^T \\
\mathbf{A}_{\epsilon_k} &\triangleq [\mathbf{a}_{-D}(\epsilon_k), ..., \mathbf{a}_0(\epsilon_k), ..., \mathbf{a}_{N_s+D-1}(\epsilon_k)] \\
\mathbf{a}_i(\epsilon_k) &\triangleq [g(-iT-\epsilon_kT), g(-iT+T_s-\epsilon_kT), ..., g(-iT+(N_sQ-1)T_s-\epsilon_kT)]^T \\
\mathbf{x}_k &\triangleq [x_k(-D), ..., x_k(0), ..., x_k(N_s+D-1)]^T. \qquad (5.3)
\end{aligned}$$

Then the observed discrete signal at the destination can be written as

$$\mathbf{d} = \sum_{k=1}^{K} \mathbf{d}_k + \mathbf{w} \qquad (5.4)$$

where $\mathbf{w}$ is the $N_sQ \times 1$ additive white Gaussian noise (AWGN) vector. Substituting (5.2) into (5.4), (5.4) can be written as

$$\mathbf{d} = \mathbf{\Omega}_{\boldsymbol{\epsilon}}\mathbf{H} + \mathbf{w} \qquad (5.5)$$

where $\mathbf{\Omega}_{\boldsymbol{\epsilon}} = [\mathbf{A}_{\epsilon_1}\mathbf{x}_1\ \mathbf{A}_{\epsilon_2}\mathbf{x}_2\ ...\mathbf{A}_{\epsilon_K}\mathbf{x}_K]$ and $\mathbf{H} = [h_1, h_2, \ldots, h_K]^T$. Then the ML estimation of the delays $\boldsymbol{\epsilon} = [\epsilon_1, \epsilon_2, ..., \epsilon_K]$ can be given by [62]

$$\hat{\boldsymbol{\epsilon}} = \arg\max_{\boldsymbol{\epsilon}} \Lambda(\boldsymbol{\epsilon}) \qquad (5.6)$$

where

$$\Lambda(\boldsymbol{\epsilon}) = \|\mathbf{\Omega}_{\boldsymbol{\epsilon}}(\mathbf{\Omega}_{\boldsymbol{\epsilon}}^H\mathbf{\Omega}_{\boldsymbol{\epsilon}})^{-1}\mathbf{\Omega}_{\boldsymbol{\epsilon}}^H\mathbf{d}\|^2. \qquad (5.7)$$

The complexity of the ML estimator depends on the number of relays K and the desired estimation resolution which is reflected by the search step size $\Delta\epsilon$ in the ML estimator. For instance, if the desired estimation resolution is $0.01T$ (normalized resolution is $\Delta\epsilon = 0.01$), (5.7) has to be computed 100^K times for K relays. Detailed complexity analysis will be given in the Section 5.3.2. It is obvious that the exhaustive search in the ML estimation in [62] is not practical in real time processing. Next, we will present a low complexity correlation based estimator.

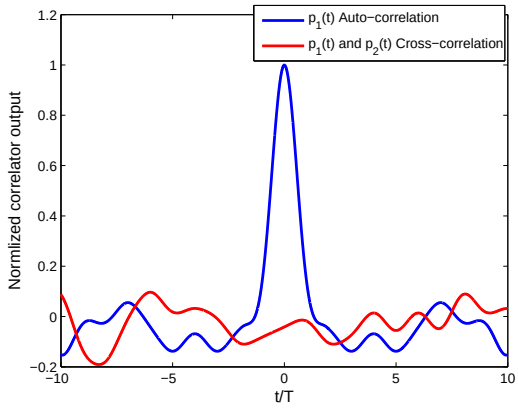

Figure 5.1: The auto-correlation and cross-correlation of $p_k(t)$.

5.3 Correlation Based Timing Estimator

5.3.1 Algorithm Description

The proposed low complexity method is based on the correlation result between the received signal and each relay's template waveform. Given an observation vector $\mathbf{d}$ in (5.4), the proposed estimator consists of 2 steps, i.e., interpolation and correlation. The interpolation is performed once per observation for a desired estimation resolution and the correlation is performed on a per relay basis. In the proposed method, $\mathbf{x}_k$ at each relay is required to be a Pseudorandom Noise (PN) sequence with length N_s. In addition, the PN sequences for the relays should have low cross-correlation. The analog baseband signal for the kth relay's PN sequence can be written as

$$p_k(t) = \sum_{n=0}^{N_s-1} x_k(n) g(t - nT - DT). \tag{5.8}$$

The continuous time correlation of $p_k(t)$ is shown in Fig. 5.1, where an m-sequence is used. We can see that the auto-correlation reaches the peak when τ is exactly 0. As a result, if the delay for relay k is $\epsilon_k T$, the peak of the auto-correlation for $p_k(t)$ should appear at $\epsilon_k T$. Therefore, correlating the received signal with each relay's template PN waveform can be used to estimate the delay for each relay separately.

According to (5.8), the received signal at the destination can be written as

$$r(t) = \sum_{k=1}^{K} h_k \sum_{n=0}^{N_s-1} x_k(n) g(t - nT - DT - \epsilon_k T) + w(t) \tag{5.9}$$

where $w(t)$ is the noise. Denote the original oversampled signal under observation with $d(n)$ $(0 < n < N_o)$, where N_o is the observation length and $N_o > (N_s + 2D)Q$ (Since the signal from different relays are misaligned). We assume that the observation interval is long enough to accommodate all the relays' arriving signal with different delays. Then $d(n)$ can be written as

$$d(n) = r(nT_S) = \sum_{k=1}^{K} h_k \sum_{i=0}^{N_s-1} x_k(i) g(n\frac{T}{Q} - iT - DT - \epsilon_k T) \tag{5.10}$$

where $T_s = \frac{T}{Q}$ is the sampling interval at the destination receiver. Since correlation of the analog waveform cannot be implemented in real system, we should consider discrete time correlation for the delay estimation. Specifically, correlation is performed on each sample and the estimate of the delay is based on the correlation result on each sample. Therefore, the estimation resolution is decided by the interval between samples. To achieve the desired estimation accuracy while maintain reasonable oversampling rate Q required on analog-to-digital converter at the analog front end, interpolation can be used to improve the sample resolution. Thus the Q times oversampled signal $d(n)$ is first interpolated to a higher oversampling rate which is denoted by $\bar{Q}$. The interpolated discrete observation is denoted with $\bar{d}(n)$ $(0 < n < \frac{\bar{Q}}{Q}N_o)$. To match the sampling rate, the pulse shaped PN template waveform $p_k(t)$ should also be sampled at rate $\bar{Q}$, and the discrete PN waveform is denoted by $\boldsymbol{\rho}_k$ with length $(N_s + 2D)\bar{Q}$. Note that the oversampling rate of the interpolated signal $\bar{d}(n)$ decides the estimation resolution, which is $\Delta\epsilon = 1/\bar{Q}$. The correlation at the lth observation sample is carried out as

$$\psi_k(l) = \sum_{m=-D\bar{Q}}^{(N_S+D)\bar{Q}-1} \rho_k(m)\bar{d}(l+m), \quad 0 \le l \le L \tag{5.11}$$

where L is the delay estimation range. It has been shown that there is supposedly only one peak for each relay's PN waveform, and the peak of $\psi_k(l)$ appears when the received signal matches the PN waveform of the kth relay. The correlation in (5.11) involves the dot product of two $((N_s + 2D)\bar{Q} \times 1)$ vectors. However, the estimation range decides the number of correlations we need to perform. The estimation range should be long enough to cover the maximum of the delay. Specifically, if the correlation in (5.11) starts from 0, then the correlation only takes place for $0 \le l \le L$ where $L > max(\boldsymbol{\epsilon})\bar{Q}$. For instance, if we assume all the delays are within one symbol

interval, we can choose $L = \bar{Q}$. In other words, with estimation range L, we should have $N_o = (N_s + 2D)\bar{Q} + L$ observation samples, and for each relay L correlations have to be computed. As a result, the estimation of ϵ_k can be written as

$$\hat{\epsilon}_k = \frac{\max_{0 \le l \le L} |\psi_k(l)|}{\bar{Q}}. \tag{5.12}$$

Once ϵ_k is estimated, the channel can be estimated using the maximal correlation output as

$$\hat{h}_k = \frac{\psi_k(l_{max})}{\lambda_{norm}} \tag{5.13}$$

where $l_{max} = \arg\max_l |\psi_k(l)|$ and $\lambda_{norm}^{(k)} = \sum_{m=-D\bar{Q}}^{(N_S+D)\bar{Q}-1} |\rho_k(m)|^2$ is the normalization factor. The channel estimation can be proved as follows. Substituting (5.11) into (5.13), we have

$$\hat{h}_k = \sum_{m=-D\bar{Q}}^{(N_S+D)\bar{Q}-1} \rho_k(m)\bar{d}(l_{max}+m). \tag{5.14}$$

Assuming $\bar{d}(n)$ is perfectly interpolated from $d(n)$, (5.14) can be further written as

$$\begin{aligned}
\hat{h}_k &= \sum_{m=-D\bar{Q}}^{(N_S+D)\bar{Q}} \frac{\rho_k(m)}{\lambda_{norm}^{(k)}} \Big(\sum_{r=1}^{K} h_r \sum_{i=0}^{N_s-1} x_r(i) g\big((m+l_{max})\frac{T}{\bar{Q}} - iT - DT - \epsilon_r T\big) + w(l_{max}+m)\Big) \\
&= \sum_{m=-D\bar{Q}}^{(N_S+D)\bar{Q}} \frac{\rho_k(m)}{\lambda_{norm}^{(k)}} \Big(\sum_{r=1}^{K} h_r \sum_{i=0}^{N_s-1} x_r(i) g\big(m\frac{T}{\bar{Q}} - iT - DT + (\frac{l_{max}}{\bar{Q}} - \epsilon_r)T\big) + w(l_{max}+m)\Big) \\
&= \sum_{m=-D\bar{Q}}^{(N_S+D)\bar{Q}} \frac{\rho_k(m)}{\lambda_{norm}^{(k)}} \Big(\sum_{r=1}^{K} h_r \rho_r(m + l_{max} - \lfloor \epsilon_r \bar{Q} \rfloor) + w(l_{max}+m)\Big)
\end{aligned} \tag{5.15}$$

where $w(n)$ is the nth sample of the AWGN $w(t)$ and $\lfloor \bullet \rfloor$ is the floor operation. Rewrite (5.15) as

$$\hat{h}_k = h_k \Lambda_{kk} + \sum_{\substack{r=1 \\ r \neq k}}^{K} h_r \Lambda_{kr} + \bar{w}_k \tag{5.16}$$

where

$$\Lambda_{kk} = \sum_{m=-D\bar{Q}}^{(N_S+D)\bar{Q}} \rho_k(m)\rho_k(m + \frac{l_{max}}{\bar{Q}} - \epsilon_k)/\lambda_{norm}^{(k)}$$
$$\Lambda_{kr} = \sum_{m=-D\bar{Q}}^{(N_S+D)\bar{Q}} \rho_k(m)\rho_r(m + \frac{l_{max}}{\bar{Q}} - \epsilon_r)/\lambda_{norm}^{(k)}$$
$$\bar{w}_k = \sum_{m=-D\bar{Q}}^{(N_S+D)\bar{Q}} \rho_k(m)w(m + l_{max})/\lambda_{norm}^{(k)}. \quad (5.17)$$

The first term Λ_{kk} in (5.17) represents the auto-correlation of the kth relay's PN modulated waveform. The second term $\sum_{\substack{r=1 \\ r\neq k}}^{K} \Lambda_{kr}$ represents the cross-correlation between the PN waveforms of the rth relay and the kth relay and the third term $\bar{w}_k$ is the correlation between the PN waveform and the AWGN, which is also Gaussian distributed. As long as $\frac{l_{max}}{\bar{Q}} \approx \epsilon_k$, i.e., the delay estimation is accurate, we have $\Lambda_{kk} \approx 1$ and $\Lambda_{kr} \ll 1$ according to the correlation property of the PN sequences. (5.16) yields the estimation of h_k.

5.3.2 Complexity Analysis

The most frequently used arithmetic operation in the synchronization algorithms is multiply-and-accumulate (MAC). Therefore, we evaluate the complexity in terms of the number of required MAC operations. Given the desired estimation resolution $T/\bar{Q}$, each correlation needs $(2D + N_s)\bar{Q}$ MAC operations. The number of correlations depends on the search range of the estimation which depends on where the observation starts. Assume that the observation starts at time $-DT$, and the signal of the kth relay arrives at $\epsilon_k T$. The maximization range L in (5.12) should be able to cover the largest propagation delay. Consequently, we have to ensure that the observation interval covers the largest propagation delay. Then L and $\bar{Q}$ determines the complexity of the correlator, which is $KL(2D + N_s)\bar{Q}$ MAC operations. Considering the interpolation involved complexity, if linear interpolation is applied, each interpolated point needs 1 MAC operation and the overall computation for the interpolation is approximately $(2D + N_s)(\bar{Q} - Q)$. Therefore, the total MAC operations required in the proposed estimator is approximately $(KL+1)(2D+N_s)\bar{Q}$ (assuming $\bar{Q} \gg Q$).

Table 5.1: Computational complexity analysis. Parameters: $K = 2$, $N_s = 31$, $Q = 4$, $D = 1$. Evaluated in the number of MAC operations. (Linear Interpolation for the proposed estimator)

	$\bar{Q} = 20$	$\bar{Q} = 40$	$\bar{Q} = 50$	$\bar{Q} = 100$
Proposed Estimator	26400	105600	165000	660000
ML Estimator	18851200	75404800	117820000	471280000

Furthermore, if the cubic spline interpolation is used, the computation required to determine the cubic splines is linear to $(2D + N_s)Q$ original samples due to the equally spaced knots [46]. For the cubic interpolation function, each interpolated sample needs 6 MAC operations (e.g., $ax^3 + bx^2 + cx + d$). Therefore the overall complexity is $KL(2D + N_s)\bar{Q} + M(2D + N_s)Q + 6(2D + N_s)(\bar{Q} - Q) \approx (KL + 6)(2D + N_s)\bar{Q}$ (assuming $\bar{Q} \gg Q$) where M is a linear factor related to the computation of the cubic spline for each interpolation segment.

On the other hand, the ML estimator in [62] needs $\bar{Q}^K$ times likelihood calculation in (5.7). Each calculation first involves the construction of $\mathbf{\Omega}_{\boldsymbol{\epsilon}}$ and the calculation of $\|\mathbf{\Omega}_{\boldsymbol{\epsilon}}(\mathbf{\Omega}_{\boldsymbol{\epsilon}}^H\mathbf{\Omega}_{\boldsymbol{\epsilon}})^{-1}\mathbf{\Omega}_{\boldsymbol{\epsilon}}^H\mathbf{d}\|^2$, which consumes approximately $(K+1)(N_sQ)^2+2K^2N_sQ+K^3$ MAC operations assuming the matrix inversion $(\mathbf{\Omega}_{\boldsymbol{\epsilon}}^H\mathbf{\Omega}_{\boldsymbol{\epsilon}})^{-1}$ consumes K^3 MAC operations. Then consider the same estimation range for the proposed estimator and the ML estimator, i.e., within one symbol interval and $L = \bar{Q}$. In this case, the total computation is approximately $K(2D + N_s)\bar{Q}^2$ for the proposed estimator and is $[(K + 1)(N_sQ)^2 + 2K^2N_sQ + K^3]\bar{Q}^K$ for the ML estimator. The comparison of the computational complexity between the proposed estimator and the ML estimator is shown in Table 5.1. It is apparent that the complexity of the proposed correlation based estimator is much lower than that of the ML estimator which increases exponentially with K for the growth rate $\bar{Q}$.

5.4 Simulation Results and Discussions

In this section, the proposed estimator is examined in terms of the mean square error (MSE) via computer simulation. Both non-fading and fading channels are simulated. For the non-fading channel, only AWGN noise is added to the received signal. Each simulation result is averaged over 10^4 program runs. For fading channels, Rayleigh fading is considered and the simulation result is averaged over 10^4 channel realizations. In the simulation, root raised cosine (RRC) filter is used for $g(t)$ with the span

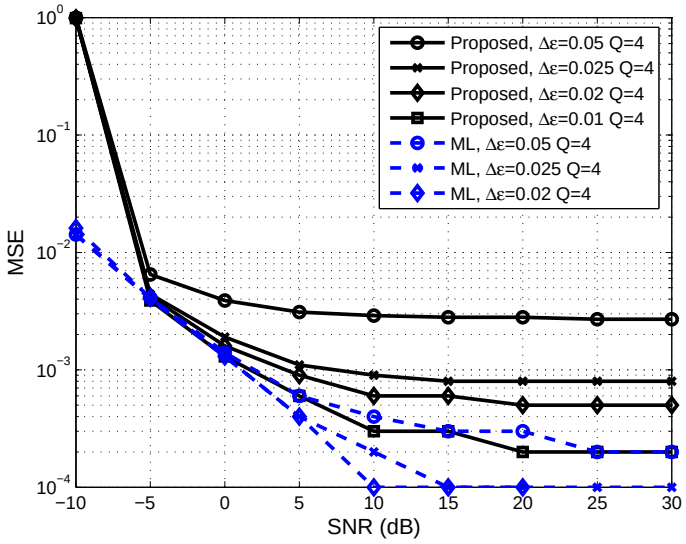

Figure 5.2: MSE performance of the correlation based delay estimator over non-fading channels compared with the ML delay estimator proposed in [62].

parameter $D = 1$. At the destination receiver, the received signal is the summation of the signals from all the relays. Therefore, to ensure that the observation interval covers the signal from all the relays, the observation interval is set to be slightly longer than the training signal duration. Specifically, given the training signal duration for all the relays as $T_p = (N_s + 2D)T$, the observation interval starts earlier than the first arriving signal and ends later than the last arriving signal. The PN sequences used are m-sequences generated with linear feedback shift registers (LFSR). Specifically, $N_s = 31$ and $N_s = 63$ have been used in the simulation, with generator polynomial $G(x) = x^5 + x^2 + 1$ for $N_s = 31$ and $G(x) = x^6 + x^4 + x^3 + x + 1$ for $N_s = 31$. The PN sequences for different relays are the cyclic shifts of the original generated sequence. For instance, for two relay systems, one relay uses the original PN sequence $\mathbf{x}$ and the other relay uses $\mathbf{x}$ shifted by $\lfloor N_s/2 \rfloor$. And for four relay systems, the relays use $\mathbf{x}$, $\mathbf{x} >> \lfloor N_s/4 \rfloor$, $\mathbf{x} >> \lfloor N_s/2 \rfloor$ and $\mathbf{x} >> \lfloor 3N_s/4 \rfloor$ where $>>$ stands for cyclic right shift operation. As for the ML estimator in [62] whose performance is also evaluated for comparison, the training sequence used is random binary phase shift keying (BPSK) (± 1) symbols.

In [62], ϵ_k is restricted within one symbol duration. On the other hand, the proposed correlation based estimator is able to deal with more severe propagation delays. However, for fair comparison, we assume the normalized delay ϵ_k is less than

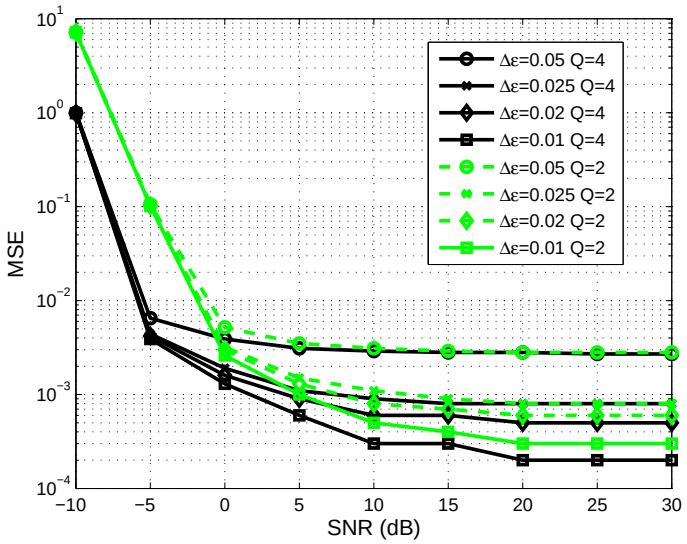

Figure 5.3: MSE performance of the correlation based delay estimator with different oversampling rate and different resolution over non-fading channels. $N_s = 31$, $D = 1$.

one symbol duration, i.e., $0 \leq \epsilon_k < 1$. The MSE performances of the proposed correlation based estimator and the ML estimator in AWGN channel are shown in Fig. 5.2 where linear interpolation is used for the proposed estimator. In Fig. 5.2, $\Delta\epsilon$ is the normalized estimation resolution which means the search step size is $\Delta\epsilon T$ for the ML estimator and the interpolation oversampling rate $\bar{Q} = 1/\Delta\epsilon$ for the proposed estimator. In the following, we will reflect the estimation resolution with $\Delta\epsilon$ rather than $\bar{Q}$ for the proposed estimator. Smaller step size leads to better estimation, but higher complexity especially for the ML estimator whose complexity increases exponentially with the resolution, as discussed in Section 5.3.2. An MSE floor can be observed as the SNR increases because of the limited estimation resolution determined by $\Delta\epsilon$. The proposed correlation based estimator has higher MSE floor than the ML estimator. The MSE of the proposed estimator drops fast at low SNRs as the SNR increases especially from -10dB to -5dB and with smaller $\Delta\epsilon$ the performance is closer to the ML estimator. Fig. 5.3 shows the performance of the proposed estimator with different oversampling rate including $Q = 2$ and $Q = 4$. It can be seen that higher oversampling rate leads to better performance at low SNRs. At low resolution ($\Delta\epsilon = 0.05$ and 0.025), the proposed estimator achieves the same MSE floor with $Q = 4$ and $Q = 2$. At high resolution ($\Delta\epsilon = 0.02$ and 0.01), increasing Q from 2 to 4 lowers the MSE floor. However, higher oversampling rate reaches the MSE floor first when the SNR increases.

For fading channels, the Rayleigh channel with unit variance is examined. The MSE performance is shown in Fig. 5.4, using the cubic spline interpolation method. It can be seen that the MSE floor of the correlation based estimator is around 0.04 with $N_s = 31$ and increasing the resolution does not improve the performance. The ML estimator is able to achieve much better performance with $N_s = 31$ than the proposed scheme over fading channels. However, the performance of the proposed estimator is significantly improved when the training sequence length is increased to $N_s = 63$. According to Section 5.3.2, doubling the training sequence length only doubles the computational complexity which is still much lower than that of the ML estimator with the shorter training length ($N_s = 31$). The timing performance with more than 2 relays is shown in Fig. 5.5, where a system with 4 relays is evaluated and compared with a 2 relay system. It can be seen that the performance with 4 relays is only slightly worse than 2 relays with the same parameters.

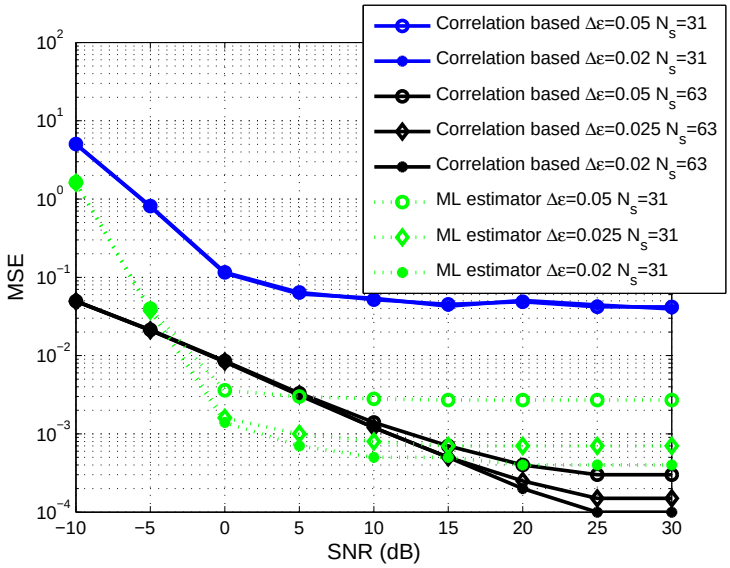

Figure 5.4: MSE performance of the correlation based delay estimator and the ML estimator over fading channels. Oversampling rate $Q = 4$, $D = 1$.

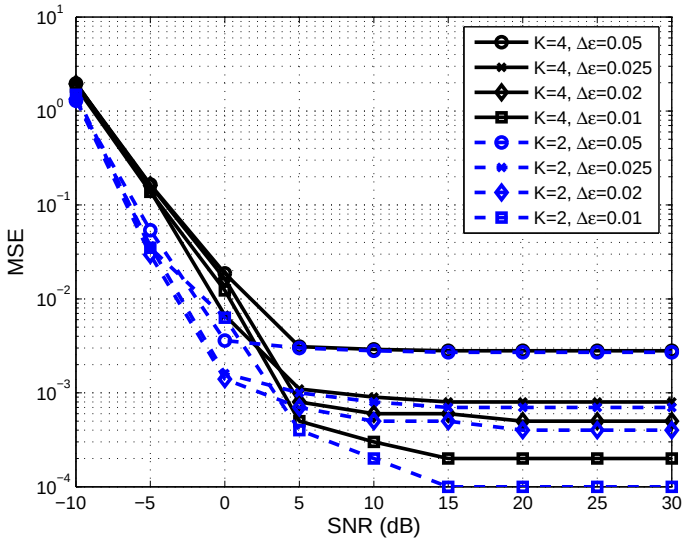

Figure 5.5: The timing MSE performance of the proposed correlation based estimator for different number of relays over fading channels. $N_s = 63$, $Q = 4$, $D = 1$.

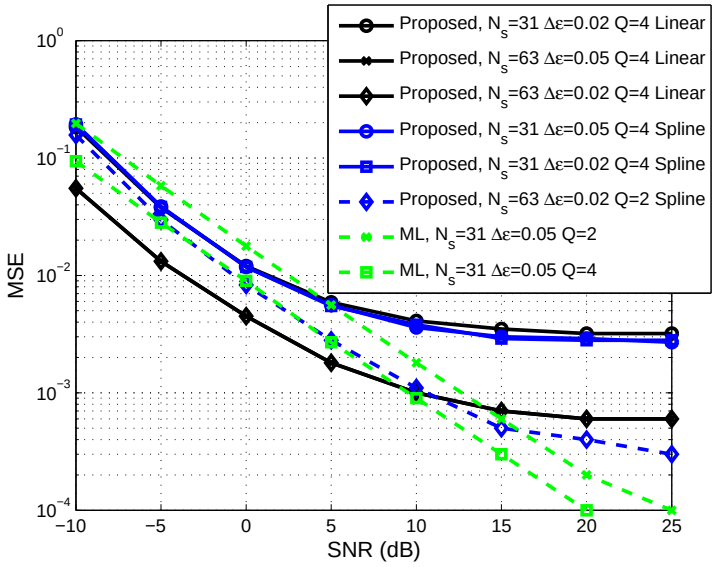

Figure 5.6: MSE performance of the channel estimation result after the timing estimation. $D = 1$.

Since the proposed scheme is also able to estimate the channel coefficient after timing is acquired using (5.13), we examine the channel estimation MSE performance of the proposed scheme compared with that of the ML scheme in Fig. 5.6. It can be seen from Fig. 5.6 that the ML scheme has better channel estimation performance than the proposed scheme with the same N_s. When comparing the proposed estimator with $N_s = 63$ and the ML estimator with $N_s = 31$, the proposed estimator is better at low SNRs but reaches an MSE floor at high SNRs which does not happen to the ML estimator. But considering the complexity, the proposed estimator is much better while still able to achieve satisfactory performance. We can also see that different interpolation schemes lead to different performances of the proposed estimation method and different resolutions achieve the same performance with the other parameters the same. Therefore, the interpolation method has more impact than the timing estimation resolution for the channel estimation.

5.5 Summary

In this chapter, a low complexity timing estimation method for DF cooperative communication system with multiple relays has been proposed. The existing ML scheme for the problem is not practical in real time processing because of the very high

complexity. The proposed estimator is a correlation based estimator that requires the training sequences among relays have good auto-correlation and cross-correlation properties. Although the performance of the proposed timing estimator is not as good as the ML estimator, the complexity is significantly reduced and it is still able to provide satisfactory performance. Not only the timing is simplified but also the channel estimation can be performed as a by-product of the timing estimation. Another benefit of the proposed estimator is that it is able to handle a larger estimation range, which is not supported in the previous ML estimator. The drawback of the proposed estimator is that in fading channel it needs longer training sequence than the ML estimator to achieve satisfactory performance.

Chapter 6

Conclusions and Future Work

6.1 Conclusions

In this dissertation, we have investigated the synchronization issues in several emerging communication systems including high rate UWB communications, OFDM based wideband cooperative communications and narrow band cooperative communication systems. Both timing and frequency synchronization have been studied. In summary, the investigated synchronization issues in this dissertation for the emerging wireless communication systems are not well solved in the literature. The objective of this dissertation is to provide new performance enhancing methods and complexity friendly methods in addition to the available study in the literature. Below is the conclusion of the contributions of each chapter.

In Chapter 2, a joint timing synchronization and channel estimation method has been proposed for block transmission high rate UWB systems. A new preamble structure has been proposed, and the coarse timing and fine timing algorithms are proposed based on the proposed preamble. The proposed fine timing estimator determines the first significant path by evaluating the energy jump for each element of the CIR vector. Moreover, the proposed energy jump detector has been analyzed against the conventional energy detector. The simulation results have shown the superior performance of the proposed scheme. In addition to that, the impact analysis of imperfect timing in SC-FDE based UWB systems has been provided, which covers a research void in the literature. The analytical results have been verified by the simulation.

In Chapter 3, the multiple CFO compensation problem in OFDM based Alamouti

DSTBC coded AF cooperative transmission has been studied. A joint TD and FD compensation and decoding approach has been proposed. Instead of immediately transforming the received signal into frequency domain, we perform a partial compensation in time domain first to remove either IBI or ICI. Then several interference suppressing methods have been proposed for the subsequent FD decoding including the sub-block equalization and iterative ML decoding. The proposed scheme outperforms the existing sub-block equalization method. On the other hand, although the proposed scheme is slightly worse than the joint ML decoding method performance-wise, it saves almost half of the computational complexity.

In Chapter 4, timing synchronization at the relay has been investigated in the TWRN system. An optimal timing estimator has been proposed for the relay nodes. The proposed estimator is actually an interference power estimator. The interference power measurement is carried out as the difference between the received signal block and a linear transformation of the received signal block. The optimal timing is then the point that minimizes the measurement metric. The effectiveness of the proposed scheme has been demonstrated by the simulation results.

In Chapter 5, the multiple delay estimation problem in DF cooperative transmission with narrow band signaling has been studied. The existing ML estimator has been found to be of prohibitive complexity. Therefore, we come up with a sub-optimal correlation based estimator. The proposed estimator is able to handle the estimation of a large delay of more than one symbol duration while the ML estimator restricts the delay to a symbol interval. The complexity analysis of the proposed estimator against the ML estimator has been provided and the substantial complexity reduction has been achieved while still keeping satisfactory performance.

6.2 Future Work

The timing and frequency synchronization methods proposed in this dissertation are ready to be extended in the following directions.

1. The joint timing and channel estimation method proposed for block transmission UWB systems is assuming perfect CFO synchronization. However, in the presence of CFO, the process should be adjusted in order to take the CFO into consideration when performing the fine timing estimation. Therefore, in this case, joint CFO and fine timing estimation should be considered based on the

current framework.

2. The joint TD and FD CFO mitigation method proposed in Chapter 3 is restricted to the Alamouti DSTBC coded two relay cooperative OFDM transmission. However, the joint TD and FD mitigation could be potentially considered in other OFDM based cooperative transmission with different coding schemes or different number of relays.

3. The optimal timing point estimation scheme proposed for the TWRN system is now evaluated in terms of the timing estimation performance at individual relay node. It is worth taking this method to the whole system performance analysis and simulation.

4. The synchronization issues studied in this dissertation consider single antenna at each terminal only. It is worth considering multiple antenna even in cooperative communication scenarios.

Bibliography

[1] Multi-band OFDM physical layer proposal for IEEE 802.15 Task Group 3a. Technical report, IEEE P802.15.3a Working Group, Mar. 2004.

[2] Part 15.4: Wireless Medium Access Control (MAC) and Physical Layer (PHY) Specifications for Low-Rate Wireless Personal Area Networks (LRW-PANs). Technical report, IEEE P802.15.4a/D4 (Amendment of IEEE Std 802.15.4), Jul. 2006.

[3] ECMA-368 high rate ultra-wideband PHY and MAC standard. Technical report, ECMA International, Dec. 2007.

[4] A. Nosratinia, T.E. Hunter and A. Hedayat. Cooperative communication in wireless networks. *IEEE Commun. Mag.* , pages 74–80, Oct. 2004.

[5] B. Can, H. Yomo and E.D. Carvalho. Hybrid forwarding scheme for cooperative relaying in OFDM based networks. In *IEEE Int. Conf. Communications (ICC)*, pages 4520 – 4525, Jul. 2006.

[6] B. Rankov and A. Wittneben. Spectral efficient signaling for half-duplex relay channels. In *Proc. of Asilomar Conf. on Signals, Systems and Computers*, pages 1066–1071, Oct. 2005.

[7] B. Rankov and A. Wittneben. Achievable rate region for the two-way relay channel. In *Proc. of IEEE Int. Symposium on Inf. Theory, (Seatle, USA)*, pages 1668–1672, Jul. 2006.

[8] P. Yang B. Zhou, Y. Xiao and S. Li. An iterative CFO compensation algorithm for distributed spatial modulation OFDM systems. In *Proc. of Int. Conf. on Wireless Commun., Networking and Mobile Computing(WiCOM)*, pages 1–4, Sept. 2011.

[9] D.S. Bernstein. *Matrix mathematics*. Princeton Univ. Press, Princeton, New Jersey, 2005.

[10] C.E. Shannon. Two-way communication channels. In *Proc. of 4th Berkeley Symp. Math. Stat. Prob.*, pages 611 – 644, 1961.

[11] C.K. Ho, R. Zhang and Y.C. Liang. Two-way relaying over OFDM: optimized tone permutation and power allocation. In *Proc. of IEEE Int. Conf. on Commun.*, pages 3908 – 3912, May 2008.

[12] C.L. Wang and H.C. Wang. An optimized joint time synchronization and channel estimation scheme for OFDM systems. In *Proc. of IEEE Veh. Techno. Conf. (VTC)*, pages 908–912, May 2008.

[13] C.R. Berger, S. Zhou, Z. Tian and P. Willett. Precise timing for multiband OFDM in a UWB system. In *Proc. of IEEE Intl. Conf. Ultra-Wideband (ICUWB)*, pages 269–274, Sept. 2006.

[14] C.R. Berger, S. Zhou, Z. Tian and P. Willett. Performance analysis on an MAP fine timing algorithm in UWB multiband OFDM. *IEEE Trans. Commun.*, pages 1606–1611, Oct. 2008.

[15] C.W. Yak , Z. Lei, S. Chattong and T.T. Tjhung. Timing synchronization and frequency offset estimation for Ultra-Wideband (UWB) Multi-Band OFDM systems. In *Proc. of Intern. Symp. on Personal, Indoor and Mobile Radio Communications (PIMRC)*, pages 471 – 475, Sept. 2005.

[16] D. Sreedhar and A. Chockalingam. ICI-ISI mitigation in cooperative SFBC-OFDM with carrier frequency offset. In *Proc. of Intern. Symp. on Personal, Indoor and Mobile Radio Communications (PIMRC)*, pages 1–5, Sept. 2007.

[17] E.G. Larsson, G. Liu, J. Li and G.B. Giannakis. Joint symbol timing and channel cstimation for OFDM based WLANs. *IEEE Commun. Lett.*, pages 325–327, Aug. 2001.

[18] F. Etezadi, L. Szczecinski and A. Ghrayeb. Correction of the CFO in OFDM relay-based space-time codes. In *Proc. of IEEE Global Telecommunications Conference (Globecom)*, pages 1 – 6, Dec. 2010.

[19] F. Gao, R. Zhang and Y.C. Liang. Channel estimation for OFDM modulated two-way relay networks. *IEEE Trans. Signal Processing*, pages 4443–4455, Nov. 2009.

[20] F. Ng and X. Li. Cooperative STBC-OFDM transmissions with imperfect synchronization in time and frequency. In *Proc. of Asilomar Conf. Signals, Systems and Computers*, pages 524–528, Oct. 2005.

[21] F. Tian, X.G. Xia and P.C. Ching. Signal detection for space-frequency coded cooperative communication system with multiple carrier offsets. In *IEEE Wireless Commun. and Networking Conf. (WCNC)*, pages 1221 – 1225, Mar. 2007.

[22] G. Scutari and S. Barbarossa. Distributed space-time coding for regenerative relay networks. *IEEE Trans. Wireless Commun.*, pages 3524–3536, Sept. 2005.

[23] G. Wang, F. Gao and C. Tellambura. Joint frequency offset and channel estimation methods for two-way relay networks. In *Proc. of Global Telecommun. Conf.*, pages 1–5, Dec. 2009.

[24] H. Gacanin, M. Salmela and F. Adachi. Performance analysis of analog network coding with imperfect channel estimation in a frequency-selective fading channel. *IEEE Trans. Wireless Commun.*, accepted for publication, 2011.

[25] H. Mehrpouyan and S.D. Blostein. Bounds and algorithms for multiple frequency offset estimation in cooperative networks. *IEEE Trans. Wireless Commun.*, pages 1300–1311, Apr. 2011.

[26] H. Mheidat, M. Uysal and N. Al-Dhahir. Equalization techniques for distributed space-Time block codes with amplify-and-forward relaying. *IEEE Trans. Signal Process.* , pages 1839–1852, May 2007.

[27] H. Minn, V.K. Bhargava and K.B. Letaief. A robust timing and frequency synchronization for OFDM systems. *IEEE Trans. Wireless Commun.*, pages 822–839, Jul 2003.

[28] H.-Q. Liu ,W.P. Siriwongpairat and K.J.R. Liu. Performance analysis of multiband OFDM UWB systems with imperfect synchronization and intersymbol interference. *IEEE J. Select. Areas Signal Proces.* , pages 521–534, Oct 2007.

[29] H. Wang, X.G Xia and Q. Yin. Distributed space-frequency codes for cooperative communication systems with multiple carrier frequency offsets. *IEEE Trans. Wireless Commun.*, pages 1045–1055, Feb. 2009.

[30] H. Xu, C.C. Chong, I. Guvenc, F. Watanabe and L. Yang. High-resolution TOA estimation with multi-band OFDM UWB signals. In *Proc. of IEEE Intl. Conf. Commun. (ICC)*, pages 4191–4196, May 2008.

[31] H. Xu, L. Yang, Y.T.J. Morton and M.M. Miller. Mistiming performance analysis of the energy detection based ToA estimator for MB-OFDM. *IEEE Trans. Wireless Commun.*, pages 3980–3984, Aug. 2009.

[32] H.-Y. Liu and C.-Y. Lee. A low-complexity synchronizer for OFDM-Based UWB system. *IEEE Trans. Circuits and Syst. -II Express Briefs*, pages 1269–1273, Nov. 2006.

[33] J.-J. van de Beek, M. Sandell and P.O. Borjesson. ML estimation of timing and frequency offset in OFDM systems. *IEEE Trans. Signal Process.*, pages 1800–1805, Jul. 1997.

[34] J.N. Laneman and G.W. Wornell. Distributed space-time coded protocols for exploiting cooperative diversity in wireless networks. In *Proc. of IEEE Global Telecommunications Conference (Globecom)*, pages 77– 81, Nov. 2002.

[35] J.N. Laneman, D.N.C. Tse and G.W. Wornell. Cooperative diversity in wireless networks: Efficient protocols and outage behavior. *IEEE Trans. Inform. Theory.*, pages 3062– 3080, Dec. 2004.

[36] T. Ketseoglou. Cooperation diversity for OFDM with iterative reception and independent CFO per node. In *Proc. of Asilomar Conference on Signals, Systems and Computers (ASILOMAR)*, pages 131–135, Nov. 2010.

[37] K.G. Seddik and K.J.R Liu. Distributed space-frequency coding over broadband relay channels. *IEEE Trans. Wireless Commun.* , pages 4748–4759, Nov. 2008.

[38] L.B. Thiagarajan, S. Sun and T. Quek. Carrier frequency offset and channel estimation in space-time non-regenerative two-way relay network. In *Proc. of IEEE 10th Workshop on Signal Processing Advances in Wireless Commun.*, pages 270 – 274, Jun. 2009.

[39] M. Morelli and U. Mengali. Carrier-frequency estimation for transmission over selective channels. *IEEE Trans. Commun.*, pages 1580–1589, Sept. 2000.

[40] M. Morelli, L. Sanguinetti and H. Vincent Poor. A robust ranging scheme for OFDMA-based networks. *IEEE Trans. Commun.*, pages 2441–2452, Aug. 2009.

[41] M. Speth, F. Classen and H. Meyr. Frame synchronization of OFDM systems in frequency selective fading channels. In *Proc. of IEEE Vehicular Technology Conference (VTC)*, pages 1807–1811, May 1997.

[42] M.K. Oh, X. Ma, G.B. Giannakis and D.J. Park. Cooperative synchronization and channel estimation in wireless sensor networks. In *Proc. of Asilomar Conf. Signals, Systems and Computers*, pages 238–242, Nov. 2003.

[43] M.L. Sichitiu and C. Veerarittiphan. Simple, accurate time synchronization for wireless sensor networks. In *IEEE Wireless Commun. and Networking Conf. (WCNC)*, pages 1266 – 1273, Mar. 2003.

[44] N. Benvenuto, S. Tomasin and D. Veronesi. Multiple frequency offsets estimation and compensation for cooperative networks. In *Proc. of IEEE Wireless Commun. and Networking Conf. (WCNC)*, pages 891 – 895, Mar. 2007.

[45] O.S. Shin, A.M. Chan, H.T. Kung and V. Tarokh. Design of an OFDM cooperative space-time diversity system. *IEEE Trans. Veh. Technol.* , pages 2203–2215, Jul. 2007.

[46] G.M. Phillips. *Interpolation and approximation by polynomials*. Spinger-Verlag Press, University of St. Andrews, St. Andrews, Scotland, 2003.

[47] Q. Huang, M. Ghogho and J. Wei. Data detection in cooperative STBC-OFDM systems with multiple frequency offsets. *IEEE Signal Processing Letters*, pages 600–603, Jul. 2009.

[48] R.U. Nabar, H. Bolcskei and F.W. Kneubuhler. Fading relay channels: performance limits and space-time signal design. *IEEE J. Select. Areas Commun.*, pages 1099–1109, Aug. 2004.

[49] S. Sadough and P. Duhamel. Improved iterative detection and achieved throughputs of OFDM systems under imperfect channel estimation. *IEEE Trans. Wireless Commun.*, pages 5039–5050, Dec. 2008.

[50] S. Zhang, S.C. Liew and P.P. Lam. Hot topic: physical layer network coding. In *Proc. of ACM Mobicom*, pages 358–365, 2006.

[51] S.V. Amari and R.B. Misra. Closed-form expressions for distribution of sum of exponential random variables. *IEEE Trans. Reliability*, pages 519–522, Dec. 1997.

[52] T. Jacobs, Y. Li, H. Minn and R.M.A.P. Rajatheva. Synchronization in MB-OFDM-based UWB systems. In *Proc. of IEEE Intl. Conf. Commun. (ICC)*, pages 1071–1076, Jun. 2007.

[53] T.D. Nguyen, O. Berder and O. Sentieys. Impact of transmission synchronization error and cooperative reception techniques on the performance of cooperative MIMO systems. In *Proc. of IEEE Intl. Conf. Commun. (ICC)*, pages 4601–4605, May 2008.

[54] T.J. Oechtering, C. Schnurr, I. Bjelakovic and H. Boche. Broadcast capacity region of two-phase bidirectional relaying. *IEEE Trans. Inform. Theory*, pages 454–458, Jan. 2008.

[55] T.M. Cover and A.A.E. Gamal. Capacity theorems for the relay channel. *IEEE Trans. Info. Theory*, pages 572–584, Sept. 1979.

[56] T.M. Schmidl and D.C. Cox. Robust frequency and timing synchronization for OFDM. *IEEE Trans. Commun.*, pages 1613–1621, Dec. 1997.

[57] D. Veronesi and D.L. Goeckel. Multiple frequency offset compensation in cooperative wireless systems. In *Proc. of IEEE Global Telecommunications Conference (Globecom)*, pages 1 – 5, Nov. 2006.

[58] W. Nam, S.Y. Chung and Y.H. Lee. Capacity bounds for two-way relay channels. In *Proc. of IEEE Int. Zurich Senimar on Commun.*, pages 144–147, Mar. 2008.

[59] W.G. Jeon, K.H. Chang and Y.S. Cho. An equalization technique for orthogonal frequency-division multiplexing systems in time-variant multipath channels. *IEEE Trans. Commun.*, pages 27–32, Jan. 1999.

[60] F. Ng X. Li and T. Han. Carrier frequency offset mitigation in asynchronous cooperative OFDM transmissions. *IEEE Trans. Signal Process.* , pages 675 – 685, Feb. 2008.

[61] X. Li and F. Ng. Using cyclic prefix to mitigate carrier frequency and timing asynchronism in cooperative OFDM transmissions. In *Proc. of Asilomar Conf. Signals, Systems and Computers*, pages 1791 – 1795, Oct. 2006.

[62] X. Li, Y.C. Wu and E. Serpedin. Timing synchronization in decode-and-forward cooperative communication systems. *IEEE Trans. Signal Processing*, pages 1444–1455, Apr. 2009.

[63] X. Wang and Z. Wu. PIC detector for joint distributed STBC under imperfect synchronization. In *Proc. of IEEE Intl. Conf. on Wireless Commun., Networking and Mobile Computing*, pages 1–4, Sept. 2009.

[64] Y. Jing and B. Hassibi. Distributed space-time coding in wireless relay networks. *IEEE Trans. Wireless Commun.*, pages 3524–3536, Dec. 2006.

[65] Y. Li, W. Zhang and X-G. Xia. Distributed high-rate full-diversity space-frequency codes for asynchronous cooperative communications. In *IEEE International Symposium on Information Theory (ISIT)*, pages 5612 – 5616, Seattle, USA, Jul. 2006.

[66] Y. Mei, Y. Hua, A. Swami and B. Daneshrad. Combating synchronization errors in cooperative relays. In *Proc. of IEEE Intl. Conf. on Acoustics Speech and Signal Process. (ICASSP)*, pages 369–372, Mar. 2005.

[67] Y. Mostofi and D.C. Cox. Mathematical analysis of the impact of timing synchronization errors on the performance of an OFDM system. *IEEE Trans. Commun.*, pages 226–230, Feb. 2006.

[68] Y. Wang and X. Dong. Cyclic prefixed single carrier transmission in ultra-wideband communications. *IEEE Trans. Wireless Commun.*, pages 2017–2021, Aug. 2006.

[69] Y. Wang and X. Dong. Frequency-domain channel estimation for SC-FDE in UWB communications. *IEEE Trans. Commun.*, pages 2155–2163, Dec. 2006.

[70] Y. Wang and X. Dong. Comparison of frequency offset and timing offset effects on the performance of SC-FDE and OFDM over UWB channels. *IEEE Trans. Veh. Techno.*, pages 242 – 250, Jan. 2009.

[71] Y. Yao and X. Dong. On the detection of distributed STBC AF cooperative OFDM signal in the presence of multiple CFOs. In *IEEE Int. Conf. Communications (ICC)*, pages 1 – 6, May 2010.

[72] Y.J. Kim, H. Lee, H.K. Chung and Y.S. Cho. An iterative decoding technique for cooperative STBC-OFDM systems with multiple carrier frequency offsets. In *Proc. of Intern. Symp. on Personal, Indoor and Mobile Radio Communications (PIMRC)*, pages 1–4, Sept. 2007.

[73] Z. Li and X-G. Xia. An alamouti coded OFDM transmission for cooperative systems robust to both timing errors and frequency offsets. *IEEE Trans. Wireless Commun.* , pages 1839–1844, May 2008.

[74] Z. Li, D. Qu and G. Zhu. An equalization technique for distributed STBC-OFDM system with multiple carrier frequency offsets. In *IEEE Wireless Commun. and Networking Conf. (WCNC)*, pages 839–843, Apr. 2006.

[75] Z. Li, X.G. Xia and B. Li. Achieving full diversity and fast ML decoding via simple analog network coding for asynchronous two-way relay networks. *IEEE Trans. Commun*, pages 3672 – 3681, Dec. 2009.

[76] Z. Ye, C. Duan, P. Orlik and J. Zhang. A low-complexity synchronization design for MB-OFDM ultra-Wideband systems. In *Proc. of IEEE Intl. Conf. Commun. (ICC)*, pages 3807–3813, May 2008.

Appendix A

Appendices

A.1 Derivation of the received block representation in (2.1)

With a timing error of m (> 0), the pth received data block can be written as $\mathbf{y}(p) = \bar{\mathbf{h}}\bar{\mathbf{x}}^m(p) + \mathbf{n}$ where

$$\bar{\mathbf{h}} = \begin{bmatrix} \overbrace{0 \ \dots \ 0}^{N_g - L} & h_L & \dots & h_0 & 0 & \dots & 0 & 0 \\ \vdots & 0 & h_L & \dots & h_0 & 0 & \dots & 0 \\ \vdots & \vdots & \ddots & \ddots & \ddots & \ddots & \ddots & \vdots \\ \vdots & \vdots & \vdots & \ddots & \ddots & \ddots & \ddots & 0 \\ 0 & \dots & \dots & \dots & 0 & h_L & \dots & h_0 \end{bmatrix}_{N \times (N+N_g)} \tag{A.1}$$

and

$$\bar{\mathbf{x}}^m(p) = [x_{p,-N_g+m}, \dots, x_{p,0}, \dots, x_{p,N-1}, \ x_{p+1,-N_g}, \\ \dots, x_{p+1,-N_g+m-1}]^T_{(N+N_g)\times 1}. \tag{A.2}$$

By defining

$$\begin{aligned}
\alpha_1 =&[x_{p,-N_g+m}\ , \ldots, x_{p,0}\ , \ldots, x_{p,N-1}\ ,\ x_{p,0},\\
&\ldots, x_{p,m-1}]^T_{(N+N_g)\times 1}\\
\alpha_2 =&[\ \underbrace{0, ..., 0}_{N+N_g-m}\ ,\ x_{p+1,-N_g}\ ,\ x_{p+1,-N_g+1}\ ,\\
&\ldots, x_{p+1,-N_g+m-1}]^T_{(N+N_g)\times 1}\\
\alpha_3 =&[\ \underbrace{0, ..., 0}_{N+N_g-m}, x_{p,0}\ ,\ x_{p,1}\ ,\\
&..., \ x_{p,m-1}]^T_{(N+N_g)\times 1}
\end{aligned} \tag{A.3}$$

$\bar{\mathbf{x}}^m(p)$ can further be written as $\bar{\boldsymbol{x}}^m(p) = \boldsymbol{\alpha}_1 + \boldsymbol{\alpha}_2 - \boldsymbol{\alpha}_3$ where $\boldsymbol{\alpha}_1$ is the cyclic extended desired block component, $\boldsymbol{\alpha}_2$ and $\boldsymbol{\alpha}_3$ are the interference terms from the next block and the current block respectively. Thus $\mathbf{y}(p) = \bar{\mathbf{h}}(\boldsymbol{\alpha}_1 + \boldsymbol{\alpha}_2 - \boldsymbol{\alpha}_3) + \mathbf{n}$. Since $\boldsymbol{\alpha}_1$ is a cyclic prefixed block, then by changing $\bar{\mathbf{h}}$ to a Toeplitz matrix $\tilde{\mathbf{h}}$ in (2.1), $\bar{\mathbf{h}}\boldsymbol{\alpha}_1$ can be reduced to $\tilde{\mathbf{h}}\mathbf{x}^m(p)$ (the first term in (2.1)). Furthermore, note that there are only m non-zero terms at the end of $\boldsymbol{\alpha}_2$ and $\boldsymbol{\alpha}_3$. Then by changing $\bar{\mathbf{h}}$ to $\tilde{\mathbf{h}}_1^m$ in (2.1), $\bar{\mathbf{h}}(\boldsymbol{\alpha}_2 - \boldsymbol{\alpha}_3)$ can be written as $\tilde{\mathbf{h}}_1^m \tilde{\mathbf{x}}_1^m(p)$ (the second term in (2.1)).

A.2 Proof of the Gaussian approximation for the sum of ISI

The sum of ISI can be written as $z_{\mathcal{N}} = \sum_{n=1}^{\mathcal{N}} a_n x_n$, where $\mathcal{N}$ is the number of ISI terms, a_n is the weight of the nth ISI term and x_n is the nth independent ISI symbol. Considering an arbitrary two dimensional M-ary modulation and defining $x'_n = a_n x_n$, we have $\mathbb{E}[x'_n] = \mu_n = a_n \mu_x$ and $\mathrm{Var}[x'_n] = \sigma_n^2 = |a_n|^2 \sigma_x^2$ where μ_x and σ_x^2 are the mean and variance of the data symbol. The third central moment of the random variable $x'_n = a_n x_n$ is

$$r_n^3 := \mathbb{E}[|x'_n - \mu_n|^3] = \sum_{i=1}^{M} p_i |a_n x(i) - a_n \mu_x|^3 = |a_n|^3 \gamma^3 \tag{A.4}$$

where $x(i)$ is the ith possible symbol out of the M constellation points, p_i is the priori probability of $x(i)$, and $\gamma^3 = \sum_{i=1}^{M} p_i |x(i) - \mu_x|^3$ is always finite. Thus r_n^3 is finite for all n. Furthermore, x_n''s satisfy

$$\begin{aligned}
\lim_{\mathcal{N}\to\infty} \frac{(\sum_{n=1}^{\mathcal{N}} r_n^3)^{1/3}}{(\sum_{n=1}^{\mathcal{N}} \sigma_n^2)^{1/2}} &= \lim_{\mathcal{N}\to\infty} \frac{\gamma}{\sigma_x} \frac{(\sum_{n=1}^{\mathcal{N}} |a_n|^3)^{1/3}}{(\sum_{n=1}^{\mathcal{N}} |a_n|^2)^{1/2}} \\
&\leq \lim_{\mathcal{N}\to\infty} \frac{\gamma}{\sigma_x} \frac{(\mathcal{N} max\{|a_n|^3\})^{1/3}}{(\mathcal{N} min\{|a_n|^2\})^{1/2}} \\
&= \lim_{\mathcal{N}\to\infty} \frac{\gamma}{\sigma_x} \frac{max\{|a_n|\}}{min\{|a_n|\}} \mathcal{N}^{-1/6} = 0. \qquad \text{(A.5)}
\end{aligned}$$

Given r_n^3 is finite and (A.5), we have $z_{\mathcal{N}} = \sum_{n=1}^{\mathcal{N}} x_n'$ converges to a Gaussian distribution with $\mathbb{E}[z_{\mathcal{N}}] = \sum_{n=1}^{\mathcal{N}} a_n \mu_x$ and $\mathrm{Var}[z_{\mathcal{N}}] = \sum_{n=1}^{\mathcal{N}} |a_n|^2 \sigma_x^2$, according to the Lyapunov's central limit theorem.